CORRECTION OF HOT SPOT MUTATIONS IN DUCHENNE MUSCULAR DYSTROPHY BY CRISPR/CAS9 GENE EDITING

APPROVED BY SUPERVISORY COMMITTEE

Eric N. Olson, Ph. D.

Hesham A. Sadek, M.D., Ph.D.

Jay Schneider, M.D., Ph.D.

Joseph Hill, M.D., Ph.D.

DEDICATION

To my beloved family.

ACKNOWLEDGMENT

Foremost, I would like to express my deepest gratitude to my two mentors, Dr. Eric Olson and Dr. Rhonda Bassel-Duby. It has been an honor and privilege to be mentored by both of them. I thank Eric for giving me freedom to explore in science and for guiding me through winding roads along the way of my Ph.D. journey. It all started in Fall 2013 when he offered me a great opportunity to rotate in the awesome Olson Lab. As a student who is interested in translational research and biopharmaceutical industry, I often found that great scientists in academia do not appreciate the linkage between basic research and applied science. Eric is very different and special, he is open-minded and supportive of what I want to pursue in my career and he helps me exceed my personal potential. I am, and always will be sincerely grateful to him. He inspired me by setting himself as an example and by being energetic and passionate every single day. His enthusiasm for research is contagious and motivational for me, even during the tough times in the Ph.D. pursuit.

My Ph.D. would not have come to a successful completion, without the guidance from Rhonda. As an international student from Taiwan, she is like my mom in the States. She is not only my go-to-person for all the presentations, outside collaborations and scientific writing, she is also the go-to-person with whom I could talk about anything and be comfortable and natural. I will always remember all the word-fine tuning and proof-reading team work, as well as the up and down moments in her office. I am thankful to Rhonda for her generous contribution of time and caring to make my Ph.D. experience fruitful and possible.

I would like to acknowledge Ning, she is like a big sister for me in the lab. I've never worked with animals before I joined the Olson lab, and Ning is the person who taught me how

to work with animals from the very beginning. Additionally, she guided me when we were collaborating on the Twist2 cardiac project, and I appreciate her for all of her help and advice.

My thesis committee, Dr. Jay Schneider, Dr. Joseph Hill, and Dr. Hesham Sadek, has been a great help and support during my Ph.D. study. They provided me with precious ideas and suggestions, and advised me through scientific challenges. I thank them for always having their doors open for me.

I am fortunate enough to be in two great communities here at UT Southwestern, the Genetics, Development, and Disease Program and the Department of Molecular Biology. I am very proud to be in my graduate program. GD&D is a graduate program that really sees students' needs and provides substantial interdisciplinary training to let us achieve our goals. I am also very grateful that I have the opportunity to be immersed in an environment with cutting-edge, high-impact, and internationally recognized research built by stellar faculty members and supportive peers of the Department of Molecular Biology.

For the people on the DMD team, I thank the team members with all my heart. Hui, Cristina, Alex, John, and Efrain, I am grateful for everyday help with experiments. Leonela, Yu, Vicky, and Dileep thank you for many discussions and great collaborations. I thank Cheryl and Dylan for their help with animal work and Josh for helping with ordering and shipments. Special thanks to Chengzu for starting the Myoediting project. I thank Dr. Pradeep Mammen for helping with DMD patient donor samples, and Jian in the Mammen Lab for helping with the muscle physiology. Plus, I thank Venkat for help with bioinformatic analysis, Angie for assistance with flow cytometry and John for his excellent work and help with histology.

As an important note, I would like to express my gratitude to all the animals that were sacrificed for our research. These animals made potential human therapeutics possible.

And of course, I am grateful to the Olson lab members. It's hard to express how much I love this lab. This lab is my extended family in the States, and I am grateful to all the brilliant minds and friendships in the Olson lab. The people in the Olson Lab are just amazing to learn from: Angie and Miao as my fantastic bay mates throughout the years; Cristina, Vicky, Alex, Kelli, Jessica, and Glynnis for their friendships; and Andres, Yu, Johnny, Stephen, Tony, Akansha, and Dileep for forming the strong and happy circle of graduate students. I thank the Olsonites for all the brainstorming, the pats on the back and the hugs from the heart. These are the most important things that shed light into the darkness.

I was fortunate to encounter many great friendships in Dallas and throughout Texas. Together with the committee members of Texas Taiwanese Biotechnology Association. We made a biotech career symposium happen at UT Southwestern. I will never forget the fruitful moments that we shared.

Also, to my dearest family in Taiwan, they are the reason why I even started my Ph.D. journey. Deepest gratitude to my parents for supporting women in science since I was a little girl and for letting me fly freely across the continents to pursue my career. I will forever thank them for being my strong backing and for loving me as always.

At last, I would like to thank Chien-Fei, my wonderful husband, for seeing me as I am, for encouraging me when I had doubt, for everyday scientific discussions and for every memory we create. I am grateful to have him by my side during my Ph.D. journey.

CORRECTION OF HOT SPOT MUTATIONS IN DUCHENNE MUSCULAR DYSTROPHY BY CRISPR/CAS9 GENE EDITING

by

YI-LI MIN

DISSERTATION

Presented to the Faculty of the Graduate School of Biomedical Sciences

The University of Texas Southwestern Medical Center at Dallas

In Partial Fulfillment of the Requirements

For the Degree of

DOCTOR OF PHILOSOPHY

The University of Texas Southwestern Medical Center at Dallas

Dallas, Texas

December, 2018

CORRECTION OF HOT SPOT MUTATIONS IN DUCHENNE MUSCULAR DYSTROPHY BY CRISPR/CAS9 GENE EDITING

Publication No. _____

Yi-Li Min, Ph.D.

The University of Texas Southwestern Medical Center at Dallas, 2018

Supervising Professor: Eric N. Olson, Ph.D.

The ability to efficiently modify the genome using CRISPR technology has rapidly revolutionized biology and genetics and will soon transform medicine. Duchenne muscular dystrophy (DMD) represents one of the first monogenic disorders that has been investigated with respect to CRISPR-mediated correction of causal genetic mutations. DMD results from mutations in the gene encoding dystrophin, a scaffolding protein that maintains the integrity of striated muscles. Thousands of different dystrophin mutations have been identified in DMD patients, who suffer from a loss of ambulation followed by respiratory insufficiency, heart failure, and death by the third decade of life. Most DMD patients have an inherited or

spontaneous deletion in the dystrophin gene that disrupts the reading frame resulting in an unstable truncated product. The major DMD mutational hotspots are found between exons 6 to 8, and exons 45 to 53. Mutations that delete exon 44 of the dystrophin gene represent one of the most common causes of DMD and can be corrected in ~12% of patients by editing surrounding exons, which restores the dystrophin open reading frame. In this study, a new DMD mouse model was generated by deleting exon 44, thereby creating a human DMD hotspot mutation in a mouse animal model. Using CRISPR/Cas9-mediated genomic editing, the reading frame of the exon 44 DMD mouse model was restored and dystrophin expression was rescued. Furthermore, I present an efficient strategy for correction of exon 44 deletion mutations by CRISPR/Cas9 gene editing in cardiomyocytes obtained from patient-derived induced pluripotent stem cells and in a new mouse model harboring the same deletion mutation. Using AAV9 encoding Cas9 and single guide RNAs, I also demonstrate the importance of the dosages of these gene editing components for optimal gene correction in vivo. Our findings provide therapeutic insight to develop possible CRISPR therapies for DMD.

TABLE OF CONTENTS

PRIOR PUBLICATIONS

1. **Y.-L. Min**, H. Li, C. Rodriguez-Caycedo, A. A. Mireault, J. Huang, J. M. Shelton, J. R. McAnally, L. Amoasii, P. Mammen, R. Bassel-Duby, and E. N. Olson. (2018) Correction of Duchenne muscular dystrophy exon 44 deletion mutations in mice and human cells by CRISPR/Cas9. *Science Advances.* In revision.
2. **Y.-L. Min**, R. Bassel-Duby, and E. N. Olson. (2018) CRISPR correction of Duchenne muscular dystrophy. *Annual Review of Medicine* 70. In press.
3. **Y.-L. Min**, P. Jaichander, E. Sanchez-Ortiz, S. Bezprozvannaya, V. Malladi, B. Chen, J. M. Shelton, R. Bassel-Duby, E. N. Olson and N. Liu. (2018) Identification of a multipotent Twist2-expressing cell population in the adult heart. *Proceedings of the National Academy of Sciences* 115 (36) E8430-E8439.
4. C. Long, H. Li, M. Tiburcy, C. Rodriguez-Caycedo, V. Kyrychenko, H. Zhou, Y. Zhang, **Y.-L. Min**, J. M. Shelton, P. A. Mammen, N, Y. Liaw, W-H. Zimmermann, R. Bassel-Duby, J. W. Schneider, and E. N. Olson. (2018) Correction of diverse muscular dystrophy mutations in human engineered heart muscle by single-site genome editing. *Science Advances* 4(1):eaap9004.
5. K. Zhou, P. Kos, Y. Yan, H. Xiong, **Y.-L. Min**, K. A. Kinghorn, J. T. Minnig, J. B. Miller, D. J. Siegwart. (2016) Intercalation-mediated nucleic acid nanoparticles for siRNA delivery. *Chemical Communications* 52(82):12155-12158.
6. D. P. Millay, D. G. Gamage, M. E. Quinn, **Y.-L. Min**, Y. Mitani, R. Bassel-Duby, E. N. Olson. (2016) Structure–function analysis of myomaker domains required for myoblast fusion. *Proceedings of the National Academy of Sciences* 113(8):2116.

7. C.-D. Liu, Y.-L. Chen, **Y.-L. Min**, B. Zhao, C.-P. Cheng, M.-S. Kang, S.-J. Chiu, E. Kieff, C.-W. Peng. (2012) The Nuclear Chaperone Nucleophosmin Escorts an Epstein-Barr Virus Nuclear Antigen to Establish Transcriptional Cascades for Latent Infection in Human B Cells. *PLOS Pathogens* 8(12):e1003084.

LIST OF FIGURES

LIST OF TABLES

LIST OF DEFINITIONS

AAV – adeno-associated virus

AAV9 – adeno-associated viruses of serotype 9

AON – Anti-sense oligonucleotide

BMD – Becker muscular dystrophy

bp – base pair

CK – creatine kinase

CMs – cardiomyocytes

CPCs – cardiac progenitor cells

CRISPR – Clustered regularly interspaced short palindromic repeats

dCas9 – catalytically deficient Cas9

DMD – Duchenne Muscular Dystrophy

DSB – double-stranded break

ECs – endothelial cells

EDL – extensor digitorum longus muscle

EMT – epithelial–mesenchymal transition

FDA – Food and Drug Administration

HDR – homology-directed repair

HITI – homology-independent targeted integration

IM – intramuscular

indels – insertions and deletions

iPSCs – induced pluripotent stem cells

iPSC-CMs – induced pluripotent stem cells derived cardiomyocytes

LbCpf1 – Cpf1 from Lachnospiraceae bacterium

MI – myocardial infarction

NHEJ – nonhomologous end-joining

nCas9 – Cas9 nickase

nt – nucleotides

ORF – Open reading frame

PAM – protospacer adjacent motif

sgRNA – single guide RNA

SaCas9 – Cas9 from Staphylococcus aureus

SP – side population cells

SpCas9 – Cas9 from Streptococcus pyogenes

TA – tibialis anterior

T7E1 – T7 endonuclease I

tdTO – tdTomato

TOPO-TA – topoisomerase-based thymidine to adenosine cloning

Tw1 – Twist1

Tw2 – Twist2

Tw2-tdTO^{+} – Tw2-derived tdTO^{+} cells

Term – Definition goes here

Term – Definition goes here

CHAPTER ONE

CRISPR CORRECTION OF DUCHENNE MUSCULAR DYSTROPHY

Introduction

More than 800 monogenic disorders result in degeneration or dysfunction of skeletal muscle (Bonne et al., 2017). Among the most severe is Duchenne muscular dystrophy (DMD), which is caused by mutations in the X-linked dystrophin gene, a massive gene spanning ~2.3 megabases (Hoffman et al., 1987). DMD is the most common lethal monogenic disorder, and it primarily affects boys owing to their single X chromosome. The incidence of the disease is estimated at 1:5,000 boys worldwide. Approximately two-thirds of DMD mutations are inherited by the sons of mothers who are unknowing carriers of dystrophin mutations, and the remaining cases result from spontaneous germline mutations (Lee et al., 2014). More than 3,000 different dystrophin mutations have been shown to cause DMD, raising significant challenges for the development of gene correction therapies that might be applicable to large cohorts of patients rather than single individuals. Roughly two-thirds of dystrophin mutations involve exon deletions that disrupt the dystrophin open reading frame (ORF), and point mutations or duplications account for the rest.

DMD is typically diagnosed in the first few years of life due to muscle weakness and progresses to loss of ambulation in the early teens. Degeneration of skeletal muscle leads to skeletal deformities and respiratory insufficiency, and cardiomyopathy ultimately causes death

in the third decade of life. A subset of patients also displays cognitive impairment. Becker muscular dystrophy (BMD) is a relatively mild form of the disease caused by in-frame deletions of the dystrophin gene. Patients with BMD exhibit a spectrum of phenotypes ranging from relatively mild muscle weakness and ambulation throughout life to severe muscle dysfunction resembling DMD (Andrews and Wahl, 2018). A major clinical goal has been to convert DMD to BMD through gene replacement or gene editing.

Since the discovery of the dystrophin gene in 1987 (Hoffman et al., 1987), there have been myriad efforts to develop therapies to delay disease progression and enhance muscle function in DMD patients. Various pharmacologic approaches, oligonucleotide-mediated exon skipping to bypass mutant exons, myoblast and stem cell transfer, and gene replacement to provide truncated forms of dystrophin have been advanced in recent years, and numerous clinical trials are under way to assess their efficacy (Salmaninejad et al., 2018). While some therapies have shown transient benefits, the majority treat the consequences and symptoms of the disease rather than the underlying genetic cause, and none have yet restored long-term expression of the dystrophin protein.

Most recently, gene editing has been explored as a possible means of permanently removing genetic mutations that cause DMD, thereby restoring production of the missing dystrophin protein. No clinical trials have yet been initiated for the correction of DMD by gene editing, but the field is moving rapidly and represents a potentially transformative therapy unlike any other. In this chapter, I review recent progress toward gene editing as a means of eliminating the genetic mutations responsible for DMD and forestalling disease progression.

Dystrophin

Dystrophin functions in muscle as a mechanical link to tether the actin cytoskeleton to the inner surface of the sarcolemma (Ahn and Kunkel, 1993). Lack of dystrophin in skeletal muscle results in fragility of the sarcolemma, impaired intracellular signaling, myocyte necrosis, inflammatory infiltration, and, eventually, replacement of muscle with fibrotic and fatty tissue (Gao, 2015). During DMD progression, satellite cells, an injury-responsive stem cell population beneath the muscle basal lamina, becomes activated and fuses with damaged myofibers. Ultimately, this regenerative cell population becomes depleted and muscle degeneration ensues (Chang et al., 2016). In contrast, the adult heart lacks a robust stem cell population, so the absence of dystrophin in the heart ultimately results in myocyte dysfunction, consequent loss of pump function, and fatal cardiomyopathy (Fayssoil et al., 2009).

The dystrophin gene encompasses 79 exons that are spliced together to give rise to a 427-kDa protein (Figure 1.1). The splicing patterns of these exons are conserved from mice to humans, allowing studies in mice to be directly extrapolated to the human gene. The encoded dystrophin protein contains four functional domains: an actin-binding domain at the N terminus that anchors the protein to the cytoskeleton; a central region containing 24 spectrin-like repeats that forms the rod domain, which is interrupted by four hinge domains; a cysteine-rich domain that binds β-dystroglycan; and a C-terminal domain that binds dystrobrevin and syntrophins, mediating sarcolemma localization.

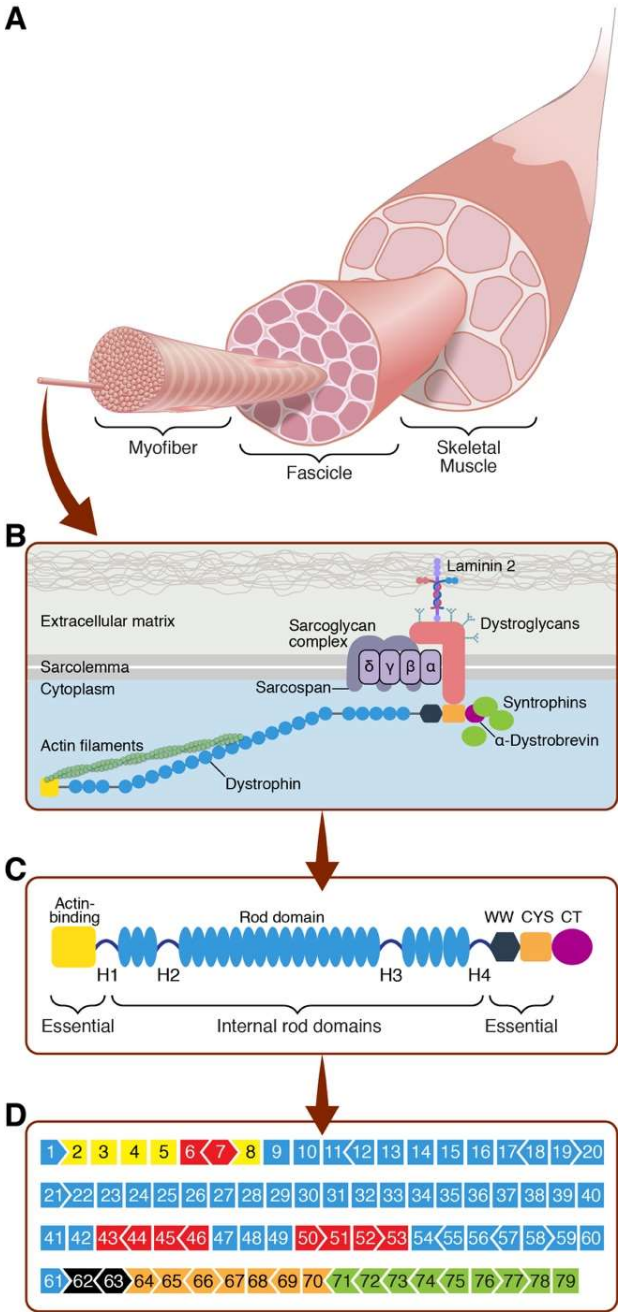

Figure 1.1 (A) Skeletal muscle is composed of thousands of multinucleated myofibers. Myofibers are held together in groups called fascicles. (B) The dystrophin-glycoprotein complex (DGC) resides on the sarcolemma of the myofiber and acts as an anchor. The N terminus of dystrophin connects with actin filaments and the C terminus interacts with the DGC, providing stability and integrity to the muscle cell. (C) Dystrophin protein structure. The N terminus of dystrophin contains the primary actin-binding domain, whereas the C terminus contains the dystroglycan-, dystrobrevin-, and syntrophin-binding sites. The N and C termini are essential for dystrophin function. The central rod domain acts like a spring between the two ends. The 24 spectrin-like repeats in the rod domain can be shortened to create a functional but less flexible dystrophin. (D) The exon structure of the dystrophin gene, showing the 79 exons. The reading frame compatibility is shown by the shape of the adjacent exons. The exons are color coded to match the major functional dystrophin protein domains in panel c. The exons within the mutational hotspot regions are indicated in red.

Dystrophin is a component of the dystrophin-glycoprotein complex (DGC), which anchors the cytoskeleton to the extracellular matrix and stabilizes the muscle membrane in response to contractions (Figure 1.1, panel B). The DGC also contains α-dystroglycan, an extracellular peripheral membrane protein and a receptor for laminin-2, which links the DGC

to the extracellular matrix; β-dystroglycan, which binds dystrophin; four sarcoglycans (α-, β-, γ-, and δ-); and sarcospan, which contributes to the stabilization of the complex. In addition, the spectrin-like repeats in the central rod domain of dystrophin bind neuronal nitric oxide synthase, targeting it to the sarcolemma.

The full-length form of dystrophin expressed in muscle tissues contains 3,684 amino acids. Interestingly, due to the modular structure of the dystrophin protein domains, internally truncated forms of dystrophin can retain function. In fact, alternatively spliced dystrophin products are found in muscle tissue of mild and asymptomatic BMD patients (Ginjaar et al., 2000). Microdystrophin, a 1,001-amino-acid truncated form of dystrophin, which lacks the redundant regions of the rod domain and contains the minimal functional regions of the protein, is currently in clinical trials as a gene therapy for DMD (Duan, 2015; Rodino-Klapac et al., 2010).

Although >3,000 different mutations have been shown to cause DMD, the majority of these mutations are positioned within so-called hotspots of the dystrophin gene and cluster around specific exons (Figure 1.1, panel D). It has been estimated that ~60% of DMD patients could benefit from gene editing strategies that skip the out-of-frame exons within these hotspots, and up to 80% of the patient population could potentially benefit if additional less common mutations were corrected. However, the remaining patients, who lack large genomic regions that include essential domains of the dystrophin protein, would not be treatable by gene editing and are therefore candidates for other gene replacement therapies.

Genome Editing

Clustered regularly interspaced short palindromic repeats (CRISPR) was first identified as a system for bacterial immunity in which segments of viral DNA are incorporated into the genome and subsequently transcribed into RNAs that can cooperate with the Cas9 endonuclease to recognize future viral pathogens and mediate their destruction (Cong et al., 2013; Jinek et al., 2012; Mali et al., 2013). In recent years, the CRISPR system has been adapted as a tool that can edit the genome of nearly any organism. The CRISPR system involves two components: a single guide RNA (sgRNA) with complementarity to any sequence in the genome, and the Cas9 endonuclease, which associates with the sgRNA at the genomic target sequence. Cas9 from Streptococcus pyogenes (SpCas9) is the most commonly used enzyme, which cuts DNA adjacent to the protospacer adjacent motif (PAM) NAG or NGG (Cong et al., 2013; Jinek et al., 2012; Mali et al., 2013). Cas9 protein from Staphylococcus aureus (SaCas9) uses the PAM motif NNGRR, which is more complex and limits the potential target sequences for gene editing (Ran et al., 2015). Another endonuclease smaller than SpCas9 is Cpf1 from Lachnospiraceae bacterium (LbCpf1), which requires a PAM sequence of 5'-TTTN-3' (Zetsche et al., 2015). These and other types of Cas9 proteins offer more options for CRISPR editing site selection (Hou et al., 2013; Müller et al., 2016). Gene editing can also be achieved using zinc-finger nucleases and transcription activator-like effector nucleases (Zhang et al., 2018).

Gene editing can occur through any of three pathways depending on the proliferative status of the cell, the presence or absence of an exogenous DNA template, and DNA sequence homologies surrounding the DNA sequence being targeted. In proliferative cells, when Cas9,

sgRNA, and a DNA template are provided, gene editing can occur through homology-directed repair (HDR), which results in replacement of the targeted genomic region by the exogenous DNA template. Since this pathway is restricted to proliferating cells, it might be applicable to satellite cells, but it cannot be readily deployed in differentiated skeletal or cardiac myocytes. In the absence of an exogenous DNA template, a sgRNA can direct Cas9 to introduce a double-stranded break (DSB) in DNA, which is subsequently repaired through an imprecise process known as nonhomologous end-joining (NHEJ), resulting in insertions and deletions (indels). This type of editing has been especially effective in deleting splice donor or acceptor site sequences in out-of-frame exons, thereby allowing restoration of the ORF of dystrophin gene. Fortuitously, the PAM sequence of Cas9, NAG, corresponds to the universal splice acceptor site sequence, thus enabling delivery of Cas9 to the splice acceptor of any exon and skipping of that exon through creation of an indel. In a variation of NHEJ, referred to as microhomology-mediated end joining, specific deletions can be introduced into a targeted genomic region flanked by regions of short homology, which recombine in a precise way. An unexpected but potentially highly useful recent discovery is that NHEJ editing with one sgRNA, a process referred to as single-cut CRISPR, results preferentially in the incorporation of a single nucleotide at the DSB (Amoasii et al., 2017). This has been attributed to the creation of a one-nucleotide overhang at the site of DNA cleavage by Cas9, which is filled by a DNA polymerase and ligated (Lemos et al., 2018). For exons that are out of frame by a single nucleotide, this type of gene editing thus allows efficient reframing of the protein.

Aside from the devastating clinical consequences of DMD and the lack of effective long-term therapy (Reinig Andrea et al., 2017), multiple features of the disease render it

amenable to gene editing as a therapeutic strategy. First, the modular structure of the rod domain of dystrophin makes it possible to delete mutant exons in this region of the gene and restore the ORF. Second, the location of the dystrophin gene on the X chromosome means that affected boys harbor only one mutant allele that needs to be corrected, and there are no concerns about inadvertently disrupting a wild-type copy of the gene. Third, only a minor fraction of normal dystrophin expression levels needs to be restored to achieve therapeutic benefit. This contrasts with disorders in which near-normal levels of a missing protein need to be produced or in which complete elimination of a toxic protein is required to achieve therapeutic efficacy. Moreover, because skeletal muscle is a syncytium in which hundreds of nuclei can share a common cytoplasm, genetic correction of even a small fraction of muscle nuclei can allow production of dystrophin and its distribution throughout the myofibers. In studies of mosaic mice generated by germline editing of a dystrophin mutation, we estimated that as little as 15% genetic correction was sufficient to restore dystrophin expression to normal levels in nearly all myofibers (Long et al., 2014).

Editing Duchenne Muscular Dystrophy Mutations in Patient-Derived Induced Pluripotent Stem Cells

The breakthrough discovery of induced pluripotent stem cells (iPSCs) has transformed our prospects for disease modeling in vitro. The use of disease-specific iPSCs provides surrogate models of human diseases, platforms for drug discovery, and possible stem cell–based cell replacement therapies. Easily accessible cell types, such as peripheral blood mononuclear cells, skin fibroblasts, or cells from urine samples, can be collected from a patient

and reprogrammed to stem cells and their derivatives, effectively recapitulating the patient's disease and genetic background in a culture dish (Kim et al., 2016; Long et al., 2018). The advantages of modeling diseases by using human iPSCs are the indefinite self-renewal capacity and pluripotency of these stem cells. In comparison to animal models of disease, patient-derived iPSCs provide an expandable and unlimited source for testing potential treatments or studying underlying disease mechanisms. Many human iPSC lines have been established to model muscular dystrophies, including DMD (Cai et al., 2016; Choi et al., 2016; Long et al., 2018; Young et al., 2016), facioscapulohumeral muscular dystrophy (Caron et al., 2016; Snider et al., 2010), limb-girdle muscular dystrophy (Kim et al., 2016; Turan et al., 2016; Wu et al., 2017), and myotonic dystrophy (Ueki et al., 2017). For DMD, multiple patient-derived iPSC lines with different types of mutations have been used to model disease-related gene expression, evaluate mutation-dependent variability, and test potential therapeutic strategies (Choi et al., 2016; Long et al., 2018).

Applications of gene editing that can be performed in human iPSC disease models include gene knockouts (Chen et al., 2015), insertion of transgenes (Adkar et al., 2016), and repair of disease-relevant mutations (Young et al., 2016). Differentiation of patient-derived iPSCs also provides a platform of cell types for CRISPR/Cas9-mediated gene editing. Thus, gene editing in iPSCs has become a standard research tool in regenerative medicine and human disease modeling.

CRISPR/Cas9-mediated gene editing has been applied to correct a variety of DMD mutations found in human myoblasts and patient-derived iPSC lines. Correction approaches for DMD include permanent exon removal, exon skipping, exon reframing, and exon knock-

in (Kyrychenko et al., 2017; Li et al., 2015; Long et al., 2018). Functional dystrophin gene restoration has been demonstrated by CRISPR/Cas9 editing in iPSCs derived from DMD patients with exon deletions, exon duplications, and point mutations (Kyrychenko et al., 2017; Long et al., 2018; Ousterout et al., 2015; Young et al., 2016). This includes the mutational hotspot regions in the repetitive rod domain and the essential actin-binding domains of dystrophin. Recently, CRISPR/Cpf1-mediated correction of DMD mutations in patient-derived iPSCs was also demonstrated (Zhang et al., 2017). Corrected DMD patient-derived iPSCs can be used to model functional improvement and study disease-related mechanisms, for example, calcium handling in DMD dilated cardiomyopathy (Kyrychenko et al., 2017), and to monitor how a modified version of dystrophin functions in a human genetic background of DMD.

An important and often ignored challenge of iPSC technology is the variability between individual iPSC lines in their differentiation properties and phenotypes caused by variations in genetic background and reprogramming methods used to generate the cell lines. These intrinsic variations between individual iPSC lines can hinder the detection of subtle phenotypes or lead to misinterpretation of disease-relevant phenotypes (Bock et al., 2011; Boulting et al., 2011). To address this issue, isogenic pairs of disease-specific and control iPSCs that differ exclusively at the specific DMD mutation have been generated using CRISPR technology and used to control for variation and defining differences in the muscle contractile profile .

It has been proposed that human iPSCs be used as a source for cell-based replacement transplantation therapy in other diseases, such as age-related macular degeneration (Mandai et al., 2017). However, iPSC transplantation is not a feasible therapy for DMD owing to inability

to access all the muscles of the body, low efficacy of engraftment of muscles, and the recognized genomic instability of iPSCs.

Mutation Correction by CRISPR/Cas9 Gene Editing In Vivo

Animal Models of Duchenne Muscular Dystrophy

To date, more than 60 spontaneous or engineered DMD animal models have been reported (McGreevy et al., 2015). Murine and canine models have been favored to elucidate pathogenic mechanisms and develop new therapeutic approaches in DMD. The most widely used DMD mouse model is the mdx mouse, with a spontaneous nonsense point mutation (cytosine-to-thymine transition) in exon 23 that leads to loss of dystrophin expression (Bulfield et al., 1984; Sicinski et al., 1989). The mdx mouse exhibits a 25% shorter lifespan than wild-type mice, but the difference is not comparable to human DMD patients, whose lifespan is reduced by 75% (Chamberlain et al., 2007). Disease progression of the mdx mouse is also relatively mild and does not mimic the human course of the disease. Following birth, the muscles of mdx mice are histologically normal. Extensive necrosis, myofiber regeneration with centrally located nuclei, and elevated levels of serum creatine kinase are evident during the crisis period at 4–6 weeks of age (Carnwath and Shotton, 1987; Dangain and Vrbova, 1984). Then disease progression slows, and the mice display a moderate myopathic disease state until 12–15 months of age, when muscle wasting, scoliosis, and cardiomyopathy develop (Bostick et al., 2008; Hakim et al., 2011; Lefaucheur Jean et al., 1995; Pastoret and Sebille, 1995). Although mdx mice develop a milder form of fibrosis and inflammatory cell infiltration in

cardiac and skeletal muscle, their diaphragm presents severe pathological changes comparable to those in human DMD patients (Stedman et al., 1991).

Four chemical variants of the mdx mouse have been developed, known as mdx2cv, mdx3cv, mdx4cv, and mdx5cv. Each of these mouse strains carries a point mutation that leads to loss of full-length dystrophin and results in expression of different dystrophin isoforms, which make these mutant mice useful for deciphering the role of these isoforms in DMD (Chapman et al., 1989). Several other dystrophin-deficient mouse lines were established using different genetic engineering techniques, including Dup2 for exon 2 duplication (Vulin et al., 2015) and MD-null for deletion of the entire dystrophin gene (Kudoh et al., 2005). Genome editing technology has played a major role in expanding DMD mouse models. For example, CRISPR/Cas9 was used to create a mouse model with deletion of exon 50 (Amoasii et al., 2017). Two other mouse models, hDMDdel45/mdx and hDMDdel52/mdx, were also generated using CRISPR/Cas9 to remove a specific exon in the knocked-in humanized dystrophin gene in the mdx mouse background (Veltrop et al., 2018; Young et al., 2017).

The relatively mild dystrophin-deficient phenotype of mice compared with DMD patients is thought to be due to the upregulation of compensatory mechanisms, such as increased utrophin expression, as well as robust skeletal muscle regenerative capacity in mice, plus differences in body size, lifespan and form of locomotion. To mimic the dystrophic phenotype in human DMD, several double-knockout mouse models have been generated with genetic elimination of the dystrophin gene and deletion of an additional gene that contributes to the compensatory mechanism, such as the genes for utrophin or α7β1-integrin (Deconinck et al., 1997; Grady et al., 1997; Guo et al., 2006; Rooney et al., 2006). Another DMD mouse

line that has features more representative of human DMD was generated by deleting telomerase RNA in mdx mice (Mourkioti et al., 2013; Sacco et al., 2010). Mice deficient in dystrophin and telomerase RNA have increased telomere shortening, which is thought to disrupt muscle stem cell maintenance.

Clinical diagnosis of muscular dystrophy has been reported in dogs (Funkquist et al., 1980; Valentine et al., 1986). Unlike mdx mice, affected dogs share a clinical resemblance to human DMD patients, exhibiting limb muscle atrophy, fibrosis, joint contracture, and hypersalivation (McGreevy et al., 2015). Several dog models of DMD with spontaneous mutations that cause dystrophinopathy have been identified (Sharp et al., 1992; Walmsley et al., 2010). The age of onset of limb weakness and cardiac defects and the expected lifespan are comparable to those of human DMD patients (Smith et al., 2011; Valentine et al., 1988). These clinically similar pathologies make DMD dogs an excellent model for preclinical gene therapy studies.

CRISPR-mediated Gene Editing Strategies

CRISPR/Cas-mediated genome editing has been shown to permanently correct DMD mutations and restore dystrophin function in mouse models. Germline editing by injecting zygotes with CRISPR/Cas9 editing components was first accomplished in mdx mice by correcting the mutated exon 23 using either HDR or NHEJ (Long et al., 2014). Postnatal editing of mdx mice was then achieved using recombinant adeno-associated virus to deliver CRISPR/Cas9 genome editing components and correct the dystrophin gene by skipping or deleting the mutated exon 23 in vivo (Bengtsson et al., 2017; Long et al., 2016; Nelson et al., 2016; Tabebordbar et al., 2016). Germline and postnatal CRISPR/Cas9 genome editing

approaches both successfully restored dystrophin expression and improved muscle function in mdx mice. Other CRISPR systems, including CRISPR/Cpf1, have been used to correct DMD mutation in both mdx mice and human-derived iPSCs by exon skipping or HDR (Zhang et al., 2017). Additionally, CRISPR/Cas9 adenine base editors have been deployed to repair a DMD mutant mouse with an exon 20 nonsense mutation by adenine-to-guanine single-nucleotide substitutions (Ryu et al., 2018). These encouraging results suggest that CRISPR technology offers therapeutic potential to correct various DMD mutations. Different strategies for correcting DMD mutations with the CRISPR system are discussed in detail in the following sections and are outlined in Figure 1.2.

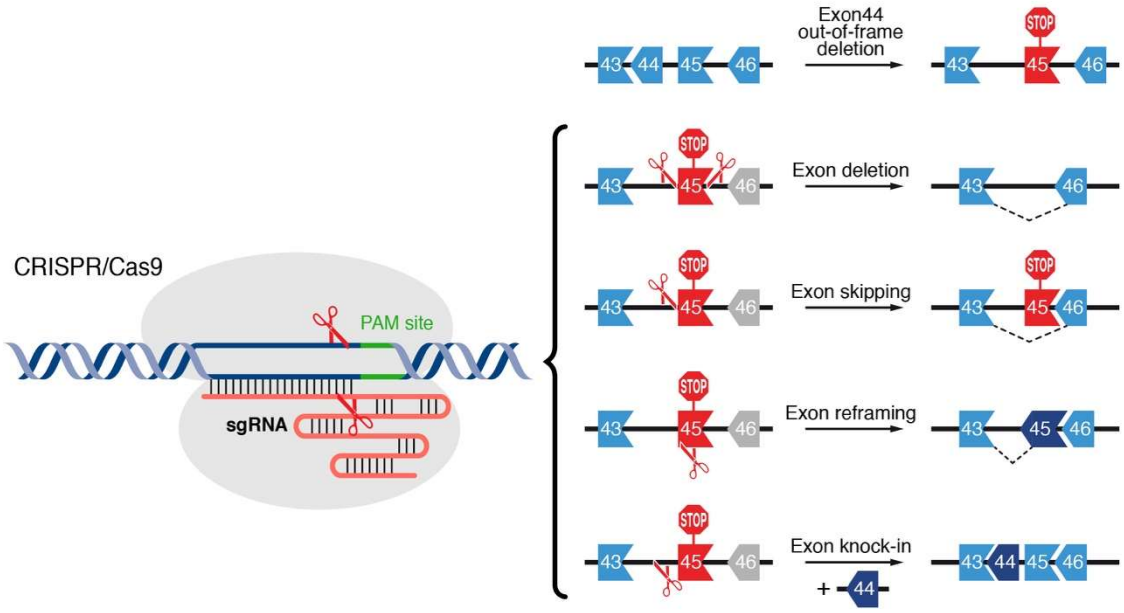

Figure 1.2 CRISPR-mediated editing strategies to correct DMD. CRISPR/Cas9-mediated strategies that require double-strand breaks, including exon deletion, exon skipping, exon reframing, and exon knock-in.

Exon deletion

Approximately 65–72% of all DMD patients carry a deletion of one or more exons. Deletions tend to cluster in a hotspot region between exons 45 and 55 of the dystrophin gene (Aartsma-Rus et al., 2006; Bladen et al., 2015). A common strategy for correcting single or multiple exon deletions is to delete the out-of-frame exon and restore the ORF. This can be achieved by deleting one exon or the entire hotspot region. Specifically, two sgRNAs flanking the targeted exon(s) can be delivered with Cas9 to excise the single or multiple mutated exons, resulting in restoration of the ORF by splicing adjacent in-frame exons (Figure 1.2) (Maggio et al., 2016; Ousterout et al., 2015; Young et al., 2016). Exon deletion strategies may also be used to correct exon duplication mutations, which occur in ~5% of DMD patients. A single sgRNA can be designed to target the intron region adjacent to the duplicated exon, and in the presence of Cas9, the single sgRNA will generate two cuts and delete one of the duplicated exons. Removal of one of the duplicated exons can renew the DMD ORF and produce full-length dystrophin protein, indistinguishable from normal dystrophin (Long et al., 2018).

Exon skipping

Skipping mutant exons leads to a shortened but semi-functional dystrophin protein, thereby transforming a severe DMD phenotype into the milder symptoms of BMD. In ~83% of DMD patients, the deletions in the dystrophin gene can be targeted by exon skipping strategies, permitting one or more exons to be excluded to restore the dystrophin ORF (Kole and Krieg, 2015). Anti-sense oligonucleotide (AON)-based exon skipping therapy for exon 51 has been approved by the US Food and Drug Administration (FDA) since 2016. However, AON-based exon skipping only modifies dystrophin mRNA, leaving the underlying mutation

still present in the dystrophin gene. Therefore, for AON-based therapy to be effective, the DMD patient must undergo lifelong biweekly administration of this drug. In contrast, CRISPR gene editing treatment would potentially be "one and done," as this technology corrects the underlying mutation in the genome.

Approaches used to correct DMD by CRISPR gene editing can be designed to minimize the loss of genomic DNA. Instead of using two sgRNAs flanking a mutant exon, one can design a single sgRNA to abolish either the splice acceptor site or splice donor site of the out-of-frame exon (Figure 1.2). Once the sgRNA has guided Cas9 to cut near the exon junction, the sequence encoding the exon splice acceptor or donor site will be destroyed by NHEJ, resulting in splicing to the next available exon and skipping the out-of-frame exon (Amoasii et al., 2017). Furthermore, a single-sgRNA approach for exon skipping also improves the editing efficiency in comparison to using two sgRNAs to flank the exon for removal.

Exon reframing

Another strategy to restore the dystrophin ORF is NHEJ-based reframing. When using a sgRNA to induce NHEJ in an out-of-frame exon, the generated indels lead to a targeted frameshift with a one-in-three possibility of putting the dystrophin gene back in frame (Figure 1.2). Several groups have demonstrated successful restoration of the dystrophin ORF through exon reframing (Bengtsson et al., 2017; Li et al., 2015; Maggio et al., 2016; Ousterout et al., 2015; Zhang et al., 2017). Since exon reframing generates small indels during the repair, this strategy is an effective approach to preserve maximal dystrophin genomic sequence while circumventing the DMD mutation.

Like exon skipping, exon reframing has the advantage of requiring only a single sgRNA. When using two sgRNAs, successful exon excision requires two DNA DSBs around the targeted exon(s), and these cuts need to occur simultaneously. In contrast, single-sgRNA-mediated NHEJ targets one intron–exon junction and requires only a single cut to restore the dystrophin ORF by either exon skipping or exon reframing.

Exon knock-in

All three strategies described above, using CRISPR gene editing to excise exons, result in a truncated form of dystrophin. In contrast, the exon knock-in strategy uses CRISPR-induced HDR, which incorporates a DNA donor template, resulting in restoration of full-length dystrophin protein (Figure 1.2). However, there is a limit to the length of the DNA donor template allowed by certain delivery approaches, making it problematic to apply this strategy to large deletion mutations of dystrophin. In addition, the efficiency of HDR is low in postmitotic cells. The HDR machinery is not readily available in G1-arrested cells, such as mature myofibers. To overcome this problem, a recently developed CRISPR/Cas9-based technology named homology-independent targeted integration (HITI) supports targeted gene insertion in nondividing cells (Suzuki et al., 2016). The HITI method precisely knocks in a missing exon(s) at a specific locus using NHEJ and bypasses the requirement of HDR.

Base editing

It is estimated that 25–35% of DMD patients have point mutations (Aartsma-Rus et al., 2006; Bladen et al., 2015). A newly developed strategy called base editing has been added to the CRISPR tool box to tackle DMD point mutations. These base editing tools can be divided into two categories: cytosine base editors that convert a C:G base pair to a T:A pair (Komor et

al., 2016; Nishida et al., 2016) and adenine base editors that convert a A:T pair to a G:C pair (Figure 1.3) (Gaudelli et al., 2017). These RNA-guided nucleotide-specific base editors, which consist of a cytidine deaminase or an engineered adenine deaminase fused with a Cas9 nickase (nCas9) or catalytically deficient Cas9 (dCas9), do not produce DNA DSBs like Cas9 and do not rely on the NHEJ repair pathway. A donor DNA template for HDR is not required, and small indels through error-prone NHEJ at the target site are not produced. Most recently, CRISPR/Cas9 adenine base editors were used to substitute a single adenine to guanine in a DMD mouse model that harbors an exon 20 nonsense mutation (Ryu et al., 2018). This strategy has been used to disrupt splicing acceptor sites (Gapinske et al., 2018) and can be used to disrupt premature stop codons for inducing exon skipping. This opens new therapeutic opportunities for DMD.

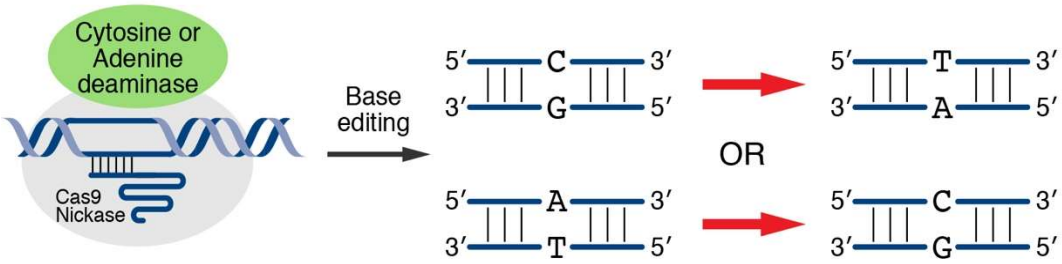

Figure 1.3. CRISPR/nCas9 attached with a cytosine or adenine deaminase carry out a C:G to T:A or A:T to C:G pair base substitution.

The alternatives

The CRISPR technology has evolved not only for gene editing but also for gene regulation. By using dCas9, a deactivated form of Cas9, fused to a transcriptional activator or a repressor, CRISPR technology can be applied to transcriptional upregulation or

downregulation (Chavez et al., 2015; Perez-Pinera et al., 2013). For example, dCas9 fused with VP160 was shown to boost utrophin expression as a compensatory therapy in DMD (Figure 1.3) (Wojtal et al., 2016). An advantage of this strategy is that it does not require a DNA DSB to regulate the target gene. However, prior to clinical use of this approach, maintenance and monitoring of the epigenetic state of the target must be ensured.

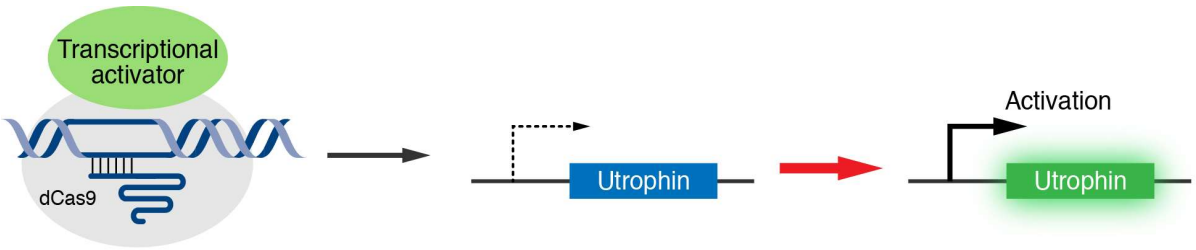

Figure 1.4 CRISPR/dCas9-mediated gene regulation. UTRN, a gene that codes for utrophin, a compensatory protein for dystrophin. UTRN can be upregulated by CRISPR/dCas9 fused with a transcriptional activator.

Delivery of CRISPR In Vivo

Effective in vivo postnatal genome editing requires an efficient delivery system. Genome editing components, Cas9 and sgRNA, can be delivered to target organs in various forms and by different systems. The forms of Cas9 and sgRNA can be DNA/DNA, mRNA/sgRNA, or protein/sgRNA, respectively. Viral and nonviral delivery systems are the CRISPR delivery systems commonly used in DMD.

Viral delivery

Lentivirus, adenovirus, and adeno-associated virus (AAV) have been used for delivery of CRISPR/Cas9 components. Among these viruses, AAV has the advantage of low immunogenicity, minimal integration risk, tissue tropism, little toxicity, and long-term

transgene expression from the episomal viral genome, making it a suitable viral vector for the delivery of gene editing components in patients with DMD (Wang et al., 2017). Indeed, the FDA has approved AAV for gene replacement therapy in spinal muscular atrophy, and clinical trials are in progress (Mendell et al., 2017).

AAV has a relatively small cargo capacity (<4.7 kb) compared to other viral vectors. The SpCas9 ORF is ~4.2 kb in length, which nears the maximum capacity of AAV cargo. This necessitates including an additional AAV vector harboring the sgRNA or the donor template. For example, a dual-AAV system has been shown to successfully edit hepatocytes and muscle cells in vivo (Yang et al., 2016). To circumvent the need for a dual-vector system, a smaller Cas9 protein such as SaCas9, which is encoded by a 3.2-kb cDNA, has been used for gene editing in mdx mouse strains (Bengtsson et al., 2017; Nelson et al., 2016; Tabebordbar et al., 2016).

AAV serotypes 1, 6, 8, 9, rh10, and rh74 have tropism for skeletal muscle and heart. Several studies have demonstrated successful delivery of CRISPR gene editing components using these AAV serotypes for postnatal genome editing (Lau and Suh, 2017; Wang et al., 2017). This approach can be modified to correct other monogenic neuromuscular disorders.

Nonviral delivery

Cas9 and sgRNAs, in various forms such as DNA, mRNA, or ribonucleoprotein (RNP), can be delivered in vivo using nonviral delivery systems. Electroporation delivers editing components by pulsing cells with high-voltage currents and creating nanometer-sized pores in the cell membrane. This allows negatively charged DNA or mRNA to enter the cells. This method has been used to deliver Cas9 and sgRNA constructs directly into skeletal muscle in

mdx mice, resulting in restoration of dystrophin expression (Xu et al., 2016). Lipid-mediated nanoparticle delivery is another delivery option to carry CRISPR components in the forms of RNP or mRNA/sgRNA into the cells (Miller Jason et al., 2016; Zuris et al., 2014). The cationic Cas9 protein is mixed with the highly anionic sgRNA to create a RNP complex that is highly anionic. This complex can be encapsulated by the cationic lipid nanoparticles and delivered into cells through endocytosis and macropinocytosis. Cationic lipid-based delivery is a relatively easy, low-cost process to deliver CRISPR components into cells. Furthermore, using RNPs as CRISPR components has been shown to reduce possible off-target mutations relative to nucleic acids (Kim et al., 2014). In addition to lipid-based nanoparticles, gold nanoparticles conjugated to DNA and complexed with cationic endosomal disruptive polymers have been reported to successfully deliver CRISPR RNP to correct the mutation in mdx mice (Lee et al., 2017). Therefore, CRISPR/Cas9 RNP and mRNA/sgRNA delivery could be a desirable method for further CRISPR/Cas9 applications in DMD therapy. However, given the requirement for body-wide delivery to muscles and the heart, major impracticalities remain to be overcome.

In this chapter (**Chapter One**), I introduced DMD and CRISPR gene editing, and provided a brief overview of several gene editing strategies for monogenic skeletal muscle disorders and delivery methods for gene editing components in skeletal and cardiac muscles. In **Chapter Two** I will describe an application of CRISPR/Cas9 gene editing in correction of exon 44 deletion, one of the most common causes of DMD. In Chapter Three I will focus on the creation of another three DMD mouse models, and the correction strategies for these models. In **Chapter Four** I will switch topics to describe the contribution of Tw2-derived cells

to adult cardiac regeneration and maintenance under homeostasis and injury conditions. In **Chapter Five** I will offer concluding remarks pertaining to my work in CRISPR gene editing to correct DMD.

CHAPTER TWO

CORRECTION OF DUCHENNE MUSCULAR DYSTROPHY EXON 44 DELETION MUTATIONS IN MICE AND HUMAN CELLS BY CRISPR/CAS9

Abstract

Mutations in the dystrophin gene cause Duchenne muscular dystrophy (DMD), which is characterized by lethal degeneration of cardiac and skeletal muscles. Mutations that delete exon 44 of the dystrophin gene represent one of the most common causes of DMD and can be corrected in ~12% of patients by editing surrounding exons, which restores the dystrophin open reading frame. Here I present a simple and efficient strategy for correction of exon 44 deletion mutations by CRISPR/Cas9 gene editing in cardiomyocytes obtained from patient-derived induced pluripotent stem cells and in a new mouse model harboring the same deletion mutation. Using AAV9 encoding Cas9 and single guide RNAs, I also demonstrate the importance of the dosages of these gene editing components for optimal gene correction in vivo. Our findings represent a significant step toward possible clinical application of gene editing for correction of DMD.

Introduction

Duchenne muscular dystrophy (DMD), caused by mutations in the dystrophin gene, is characterized by degeneration of cardiac and skeletal muscles, loss of ambulation and premature death (Hoffman et al., 1987). Dystrophin is a massive protein (>3,600 amino acids), which stabilizes muscle membranes by tethering the actin cytoskeleton to the inner surface of the sarcolemma (Ahn and Kunkel, 1993; Campbell and Kahl, 1989). Thousands of mutations that prevent dystrophin production have been identified in DMD patients (Bladen Catherine et al., 2015). These mutations cluster in hotspot regions of the gene that can, in principle, be bypassed by various exon skipping strategies to restore the dystrophin open reading frame (Echevarría et al., 2018). To date, however, there has been no effective long-term therapy for this disease and the only drug approved by the FDA for treatment of DMD allows for restoration of <1% of the normal level of dystrophin protein after extended treatment (Charleston et al., 2018). Thus, there remains a major unmet medical need for new strategies to correct the underlying cause of DMD – genetic mutations in the dystrophin gene.

A significant challenge in the development of DMD therapies has been the lack of animal models harboring the most common human mutations. Because the mouse and human dystrophin genes both contain 79 exons with highly conserved exon splicing patterns, results obtained in mouse models of the disease can be extrapolated to the human condition. One of the most common deletions in DMD patients eliminates exon 50 in the rod domain of dystrophin, which places exon 51 out of frame with preceding exons (Bladen et al., 2015; Flanigan et al., 2009; Guo et al., 2015; Takeshima et al., 2010; Vieitez et al., 2017). Our lab recently described the rescue of mice and dogs lacking exon 50 by injection of two adeno-

associated viruses of serotype 9 (AAV9) encoding CRISPR/Cas9 gene and sgRNAs that allow skipping or reframing of exon 51 and restoration of dystrophin expression (Amoasii et al., 2018; Amoasii et al., 2017).

The second most common mutational hotspot in the dystrophin gene includes exon 44, which disrupts the open reading frame in surrounding exons (Bladen et al., 2015; Flanigan et al., 2009; Takeshima et al., 2010; Vieitez et al., 2017). Here I describe the creation of a new mouse model of DMD with exon 44 deletion and we present two strategies for correction of this mutation by CRISPR/Cas9-mediated skipping of surrounding exons. These mice represent an important tool for testing and optimization of diverse therapies for DMD. I also show that sgRNAs, unexpectedly, are limiting for optimal gene editing in vivo and that editing efficiency can be enhanced ~10-fold by optimizing the dose of AAVs encoding Cas9 and sgRNAs. Our findings highlight the potential of gene editing to permanently eradicate mutations that cause DMD, thereby preventing the pathogenic sequelae of this disease.

Results

Correction of a DMD exon 44 deletion in patient-derived iPSCs

We generated patient-derived induced pluripotent stem cells (iPSCs) from a DMD patient lacking exon 44 of the dystrophin gene (*DMD*) and from the patient's brother with a normal dystrophin gene as a heathy control (Figure 2.1, panel A). Deletion of exon 44 (ΔEx44) disrupts the open reading frame of dystrophin by causing splicing of exon 43 to exon 45 and introducing a premature termination codon (Figure 2.1, panel B). The reading frame can be restored by using CRISPR/Cas9 gene editing to skip exon 43, which allows splicing between

exons 42 and 45, or to skip exon 45, which allows splicing between exons 43 and 46. Alternatively, reframing of exon 43 or 45 can restore the protein reading frame by inserting one nucleotide (+3n+1 insertion) or deleting two nucleotides (+3n-2 deletion).

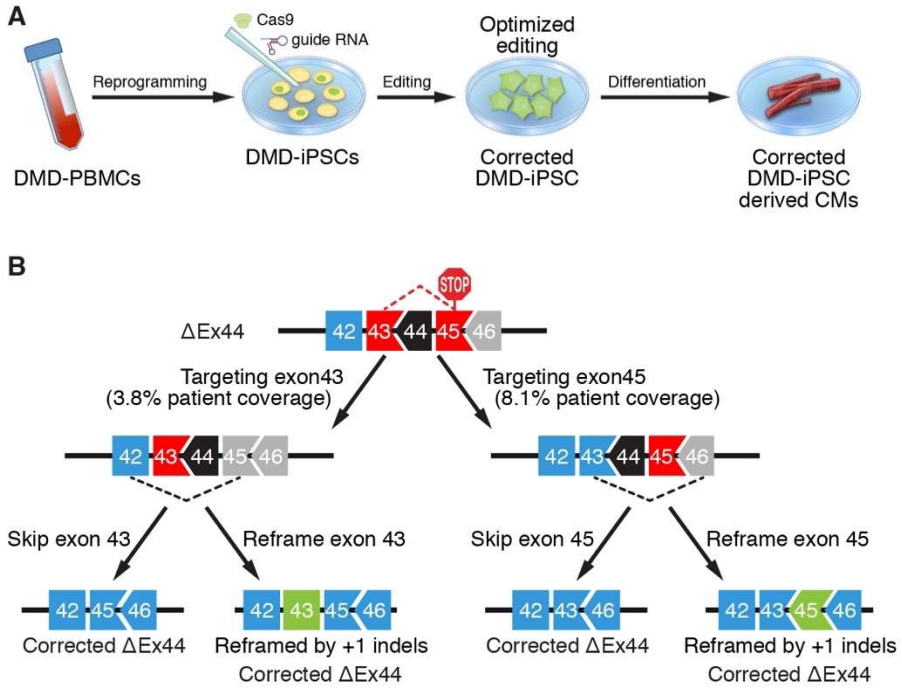

Figure 2.1 Exon 44-deleted DMD patient iPSC-derived cardiomyocytes express dystrophin after CRISPR/Cas9 mediated genome editing. (**A**) Schematic of the procedure for derivation and editing of DMD patient-derived iPSCs and iPSC-CMs. (**B**) Gene editing strategy for *DMD* exon 44 deletion. Deletion of exon 44 (black) results in splicing of exon 43 to 45, generating an out-of-frame stop mutation of dystrophin. Disruption of the splice junction of exon 43 or exon 45 results in splicing of exon 42 to 45 or exon 43 to 46, respectively, and restores the protein reading frame. The protein reading frame can also be restored by reframing exon 43 or 45 (green).

We selected sgRNAs that permit deletion of the splice acceptor or donor sites of exon 43 and 45 thereby allowing splicing between surrounding exons to recreate in-frame dystrophin. For editing exon 43, we designed four 20 nucleotides (nt) sgRNAs (G1, G2, G3

and G4) directed against sequences near the 5' and 3' boundaries of the splice junctions of exon 43 (Figure 2.2).

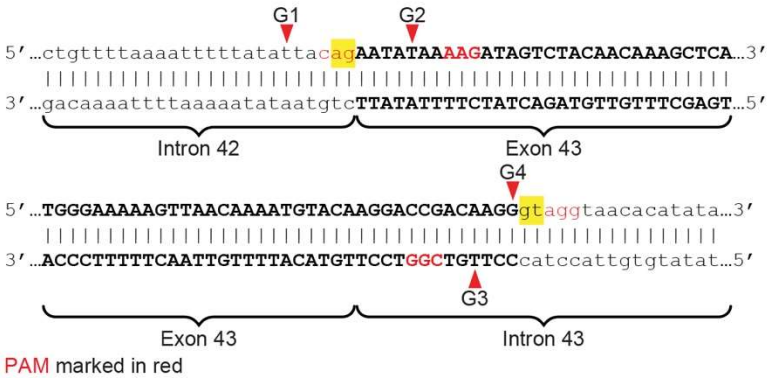

Figure 2.2 Sequence of sgRNAs targeting exon 43 splice acceptor and donor sites in the human *DMD* gene. The protospacer adjacent motif (PAM) (denoted as red nucleotides) of the sgRNAs is located near the exon 43 splice junctions. Exon sequence is bold upper case. Intron sequence is lower case. Arrowheads show sites of Cas9 DNA cutting with each sgRNA. Splice acceptor and donor sites are shaded in yellow.

For exon 45, we observed that the intron-exon junction of the splice acceptor site is contained within a 33-base pair (bp) region that is identical in the human and mouse genomes, allowing exon skipping strategies to be interchanged between the two species (Figure 2.3, panel A). We generated four 18-20nt sgRNAs (G5, G6, G7, and G8) to target the 5' boundary of exon 45, within the conserved region of the human and mouse genomes (Figure 2.3, panel B).

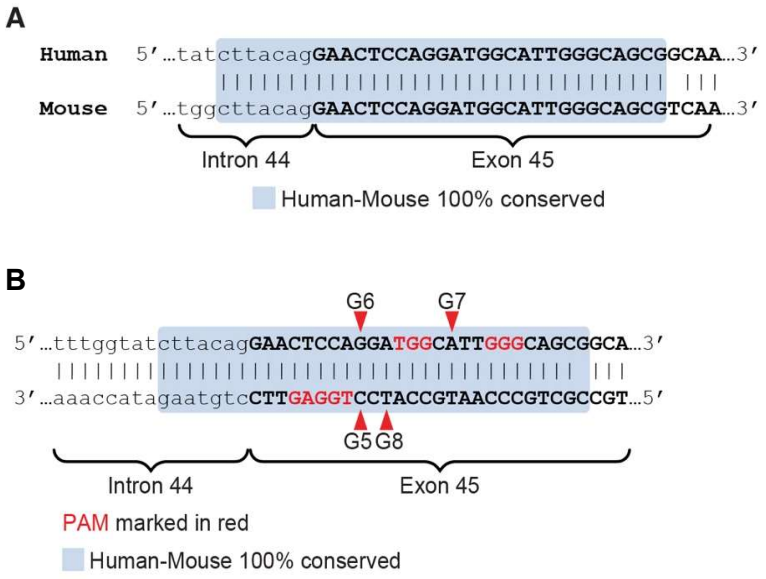

Figure 2.3 (A) Alignment of human and mouse DNA sequence at the intron-exon junction of exon 45. The conserved region is shaded in light blue. Exon sequence is in bold upper case and intron sequence is in lower case. (B) Sequence of sgRNAs targeting exon 45 splice acceptor site in the human *DMD* gene. The PAM (denoted as red nucleotides) of the sgRNAs is located near the exon 45 splice acceptor site. Human and mouse conserved sequence is shaded in light blue. Exon sequence is bold upper case. Intron sequence is lower case.

By the mismatch-specific T7 endonuclease I (T7E1) assay, we compared the sgRNAs for their ability to direct Cas9-mediated gene editing in human 293 cells (Figure 2.4, panel A). Two out of four sgRNAs for exon 43 efficiently edited the targeted region, and all four sgRNAs for exon 45 generated precise cuts at the conserved region (Figure 2.4, panel B). We concurrently tested the editing activity of the same four sgRNAs for exon 45 in mouse 10T½ cells and confirmed the effectiveness of the four sgRNAs in both the human and mouse genomes (Figure 2.4, panel B).

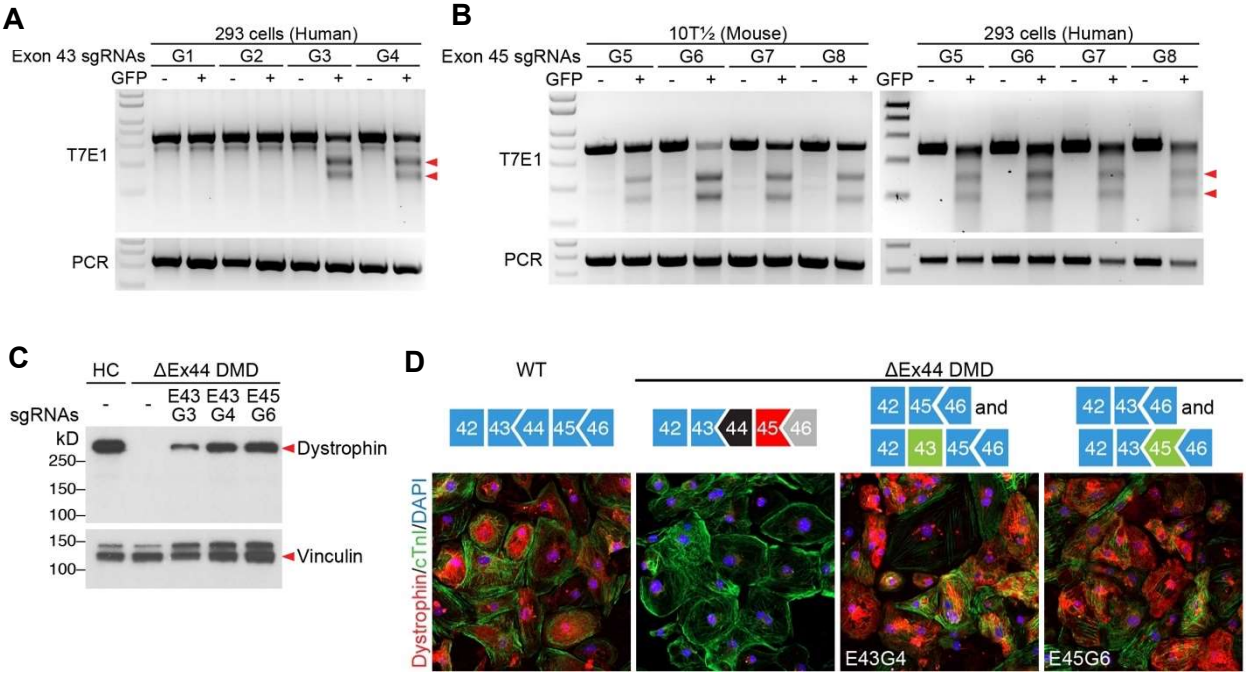

Figure 2.4 (A) T7E1 assay using human 293 cells transfected with plasmids that express SpCas9 and exon 43 sgRNA1 (G1), sgRNA2 (G2), sgRNA3 (G3) or sgRNA4 (G4) shows cleavage of the *DMD* locus at the intron-exon junctions of exon 43. Red arrowheads denote cleavage products. PCR indicates the undigested PCR product. (B) T7E1 assay using mouse 10T½ and human 293 cells transfected with plasmids that express SpCas9 and exon 45 sgRNA5 (G5), sgRNA6 (G6), sgRNA7 (G7) or sgRNA8 (G8) shows cleavage of the *Dmd* locus at the intron-exon junction of exon 45. Red arrowheads denote cleavage products. PCR indicates the undigested PCR product. (C) Western blot analysis shows restoration of dystrophin expression in exon 43-edited (E43) and exon 45-edited (E45) ΔEx44 patient iPSC-CMs with sgRNAs (G) 3, 4 and 6, as indicated. Vinculin is loading control. HC, iPSC-CMs from a healthy control. The second lane is unedited ΔEx44 patient iPSC-CMs. (D) Immunostaining shows restoration of dystrophin expression in exon 43-edited and exon 45-edited ΔEx44 patient iPSC-CMs. Dystrophin is shown in red. Cardiac troponin I is shown in green. Nuclei are marked by DAPI stain in blue.

sgRNAs with the highest gene editing activity based on T7E1 assays were then tested for the ability to efficiently edit the corresponding exons in patient-derived iPSCs lacking exon 44 (referred to as ΔEx44). A single plasmid encoding optimized sgRNAs (G3 or G4 for exon 43, or G6 for exon 45) and *Sp*Cas9 was introduced into ΔEx44 patient-derived iPSCs by electroporation, and the edited iPSCs were differentiated into cardiomyocytes (iPSC-CMs). Dystrophin expression was assessed by Western blot analysis and immunostaining, confirming restoration of dystrophin protein expression in edited ΔEx44 iPSC-CMs (Figure 2.4, panel C and D). Levels of dystrophin protein expression in ΔEx44 iPSC-CMs edited with sgRNAs G4 and G6 were approximately comparable to those seen in healthy control iPSC-CMs (Figure 2.4, panel C).

Due to the high efficiency of editing in the T7E1 assay and the complete conservation of sequence between human and mouse genomes, we chose to use sgRNA G6 to derive single clones of ΔEx44 iPSCs that were edited within exon 45. Thirty-four single clones were isolated and expanded. Sequence analysis of the clones showed exon skipping events in 3 out of 34 clones, and dystrophin reframing by either +3n+1 or +3n-2 in 13 out of 34 clones (Figure 2.5). Western blot analysis confirmed the restoration of dystrophin expression in three of the CRISPR/Cas9 corrected clones (Figure 2.6).

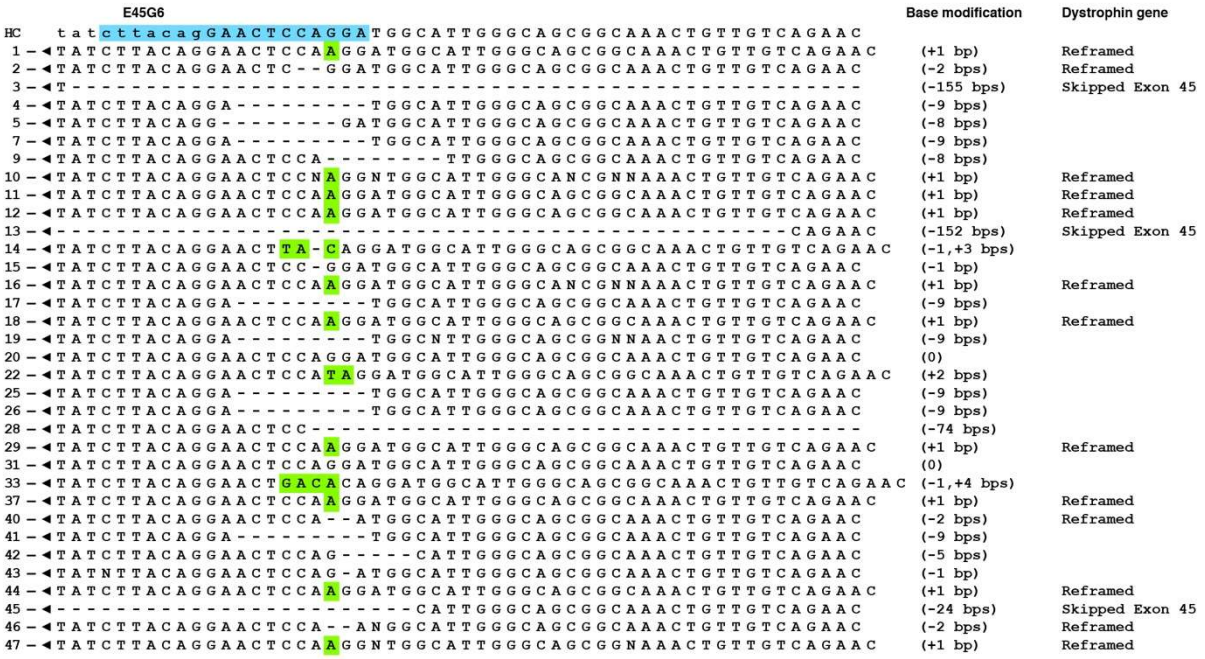

Figure 2.5 Sequences of the G6 edited 34 single clones. HC is sequence of the healthy human control. G6 sequence is shaded in blue. Insertions are shaded in green. Base modification and dystrophin gene status are listed on the right.

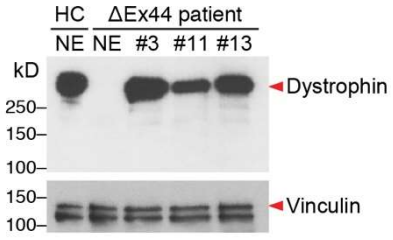

Figure 2.6 Western blot analysis showing restoration of dystrophin expression in three corrected single iPSC clones (clones #3, #11 and #13). HC, iPSC-CM from a healthy human control. NE, non-edited. Vinculin is loading control.

Generation of mice with a DMD exon 44 deletion

To optimize gene editing for correction of an exon 44 deletion in vivo, we generated a mouse model bearing an exon 44 deletion in the *Dmd* gene by CRISPR/Cas9 gene editing (Figure 2.7). We injected zygotes of C57BL/6 mice with two sgRNAs that target the introns flanking exon 44 and implanted the zygotes into surrogate female mice. An F0 founder with a 957 bp deletion that eliminated exon 44 was chosen for further studies. These ΔEx44 DMD mice contain one of the most common deletions responsible for DMD in humans. In principle, correction of exon 44 deletions by gene editing of surrounding exons could potentially restore the reading frame of dystrophin in ~12% of DMD patients.

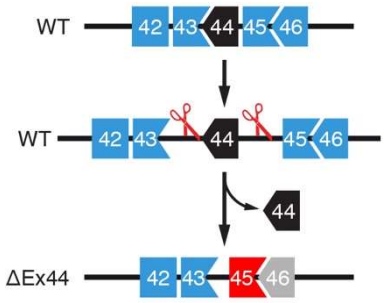

Figure 2.7 Generation of mice with a DMD exon 44 deletion. CRISPR/Cas9 editing strategy used for generation of exon 44 deleted mice (ΔEx44). Exon 45 (red) is out of frame with Exon 43.

Deletion of exon 44 was confirmed by RT-PCR analysis (Figure 2.8, panel A). Sequencing of the RT-PCR products using primers for sequences in exons 43 and 46 confirmed the removal of exon 44 in these mice (Figure 2.8, panel B). At 4 weeks of age, immunostaining of tibialis anterior (TA) muscle, diaphragm, and heart in the ΔEx44 DMD mice showed complete absence of dystrophin protein expression (Figure 2.9, panel A). Western blot analysis confirmed loss of dystrophin protein (Figure 2.9, panel B). Necrotic fibers, inflammatory infiltration, and regenerative fibers with centralized nuclei were observed in 4-week old ΔEx44

DMD mice, indicative of a severe muscular dystrophy phenotype (Figure 2.9, panel C). Serum creatine kinase levels in the ΔEx44 DMD mice were elevated 22-fold compared to WT littermates, similar to *mdx* mice, an established DMD mouse model (Figure 2.9, panel D).

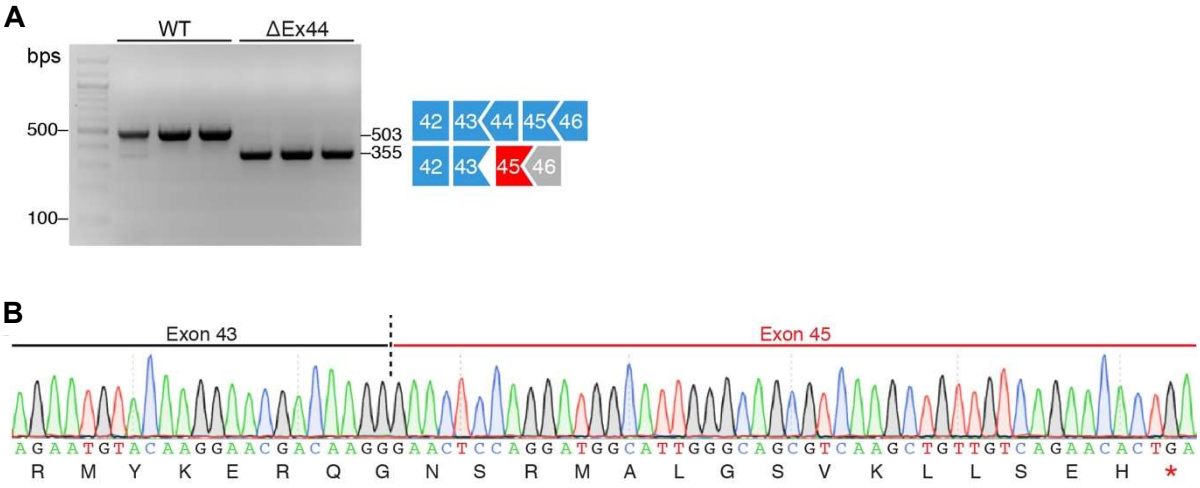

Figure 2.8 (A) RT-PCR analysis of TA muscles to validate deletion of exon 44. RT-PCR primers were in exons 43 and 46, and the amplicon size is 503 base pairs (bp) for WT mice and 355 bp for ΔEx44 DMD mice. RT-PCR products are schematized on the right. (n=3) (B) Sequencing of RT-PCR products from ΔEx44 DMD mouse muscle confirmed deletion of exon 44 and generation of a premature stop codon in exon 45, indicated by red asterisk.

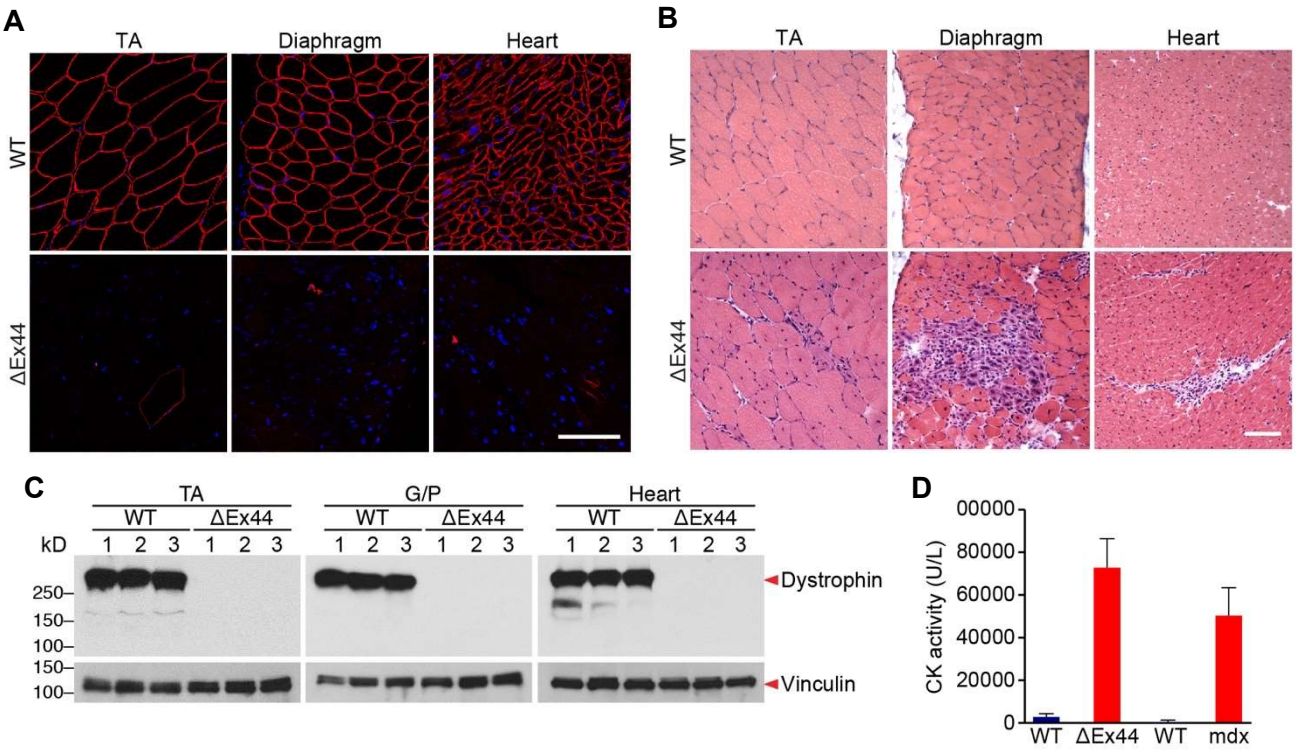

Figure 2.9 (A) Dystrophin staining of TA, diaphragm and heart of WT and ΔEx44 DMD mice. Dystrophin is shown in red. Nuclei are marked by DAPI stain in blue. (B) Western blot analysis shows loss of dystrophin expression in TA, gastrocnemius/plantaris (G/P) muscle, and heart of ΔEx44 mice. Vinculin is loading control. (n=3) (C) H&E staining of TA, diaphragm and heart. Note extensive inflammatory infiltrate and centralized myonuclei in ΔEx44 sections. (D) Serum creatine kinase (CK), a marker of muscle damage and membrane leakage, was measured in WT (C57BL/6 and C57BL/10), ΔEx44 and mdx mice.

Shear force generated during muscle contraction leads to muscle membrane tearing in muscle lacking dystrophin, eventually causing myofiber degeneration and muscle fibrosis (Allen et al., 2015). Fibrotic tissue increases muscle stiffness and compromises contractility of muscles. To further analyze muscle function of ΔEx44 DMD mice, we measured maximal tetanic force in the extensor digitorum longus (EDL) muscle *ex vivo*. Compared with WT

littermates at 4 weeks of age, ΔEx44 DMD mice showed an ~50% decrease in the specific and absolute tetanic force in the EDL muscle (Figure 2.10, panel A and B). A similar decrease of muscle strength was observed by grip strength analysis in 8-week old ΔEx44 DMD mice (Figure 2.10, panel C).

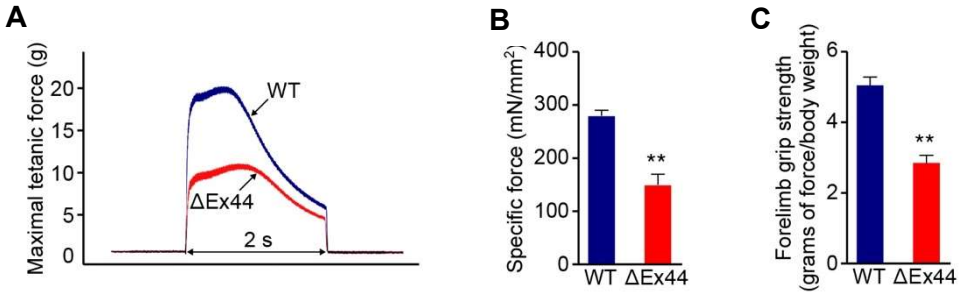

Figure 2.10 (A) Maximal tetanic force of EDL muscles in WT and ΔEx44 mice. (B) Specific force of EDL muscles in WT (blue) and ΔEx44 mice (red) (n=6) (C) Forelimb grip strength analysis of WT and ΔEx44 mice (n=4).

Correction of DMD exon 44 deletion in mice by intramuscular AAV9 delivery of gene editing components

To deliver *Sp*Cas9 and sgRNA in vivo, we utilized AAV9 to package the gene editing components. AAV9 is a single-stranded DNA virus that displays tropism to both skeletal muscle and heart and has been used in numerous clinical trials (Lau and Suh, 2017; Mendell et al., 2017; Wang et al., 2017; Zincarelli et al., 2008). To further achieve muscle-specific gene editing, we used the CK8e regulatory cassette that combines key elements of the enhancer and promoter regions of the muscle creatine kinase gene to drive *Sp*Cas9 expression in skeletal muscle and heart (Büning et al., 2008; Martari et al., 2009). For delivery of sgRNA, we used

three RNA polymerase III promoters (U6, H1, and 7SK) to express three copies of a sgRNA (Figure 2.11, panel A) (Schmidt et al., 2015a).

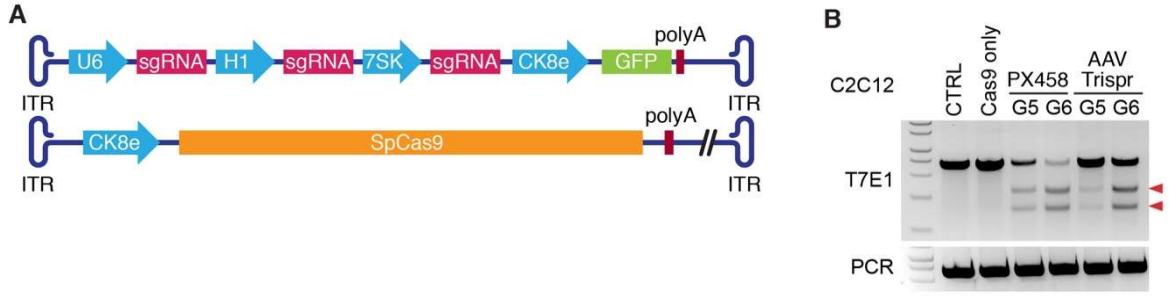

Figure 2.11 (A) Illustration of the AAV construct for CRISPR/Cas9 delivery. The muscle creatine kinase 8 (CK8e) regulatory cassette was used to express SpCas9 and GFP. The U6, H1, and 7SK RNA polymerase III promoters were used to express sgRNAs. ITR is inverted terminal repeats. (B) T7E1 assay shows cleavage of the Dmd locus at the intron-exon junction of exon 45 in mouse C2C12 cells with electroporation of G5 or G6 in PX458 or Trispr backbone. Red arrowheads show cleavage products of genome editing. PCR indicates the undigested PCR product.

We first compared the efficiency of gene editing with different expression constructs encoding Cas9 and sgRNAs. The PX458 plasmid encodes both editing components (Ran et al., 2013), whereas we used two AAV expression plasmids to express Cas9 and another to express three copies of the sgRNA that targeted exon 45 in mouse C2C12 muscle cells. By T7E1 assay, we observed comparable editing efficiency with both constructs (Figure 2.12, panel B). Among the two sgRNAs tested, G6 showed better cutting efficiency than G5, consistent with the observations in mouse 10T½ cells and human 293 cells (Figure 2.4, panel B).

To validate the efficacy of the single cut gene editing strategy in the ΔEx44 DMD mouse model, we performed localized intramuscular (IM) injection of AAV9 encoding *Sp*Cas9 (AAV-Cas9) and AAV9 encoding sgRNA (AAV-G5 or AAV-G6) in TA muscle of postnatal day 12 (P12) mice. As a control group, WT and ΔEx44 DMD mice were injected with AAV-Cas9 without AAV-sgRNA. In initial studies, 50 µl of AAV9 (1×10^{12} vg/ml) was injected per leg, containing equal amounts of AAV-Cas9 and AAV-G5 or AAV-G6. Three weeks after IM injection, we collected the TA muscles for analysis. In vivo gene editing by AAV-G5 and AAV-G6 was compared by the T7E1 assay and RT-PCR of the targeted region (Figure 2.12, panel A and B). Gene editing with AAV-G6 showed higher efficiency based on DNA cutting in vivo (Figure 2.12, panel B). RT-PCR with primers that amplify the region from exon 43 to exon 46 revealed deletion of exon 45 in TA muscle injected with AAV-Cas9 and AAV-G6 (Figure 2.12, panel A). This allows exon 43 to skip exon 45 and directly splice to exon 46 when processing the pre-mRNA. As a result, the alternate mRNA enables the production of a truncated dystrophin protein in corrected TA muscle of ΔEx44 DMD mice.

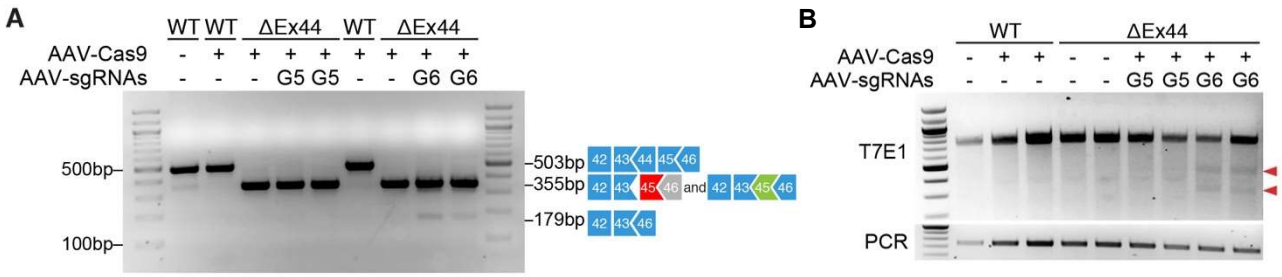

Figure 2.12 Correction of *Dmd* exon 44 deletion in mice by intramuscular AAV9 delivery of gene editing components. (A) RT-PCR analysis of TA muscles from WT and ΔEx44 mice 3 weeks after intramuscular injection of gene editing components carried by AAV9. Lower dystrophin bands (179 bp) indicate skipping of exon 45. (B) T7E1 assay shows cleavage of the *Dmd* locus at the intron-exon junction of exon 45 in TA muscle

of corrected ΔEx44 mice. Red arrowheads show cleavage products of genome editing. PCR indicates the undigested PCR product.

To further evaluate the mutations generated by gene editing, we performed topoisomerase-based thymidine to adenosine (TOPO-TA) cloning using the RT-PCR amplification products and sequenced the cDNA products. Sequencing results demonstrated that 7% of sequenced clones represented exon 45-skipped cDNA products, and 42% of sequenced clones contained a single adenosine (A) insertion in exon 45 that resulted in reframing of dystrophin protein (Figure 2.13, panel A and B). The predominance of reframing explains the high abundance of the RT-PCR band at 355 bp and the lower abundance of the smaller RT-PCR product of 179 bp that reflects exon skipping (Figure 2.12, panel A).

Figure 2.13 (A) Percentage of events detected at exon 45 after AAV-Cas9 and AAV-G6 treatment using RT-PCR sequence analysis of TOPO-TA (topoisomerase-based thymidine to adenosine) generated clones. RT-PCR products were divided into four groups: Not edited (NE), exon 45–skipped (SK), reframed (RF), and out of frame (OF) are indicated. (B) Sequences of RT-PCR products of WT, ΔEx44 and corrected ΔEx44 mice. In-frame sequences are shown in blue, including WT and exon 45-skipped sequences. Reframed sequence is shown in green, and out of frame sequence is shown in red.

Genomic and cDNA amplicon deep sequencing on the target region of the TA muscles with AAV-G6 IM injection also confirmed that 9.8% of mutations at the genomic level and 35.7% of mutations at the mRNA level contain a single A insertion at the cutting site after gene editing with AAV-G6 (Figure 2.14, panel A and B). This single A insertion leads to reframing of exon 45 and restores the dystrophin protein reading frame. We also observed minor AAV ITR integration events at the cutting site, with a frequency of 0.21% at the genomic level (Figure 2.14, panel A), and 1.15% at the mRNA level (Figure 2.14, panel B).

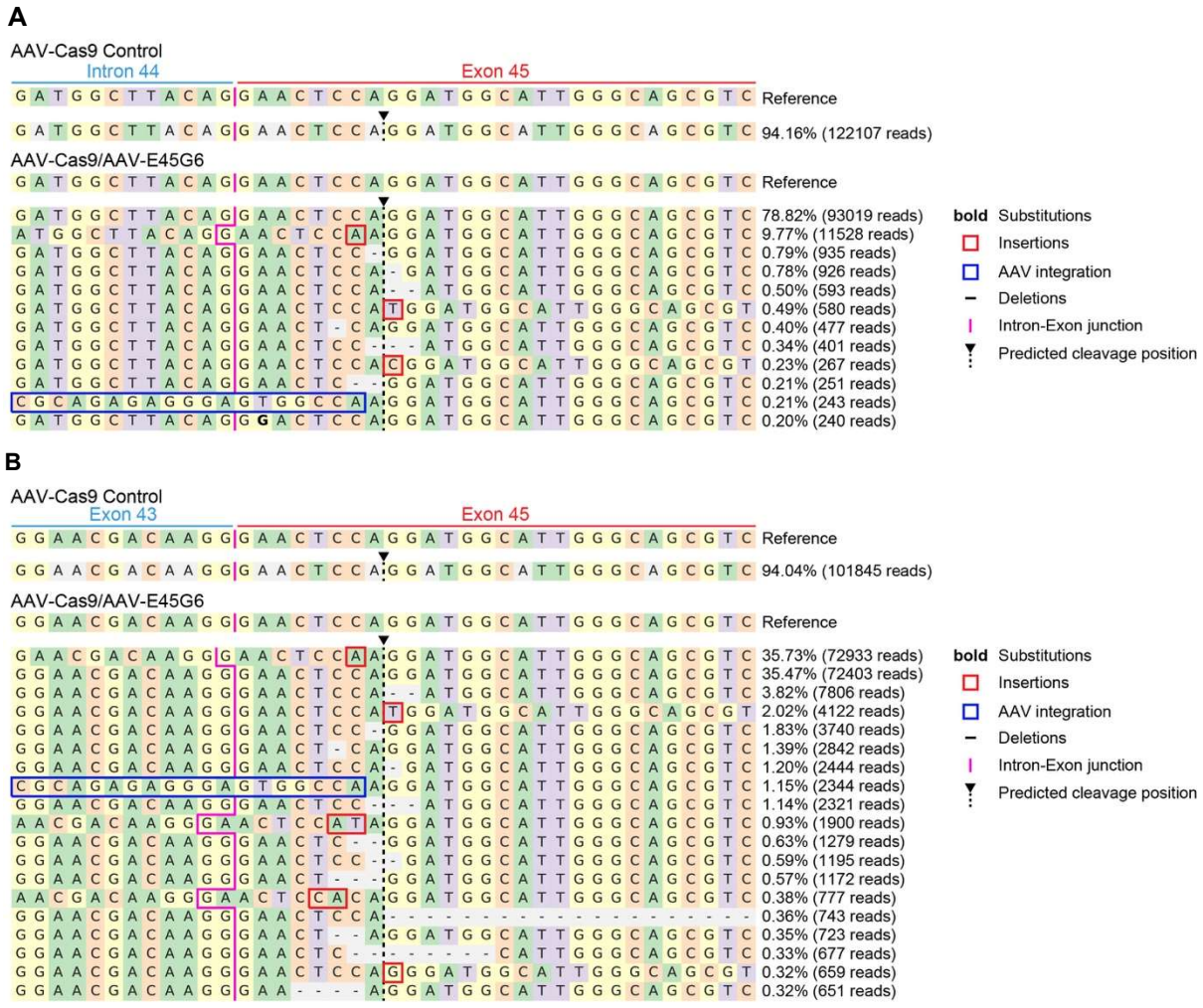

Figure 2.14 On-target (A) genomic and (B) cDNA amplicon deep sequencing of ΔEx44 DMD, and corrected ΔEx44 DMD mice after 3 weeks of AAV-Cas9 and AAV-G6 intramuscular injection (2.5×10^{10} vg of AAV9-Cas9 and 2.5×10^{10} vg of AAV-G6). Bold represents substitutions, red square is insertions, "-" is deletion. Vertical pink line indicates intron-exon junction in (A) and exon-exon junction in (B). Black arrowhead points to dotted vertical line representing the predicted cleavage site.

To evaluate dystrophin protein restoration after IM injection with AAV-Cas9 and AAV-G5 or AAV-G6, we performed Western blot analysis on TA muscle and the heart (Figure 2.15, panel A). We observed restoration of dystrophin protein expression to 74% of the WT level in edited TA muscles of ΔEx44 DMD mice (Figure 2.15, panel B). Interestingly, although the injection was localized to the TA muscle, we observed expression of dystrophin in the heart at 21% of WT level (Figure 2.15, panel A). This suggests leakage of AAV into the circulation and delivery of the gene editing components to the heart.

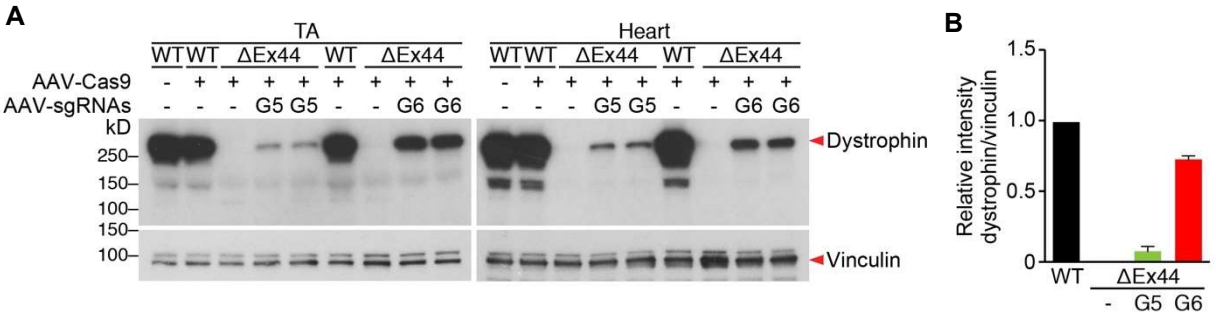

Figure 2.15 (A) Western blot analysis shows restoration of dystrophin expression in TA muscle and heart of ΔEx44 mice. Vinculin is loading control. (**B**) Quantification of the Western blot analysis in TA muscle. Relative dystrophin intensity was calibrated with vinculin internal control.

Immunostaining showed that dystrophin protein expression was restored in 99% of the myofibers in TA muscle injected with AAV-Cas9 and AAV-G6 (Figure 2.16, panel A and B). Histological analysis and hematoxylin and eosin (H&E) staining showed a pronounced reduction in fibrosis, necrotic myofibers and regenerating fibers with central nuclei, indicating amelioration of the abnormalities associated with muscular dystrophy in the TA muscle 3 weeks after AAV9-Cas9 and AAV-G6 injection (Figure 2.16, panel C).

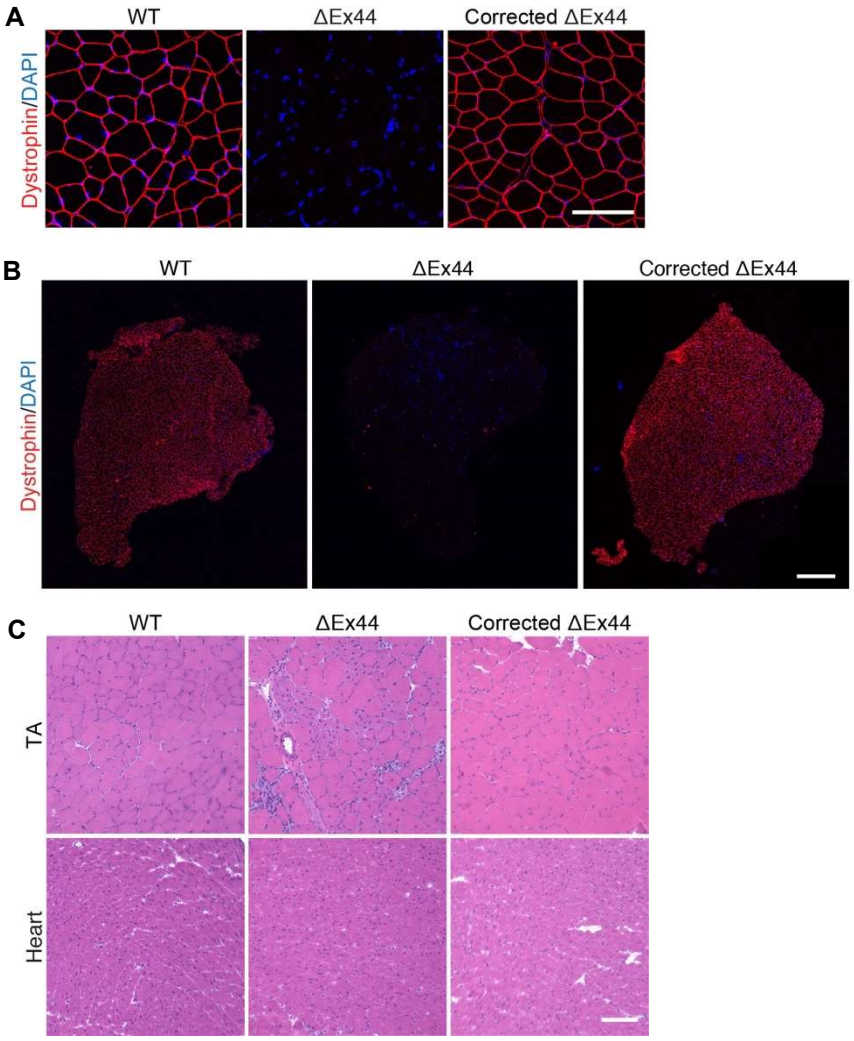

Figure 2.16 (A) Immunostaining shows restoration of dystrophin in TA muscle of ΔEx44 mice 3 weeks after intramuscular injection of gene editing components carried by AAV9. Dystrophin is shown in red. Nuclei are marked by DAPI stain in blue. (B) Dystrophin immunostaining of TA muscle in WT, ΔEx44 DMD, and corrected ΔEx44 DMD mice after 3 weeks of AAV-Cas9 and AAV-G6 intramuscular injection (2.5×10^{10} vg of AAV9-Cas9 and 2.5×10^{10} vg of AAV-G6). Dystrophin is shown in red. Nuclei are marked by DAPI stain in blue. 10X tile scan of the entire TA muscle. Scale bar is 500 µm. (**C**) H&E staining of TA and heart in WT, ΔEx44, and corrected ΔEx44 mice (n=3).

Based on CRISPR design tools (http://crispr.mit.edu/ and https://benchling.com/), we determined the top 10 potential off-target sites and, based on sequencing analysis, we did not detect off-target effects at these sites (Figure 2.17). T7E1 analysis confirmed the absence of off-target cutting in the top 10 potential off-target sites, and DNA sequencing of the isolated genomic PCR amplification products spanning the potential off-target sites confirmed the absence of sgRNA/Cas9-mediated mutations at the predicted sites (Figure 2.17, panel A). In addition, we performed genomic amplicon deep sequencing of the top 10 predicted off-target sites within protein-coding exons. None of these sites showed significant sequence alterations (Figure 2.17, panel B and Table 2.1).

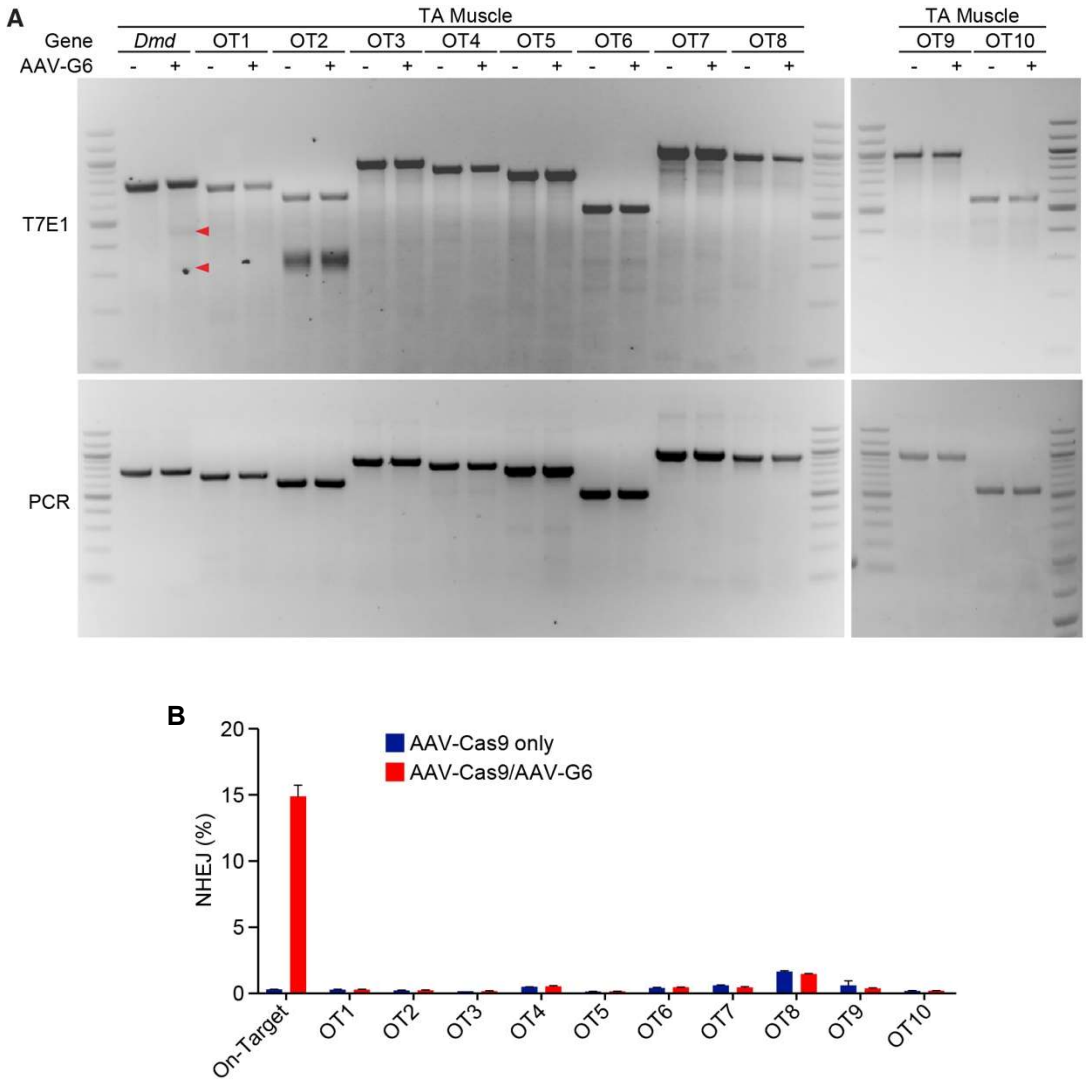

Figure 2.17 (A) Analysis of top ten potential off-target sites. (A) T7E1 analysis of the top 10 predicted off-target (OT) sites of sgRNA-G6 assayed in TA muscle 3 weeks following intramuscular injection of 2.5×10^{10} vg AAV9-Cas9 and 2.5×10^{10} vg AAV-G6. Red arrowheads denote on-target cleavage products. No off-target cleavage products were detected. PCR indicates the undigested PCR product. (B) Percentage of NHEJ in amplicon genomic deep sequencing analysis on the top 10 predicted off-target sites of G6. Blue indicates AAV-Cas9 only control, and red indicates AAV-Cas9/AAV-G6 injected TA muscle.

Selected OT site	Sequence	PAM	Gene	Chromosome	Samples	Total Reads	Unmodified	NHEJ	NHEJ%	AVG
E45G6 On-target	CTTACAGGAACTCCAGGA	TGG	ENSMUSG00000045103	chrX	Δ44-AAV-Cas9 control-1	129677	129273	404	0.31%	0.31%
					Δ44-AAV-Cas9 control-2	118099	117724	375	0.32%	
					Δ44-AAV-Cas9.AAV-E45G6-1	118011	99440	18571	15.74%	14.89%
					Δ44-AAV-Cas9.AAV-E45G6-2	79958	68732	11226	14.04%	
E45G6 OT1	CTCACAGAAACTCCAGGA	AAG	ENSMUSG00000018168	chr11	Δ44-AAV-Cas9 control-1	148291	147900	391	0.26%	0.30%
					Δ44-AAV-Cas9 control-2	140851	140391	460	0.33%	
					Δ44-AAV-Cas9.AAV-E45G6-1	146193	145718	475	0.32%	0.29%
					Δ44-AAV-Cas9.AAV-E45G6-2	141836	141485	351	0.25%	
E45G6 OT2	TTGACAGGAACTCCAGGA	AAG	ENSMUSG00000087615	chr17	Δ44-AAV-Cas9 control-1	195414	195077	337	0.17%	0.21%
					Δ44-AAV-Cas9 control-2	164408	164011	397	0.24%	
					Δ44-AAV-Cas9.AAV-E45G6-1	163644	163237	407	0.25%	0.22%
					Δ44-AAV-Cas9.AAV-E45G6-2	224318	223898	420	0.19%	
E45G6 OT3	CTTCCAGGAACTCCAGCA	CAG	ENSMUSG00000024087	chr17	Δ44-AAV-Cas9 control-1	118944	118753	191	0.16%	0.16%
					Δ44-AAV-Cas9 control-2	137789	137573	216	0.16%	
					Δ44-AAV-Cas9.AAV-E45G6-1	115015	114797	218	0.19%	0.16%
					Δ44-AAV-Cas9.AAV-E45G6-2	115647	115493	154	0.13%	
E45G6 OT4	CTTATAGGAATTCCAGGA	AGG	ENSMUSG00000001123	chr11	Δ44-AAV-Cas9 control-1	112923	112346	577	0.51%	0.50%
					Δ44-AAV-Cas9 control-2	80286	79896	390	0.49%	
					Δ44-AAV-Cas9.AAV-E45G6-1	72867	72514	353	0.48%	0.54%
					Δ44-AAV-Cas9.AAV-E45G6-2	102712	102102	610	0.59%	
E45G6 OT5	GTGACATGAACTCCAGGA	AAG	ENSMUSG00000097736	chr9	Δ44-AAV-Cas9 control-1	132220	132032	188	0.14%	0.15%
					Δ44-AAV-Cas9 control-2	100491	100341	150	0.15%	
					Δ44-AAV-Cas9.AAV-E45G6-1	111366	111173	193	0.17%	0.16%
					Δ44-AAV-Cas9.AAV-E45G6-2	114976	114805	171	0.15%	
E45G6 OT6	TTTCCAGGAATTCCAGGA	AGG	ENSMUSG00000026835	chr2	Δ44-AAV-Cas9 control-1	95824	95395	429	0.45%	0.42%
					Δ44-AAV-Cas9 control-2	103709	103292	417	0.40%	
					Δ44-AAV-Cas9.AAV-E45G6-1	112059	111548	511	0.46%	0.47%
					Δ44-AAV-Cas9.AAV-E45G6-2	128665	128037	628	0.49%	
E45G6 OT7	CTCACCGGAACTCCAGGA	GGG	ENSMUSG00000025650	chr9	Δ44-AAV-Cas9 control-1	131416	130646	770	0.59%	0.61%
					Δ44-AAV-Cas9 control-2	122440	121656	784	0.64%	
					Δ44-AAV-Cas9.AAV-E45G6-1	122052	121559	493	0.40%	0.47%
					Δ44-AAV-Cas9.AAV-E45G6-2	134661	133948	713	0.53%	
E45G6 OT8	ATGACAGAAACTCCAGGA	AAG	ENSMUSG00000056952	chr6	Δ44-AAV-Cas9 control-1	87995	86485	1510	1.72%	1.65%
					Δ44-AAV-Cas9 control-2	130159	128107	2052	1.58%	
					Δ44-AAV-Cas9.AAV-E45G6-1	136626	134574	2052	1.50%	1.48%
					Δ44-AAV-Cas9.AAV-E45G6-2	121227	119468	1759	1.45%	
E45G6 OT9	CTACCAGGAACTCCAGGC	TGG	ENSMUSG00000021275	chr12	Δ44-AAV-Cas9 control-1	123165	122861	304	0.25%	0.60%
					Δ44-AAV-Cas9 control-2	116857	115745	1112	0.95%	
					Δ44-AAV-Cas9.AAV-E45G6-1	135673	135192	481	0.35%	0.39%
					Δ44-AAV-Cas9.AAV-E45G6-2	134603	134030	573	0.43%	
E45G6 OT10	CTTTCAGAGACTCCAGGA	CAG	ENSMUSG00000034731	chr14	Δ44-AAV-Cas9 control-1	89824	89681	143	0.16%	0.19%
					Δ44-AAV-Cas9 control-2	94091	93884	207	0.22%	
					Δ44-AAV-Cas9.AAV-E45G6-1	80995	80807	188	0.23%	0.22%
					Δ44-AAV-Cas9.AAV-E45G6-2	100775	100570	205	0.20%	

Table 2.1 Amplicon genomic deep sequencing analysis on the top 10 predicted off-target sites of G6. Muscle was analyzed 3 weeks following intramuscular injection of 2.5×10^{10} vg AAV9-Cas9 and 2.5×10^{10} vg AAV-G6. Mismatches in the target sequence are highlighted in red.

Systemic delivery of AAV9 expressing gene editing components rescues dystrophin expression in ΔEx44 mice.

To achieve body-wide rescue of the disease phenotype in ΔEx44 DMD mice, we delivered AAV-Cas9 and AAV-G6 systemically through intraperitoneal (IP) injection. AAV-Cas9 was injected at a dosage of 5×10^{13} vg/kg. Multiple ratios of AAV-G6 to AAV-Cas9 were tested to determine whether there might be an optimal ratio of the viruses for maximal systemic editing efficiency. Four weeks after injection, we assessed dystrophin protein expression in several muscle tissues, including TA muscle of the hindlimb, triceps of the forelimb, diaphragm, and cardiac muscle. By immunostaining, we observed dystrophin expression in 94%, 90% and 95% of myofibers in the TA, triceps, and diaphragm, respectively, and in 94% of cardiomyocytes when ΔEx44 mice were injected with a 1:10 ratio of AAV-Cas9:AAV-G6 (5×10^{13} vg/kg of AAV-Cas9 and 5×10^{14} vg/kg of AAV-G6) (Figure 2.18, panel A and B). The restoration of dystrophin protein in skeletal muscles correlated with the dosage of AAV-G6 delivered through IP injection. In contrast, in the heart, dystrophin positive cardiomyocytes were seen at a low dosage of AAV-G6 and remained consistent at higher dosages. Western blot analysis of the same muscle groups after systemic delivery showed similar trends of dystrophin correction (Fig. 2.19 and Fig 2.20). At every ratio of AAV-Cas9:AAV-G6 tested by systemic delivery, cardiac muscle showed higher dystrophin restoration than skeletal muscle. Correction of cardiac muscle reached 82% when injected at a 1:1 ratio of AAV-Cas9:AAV-G6 and increased an additional 12% at a 1:10 ratio. In contrast, we observed an increase of dystrophin-expressing myofibers from 10% to 94% when the sgRNA was increased. H&E staining showed that histopathologic hallmarks of muscular

dystrophy, such as necrotic myofibers and regenerated fibers with central nuclei, were diminished in the TA, diaphragm, and triceps muscles at 4 weeks after AAV-Cas9/AAV-G6 delivery (Figure 2.21 and Figure 2.22).

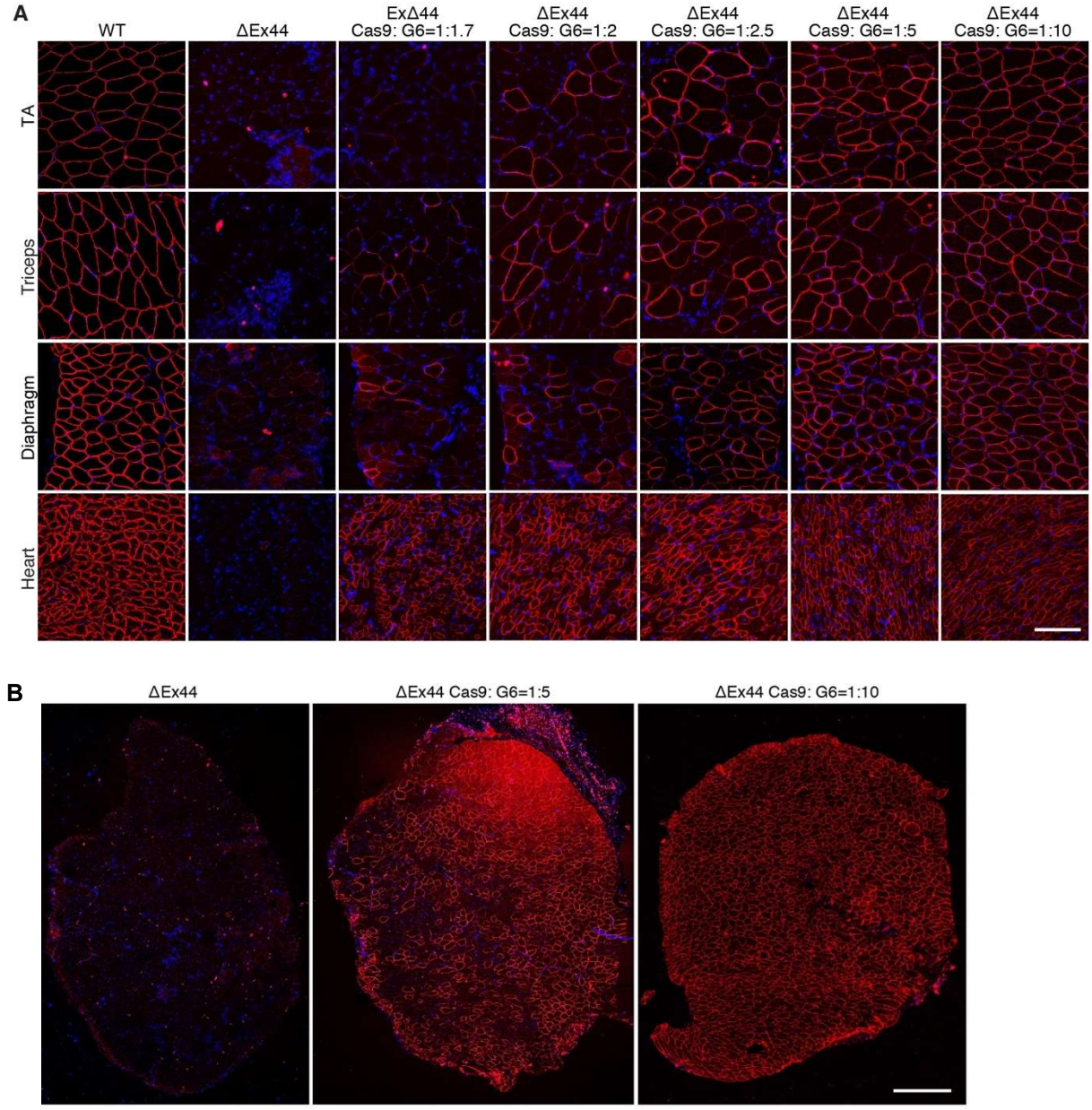

Figure 2.18 Systemic AAV9 delivery of gene editing components to ΔEx44 mice rescues dystrophin expression. (A) Immunostaining shows restoration of dystrophin in TA, triceps, diaphragm, and heart of ΔEx44 mice 4 weeks

after systemic delivery of AAV-Cas9 and AAV-G6 at the indicated ratios. Dystrophin is shown in red. Nuclei are marked by DAPI stain in blue. (B) Whole TA muscle scanning of ΔEx44 DMD and corrected ΔEx44 DMD 4 weeks after systemic injection of a 1:5 ratio and 1:10 ratio of AAV-Cas9 to AAV-G6. AAV-Cas9 was administered at 5×10^{13} vg/kg. Dystrophin is shown in red. Nuclei are marked by DAPI stain in blue. 10X tile scan of the entire TA muscle. Scale bar is 500 μm.

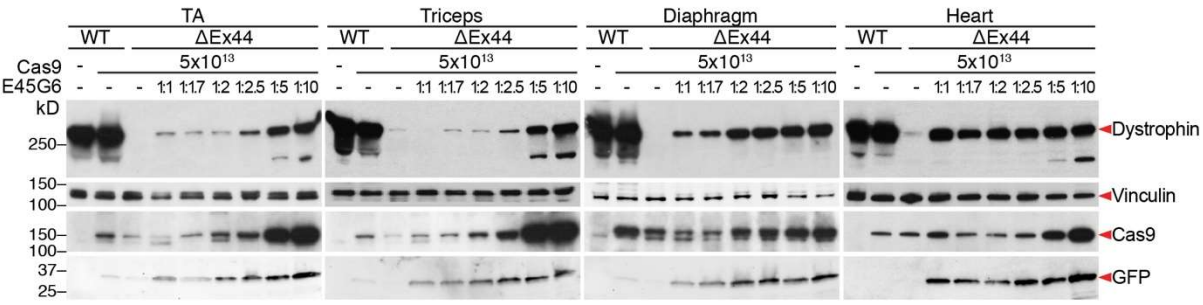

Figure 2.19 Western blot analysis shows restoration of dystrophin expression in TA, triceps, diaphragm, and heart of ΔEx44 mice 4 weeks after systemic delivery of AAV-Cas9 and AAV-G6 at the indicated ratios. Vinculin is loading control. (n= 4)

To further assess systemic delivery of AAV-Cas9 in the presence of different amounts of AAV-G6, we performed Western blot analysis to evaluate the amount of Cas9 protein expressed in the muscles. Although we kept the total AAV-Cas9 dosage constant (5×10^{13} vg/kg), the mice that received higher doses of AAV-G6 showed greater expression of Cas9 protein in corrected muscles (Figure 2.19 and Figure 2.20).

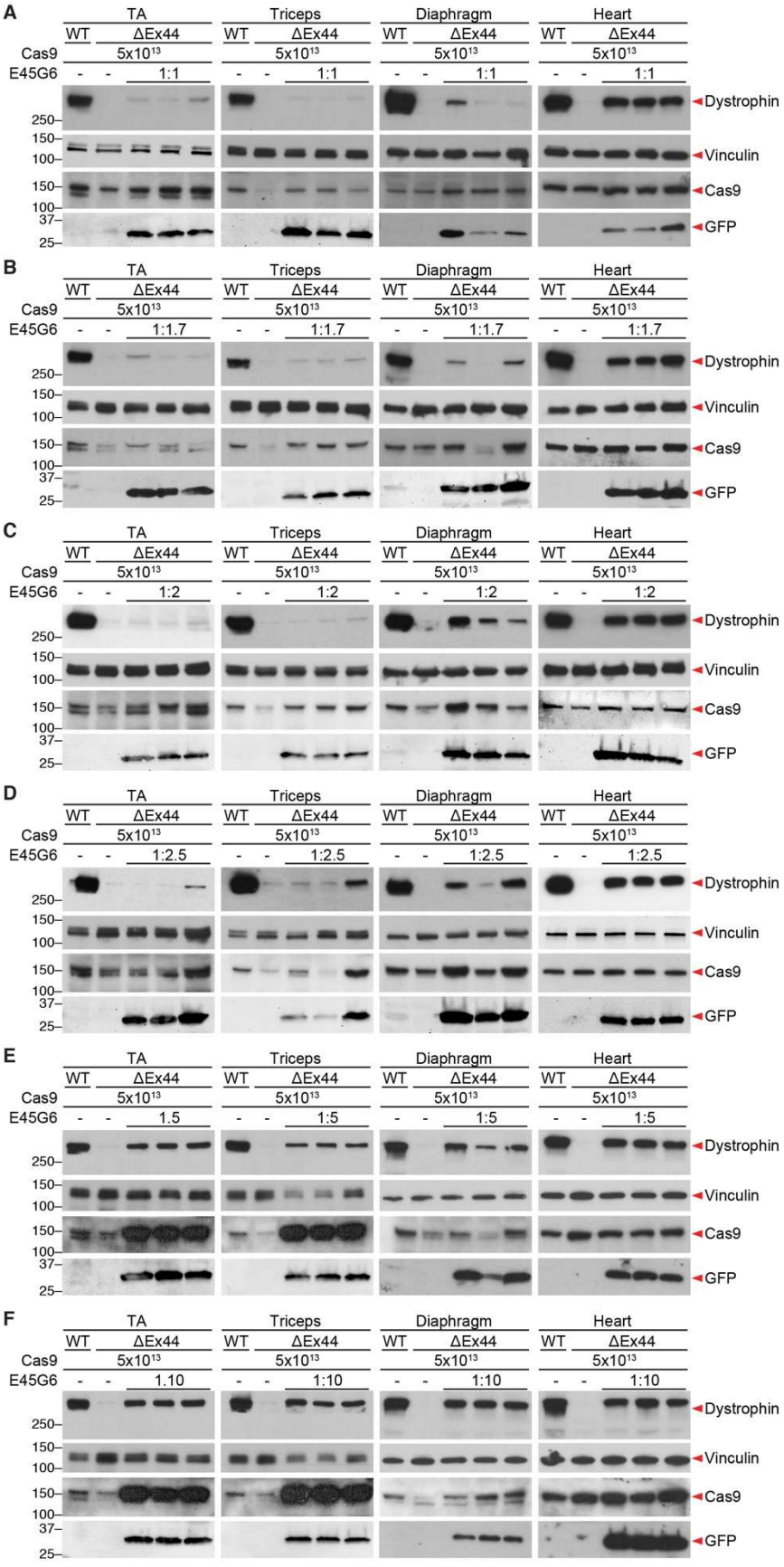
A
TA
Triceps
Diaphragm
Heart
WT
ΔEx44
Cas9
5x10^13
E45G6
1:1
B
1:1.7
C
1:2
D
1:2.5
E
1:5
F
1:10
250–
150–
100–
37–
25–
Dystrophin
Vinculin
Cas9
GFP

Figure 2.20 Western blot analysis of corrected ΔEx44 mice by systemic delivery of AAV9 expressing gene editing components. (A)–(F) Western blot analysis of dystrophin, Cas9, and GFP protein expression in TA, triceps, diaphragm, and heart of ΔEx44 mice 4 weeks after systemic delivery of AAV-Cas9 and AAV-G6 at the indicated ratios. AAV-Cas9 was administered at 5×10^{13} vg/kg. Vinculin is loading control. (n= 3)

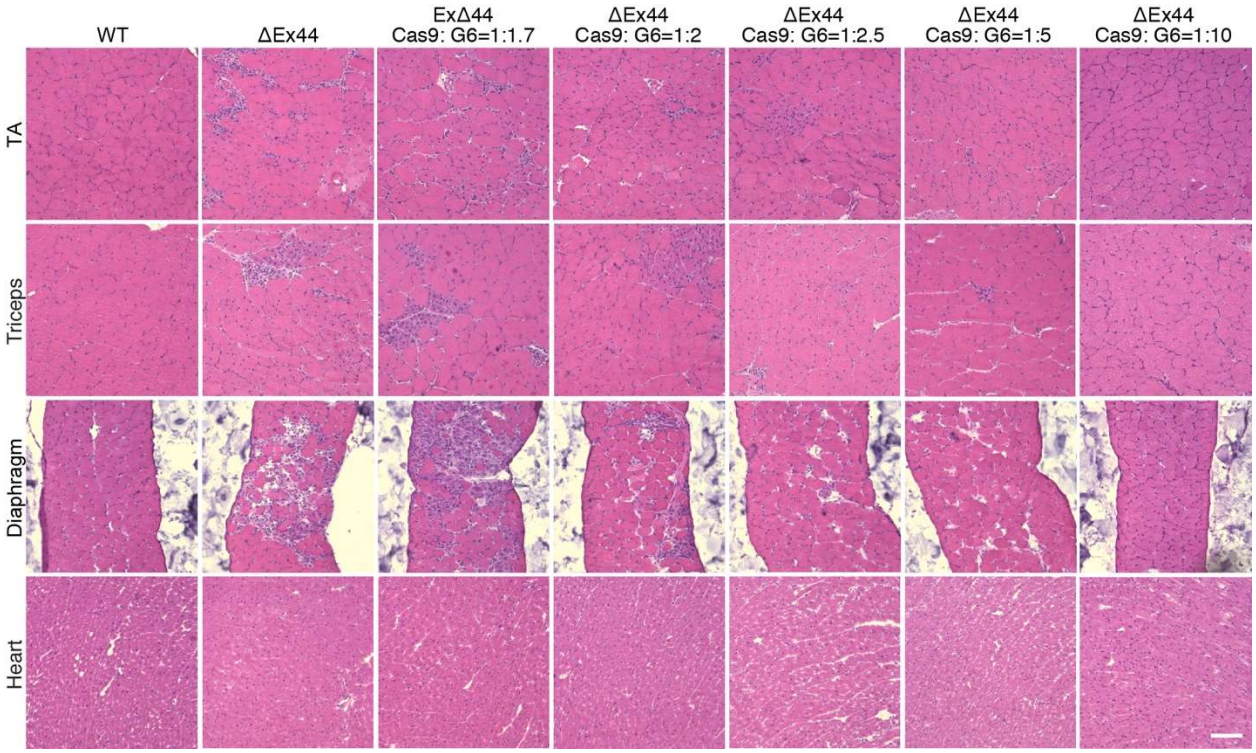

Figure 2.21 Histology of ΔEx44 mice after systemic delivery of AAV9 expressing gene editing components H&E staining of TA, triceps, diaphragm and heart of ΔEx44 mice 4 weeks after systemic delivery of AAV-Cas9 and AAV-G6 at the indicated ratios. AAV-Cas9 was administered at 5×10^{13} vg/kg.

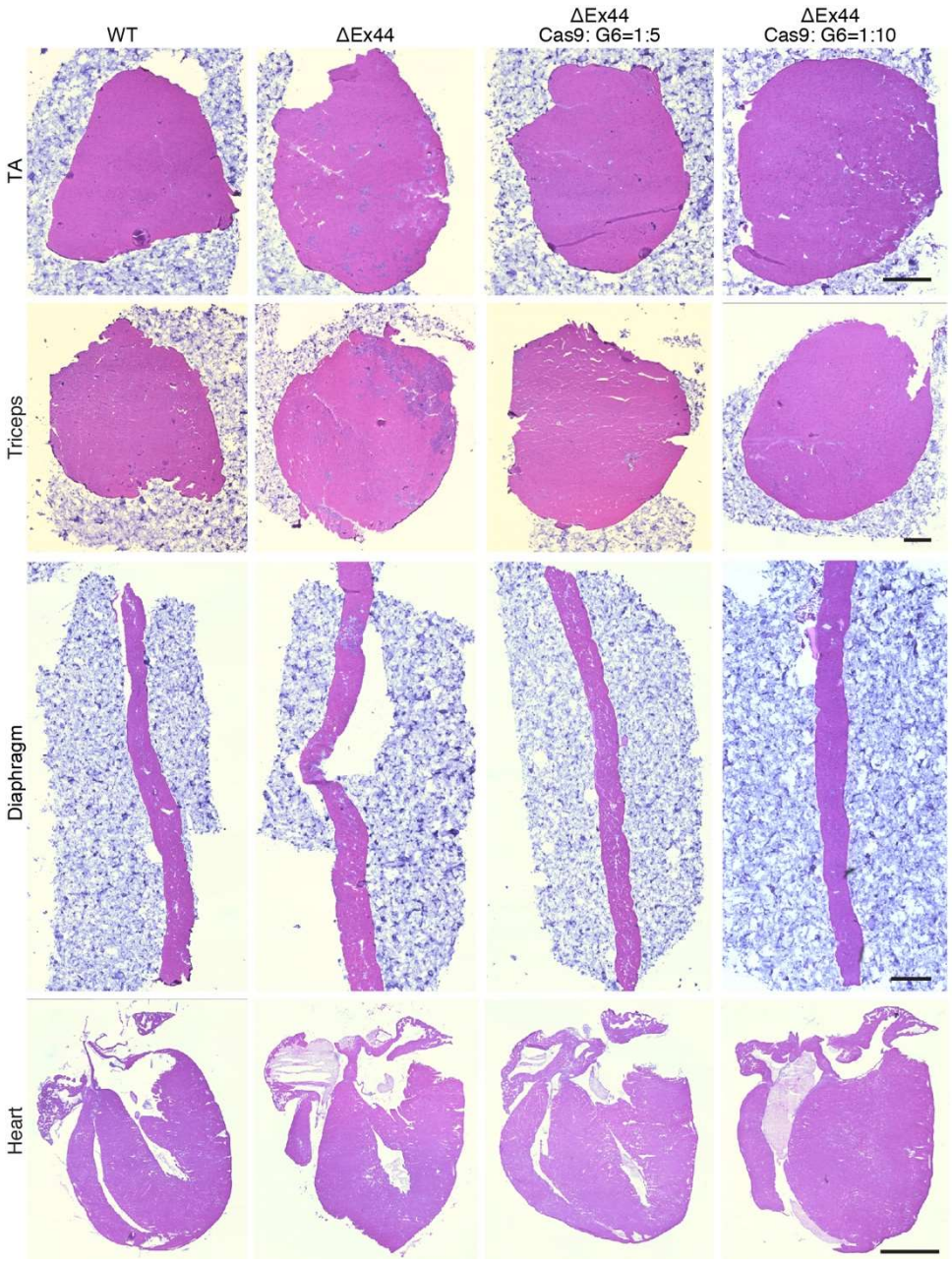

Figure 2.22 Whole muscle scanning of TA, triceps, diaphragm and heart of corrected ΔEx44 DMD mice. H&E staining of WT, ΔEx44 DMD and corrected ΔEx44 DMD 4 weeks after systemic injection of a 1:5 ratio and 1:10 ratio of AAV-Cas9 to AAV-G6. AAV-Cas9 was administered at 5×10^{13} vg/kg. 4X tile scan of the entire muscle. Scale bar in TA, triceps, diaphragm is 500 μm, in heart is 1.5mm.

qPCR analysis of Cas9 mRNA in muscle groups comparing low and high doses of AAV-G6 revealed increased Cas9 mRNA expression in skeletal muscle in the presence of high doses of AAV-G6 (Figure 2.23). These results indicate that Cas9 expression is affected by the amount of sgRNA present, and thus sgRNA is limiting for optimal gene editing in vivo. These results also suggest that the extent of dystrophin restoration and muscle recovery may provide an environment that favors Cas9 expression.

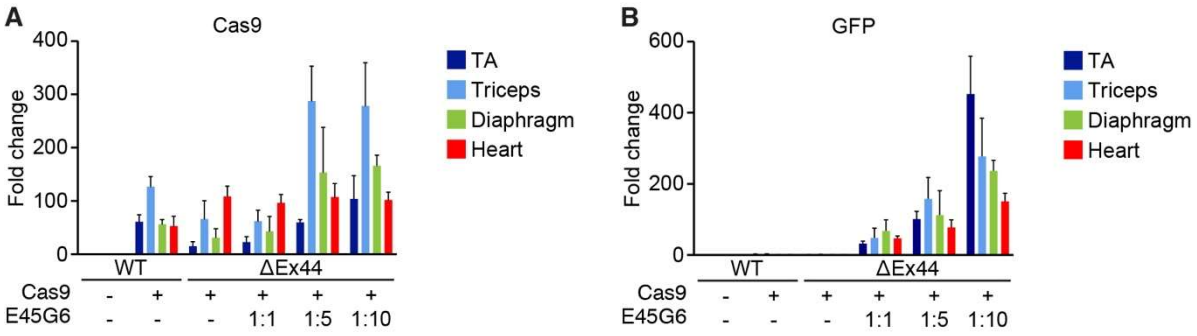

Figure 2.23 qPCR analysis of the skeletal and cardiac muscle groups comparing low and high doses of AAV-G6. (A) qPCR analysis of Cas9 mRNA expression in TA, triceps, diaphragm, and heart of ΔEx44 mice 4 weeks after systemic delivery of AAV-Cas9 and AAV-G6 at the indicated ratios. AAV-Cas9 was administered at 5×10^{13} vg/kg. Normalized to 18S ribosomal RNA. (n= 3) (B) qPCR analysis of GFP mRNA expression in TA, triceps, diaphragm, and heart of ΔEx44 mice 4 weeks after systemic delivery of AAV-Cas9 and AAV-G6 at the indicated ratios. AAV-Cas9 was administered at 5×10^{13} vg/kg. Normalized to 18S ribosomal RNA. (n= 3)

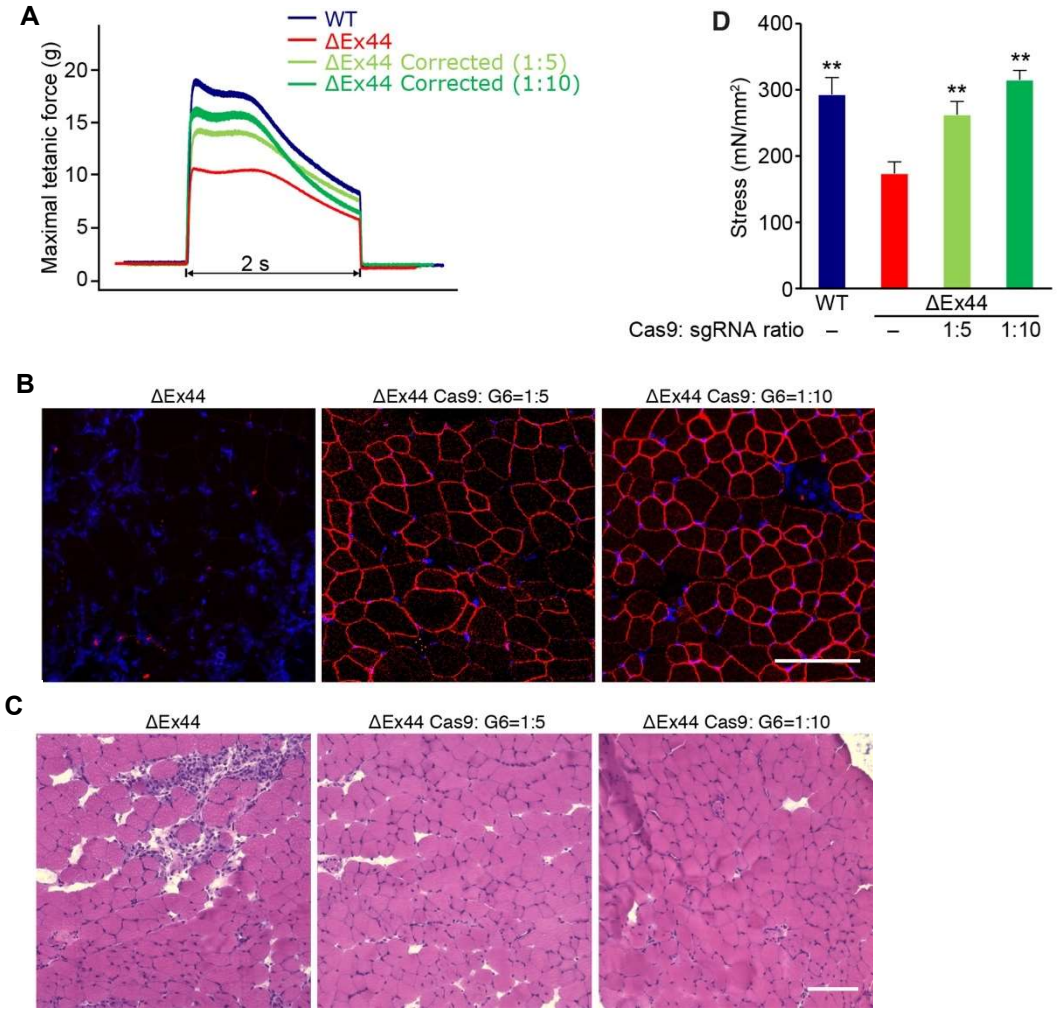

Figure 2.24 (A) Maximal tetanic force of EDL muscles in WT (blue), ΔEx44 DMD (red), and corrected ΔEx44 DMD (green) mice 4 weeks after systemic delivery of AAV-Cas9 and AAV-sgRNA at 1:5 and 1:10 ratios. (n=6) (B) Dystrophin immunostaining of EDL muscle in ΔEx44 DMD and corrected ΔEx44 DMD 4 weeks after systemic injection of a 1:5 ratio and 1:10 ratio of AAV-Cas9 to AAV-G6. AAV-Cas9 was administered at 5×10^{13} vg/kg. Dystrophin is shown in red. Nuclei are marked by DAPI stain in blue. (C) H&E staining of EDL muscle in ΔEx44 DMD and corrected ΔEx44 DMD 4 weeks after systemic injection of a 1:5 ratio and 1:10 ratio of AAV-Cas9 to AAV-G6. AAV-Cas9 was administered at 5×10^{13} vg/kg. (D) Specific force (mN/mm^2) of EDL muscles in WT (blue), ΔEx44 DMD (red), and corrected ΔEx44 DMD (green) mice 4 weeks after systemic delivery of AAV-Cas9 and AAV-sgRNA at 1:5 and 1:10 ratios. (n=6).

To examine the effect of dystrophin restoration on muscle function in systemically corrected ΔEx44 DMD mice, we performed electrophysiology on EDL muscle of ΔEx44 DMD mice at 4 weeks post-injection with AAV-Cas9 and AAV-G6. We observed rescue of maximal tetanic force in the EDL of the corrected ΔEx44 DMD mice (Figure 2.24, panel A). Improvement of muscle function correlated with increased dystrophin expression and decreased muscle degeneration and was associated with administration of increasing amounts of AAV-G6 relative to AAV-Cas9 (Figure 2.24, panel B and C). For measurement of muscle-specific force, which is calibrated with the muscle cross-sectional area, we observed an increase in force from 59% to 89% for a 1:5 ratio and to 107% for a 1:10 ratio of AAV-Cas9:AAV-G6 in EDL of systemically corrected ΔEx44 DMD mice (Figure 2.24, panel D). We conclude that systemic delivery of AAV-Cas9 and AAV-G6 efficiently restores dystrophin expression and improves muscle function in corrected ΔEx44 DMD mice, and the amount of sgRNA delivered to muscle is critical to the efficiency of genome editing in vivo.

Discussion

Our results establish a new mouse model of DMD lacking exon 44 of the dystrophin gene, representing one of most prevalent hotspot regions for dystrophin gene mutations in humans. Correction of exon 44 deletions through exon skipping or reframing of surrounding exons could potentially treat ~12% of DMD patients. These ΔEx44 DMD mice display the hallmarks of DMD, including myocyte degeneration, regeneration, fibrosis and fatty infiltration of muscle, as well as loss of contractile function, and will provide a platform for testing and optimizing gene editing strategies, as well as other therapies. The dystrophin exon

44 deletion in these mice and the strategy for restoration of dystrophin expression by skipping exon 45 are analogous to the correction strategy using the oligonucleotide Casimersen (SRP-4045), developed by Sarepta, which is designed to restore dystrophin expression in patients with exon 44 deletions by masking the splice acceptor site on exon 45. In a recent clinical trial, Eteplirsen, an oligonucleotide that allows exon 51 skipping in patients lacking exon 50, was reported to allow the expression of ~0.5% of the normal level of dystrophin, as measured in biopsy samples from treated DMD patients, after approximately one year of continuous treatment (Charleston et al., 2018). By comparison, we observed ~90% restoration of dystrophin protein expression in all muscles and the heart of mice with exon 44 deletion within 4 weeks of a single systemic dose of gene editing components encoded by AAV9. It has been estimated that only 15-30% of normal dystrophin levels could provide therapeutic benefits in patients (Aslesh et al., 2018; Neri et al., 2007).

We show that the ratio of AAVs encoding sgRNA and Cas9 can have a profound effect on the efficiency of gene correction in vivo. Increasing the ratio of AAV-sgRNA to AAV-Cas9 dramatically increases gene correction by single-cut CRISPR. There are several potential explanations to account for these observations: 1) AAV-sgRNA may be limiting in vivo, such that more virus enables greater gene editing. Moreover, because association of Cas9 with sgRNA has been reported to induce a conformational change in Cas9 that potentiates gene editing (Jinek et al., 2014), higher levels of sgRNA may ensure higher Cas9 activity in vivo. 2) sgRNAs are transcribed by RNA polymerase III and are likely to be confined to the nucleus (Jinek et al., 2012; Qi et al., 2018). Cas9 protein, derived from translation of Cas9 mRNA in the cytoplasm can enter nuclei other than those in which the sgRNA was transcribed.

Increasing the level of AAV-sgRNA may allow for a higher percentage of nuclei within myofibers to express the sgRNA thereby enhancing CRISPR/Cas9 genomic editing. 3) Depletion of sgRNA may occur over time in vivo, and increasing the abundance of sgRNA may ensure continuous editing in myofibers.

When a constant dosage of AAV-Cas9 was administered with higher amounts of AAV-sgRNA, we observed increased Cas9 protein and mRNA expression. Perhaps the increase in Cas9 expression with sgRNA dosage and the consequent increase in dystrophin restoration leads to a healthier cellular environment for Cas9 expression. The difference in rescue efficiency at different ratios of AAV-sgRNA and AAV-Cas9 potentially correlates with the number of nuclei edited in each cell. Although both cardiac muscle and skeletal muscle are multi-nucleated, a single cardiomyocyte contains 1-4 nuclei on average, but one myofiber may contain hundreds of nuclei. Thus, generating dystrophin-expressing myocytes by editing nuclei in one cardiomyocyte is more efficient than in one myofiber. As a result, when supplied with the same amount of sgRNA, cardiac muscle shows better editing efficacy than skeletal muscle. In addition, based on previous reports it is likely that AAV9 has better tropism for heart tissue than skeletal muscle (Zincarelli et al., 2010).

Using a single sgRNA against a sequence within exon 45, we observed a high fraction of single nucleotide insertions immediately adjacent to the DNA cut and these insertions were most commonly an adenosine, corresponding to the next nucleotide adjacent to the site of the initial double-strand DNA break. We made similar observations with single-cut gene editing of exon 51 in mice and dogs lacking exon 50 (Amoasii et al., 2017). Because cutting with Cas9 has a propensity for a single nucleotide 5’ overhang four nucleotides 5’ to the cut site, the

presence of a thymidine at this position favors the insertion of an adenosine on the complementary strand during DNA repair (Lemos et al., 2018). This single nucleotide insertion has the potential to restore the open reading frame if the exon is out of frame with the preceding exon by a single nucleotide, as in the case of exons 43 and 45. However, this strategy is less likely to restore the open reading frame if two nucleotides are required to reframe the protein due to the low frequency of two-nucleotide insertions after NHEJ. Nevertheless, deletions that remove the splice acceptor or donor sequence of the out of frame exon can restore dystrophin in such cases. Of note, we observed a low frequency of integration of AAV ITR sequences at the site of Cas9 cutting in vivo as observed by previous reports (Barzel et al., 2015; Donsante et al., 2007). In contrast, we have not previously observed integration of AAV sequences at sites of genomic cutting within exon 51 in either dogs or mice (Amoasii et al., 2018; Amoasii et al., 2017), suggesting that such integrations may be dependent on surrounding genomic sequences, sgRNAs or chromatin configuration.

Our results highlight the effectiveness of single-cut CRISPR gene editing for efficient restoration of dystrophin in vivo. While several studies have also shown that the use of two sgRNAs to mediate Cas9 cutting at distal genomic sites can allow for excision of large intervening genomic regions and restoration of dystrophin expression from mutant alleles (Bengtsson et al., 2017; Nelson et al., 2016; Ousterout et al., 2015), the efficiency of the double-cut approach is low and is associated with unpredictable genomic rearrangements that we have not observed using only a single sgRNA to direct Cas9 cutting. Thus, we believe the single-cut CRISPR editing approach represents the most viable clinical approach for correction of dystrophin mutations by gene editing. Of course, it also remains to be determined if the

dramatic effects we have observed here in mice can be scaled up to humans with much larger muscles over a longer time frame.

There are several limitations of our study that should be considered. While we have shown dramatic restoration of dystrophin protein and muscle structure within 4 weeks of AAV delivery, we do not yet know if these effects will be sustained or, alternatively, may fade over time. Considering that the majority of cardiomyocytes do not turn over, we expect that the benefits of dystrophin restoration in the heart will be lifelong. However, it remains to be determined if there will be gradual turnover of skeletal muscle following delivery of gene editing components by AAV9. In this regard, Wagers and coworkers have reported that AAV9 infects satellite cells in vivo (Tabebordbar et al., 2016), which could provide a sustained reservoir of cells for long-term maintenance of dystrophin expression. However, we and others have not observed efficient AAV infection of satellite cells in vivo (Amoasii et al., 2017; Arnett et al., 2014). Whether this represents technical differences in delivery approaches remains to be determined. Nevertheless, even if satellite cells cannot be efficiently infected with AAV, the fusion of satellite cells with dystrophic myofibers that express Cas9 and sgRNAs would expose the mutant dystrophin alleles in the satellite cells to the gene editing components and might therefore allow for prolonged gene correction.

Possible immunological responses to Cas9 or dystrophin also remain to be investigated over the long-term. While we have not observed an immune response to AAV or Cas9, nor to dystrophin, in our prior studies (Amoasii et al., 2017), it is conceivable such responses might be seen over longer times. Finally, we have tested for possible off-target genomic cutting at sites predicted to have highest homology with the sgRNAs used to correct the ΔEx44 deletion

but have not observed any off-target cutting above background. Indeed, there has been little evidence of off-target effects of CRISPR-Cas9 editing in mice, other than one report that was retracted (Schaefer et al., 2017).

In summary, the ΔEx44 DMD mice described here, combined with the optimized sgRNA and AAV vectors for delivery, should facilitate progress toward long-term correction of dystrophin mutations in mice as a prelude to possible clinical translation.

Materials and Methods

Study design

This study was designed with the primary aim to identify the most efficient way to correct an exon 44 mutation in a mouse model of DMD and human DMD patient-derived iPSCs. Secondary objectives were to investigate the amount of exon skipping, expression of dystrophin protein, and various indicators of disease progression in corrected DMD mice. PBMCs from healthy individuals and DMD patients were generated at the UT Southwestern Wellstone Myoediting Core. Male donors' PBMCs were used in all experiments. PBMCs were collected based on the mutation of the patients; we did not use exclusion, randomization, or blinding approaches to select the donors. Animal work described in this manuscript has been approved and conducted under the oversight of the UT Southwestern Institutional Animal Care and Use Committee. Animals were allocated to experimental groups based on genotype; we did not use exclusion, randomization, or blinding approaches to assign the animals for the experiments. AAV injection and dissection experiments were conducted in a nonblinded fashion. Blinding approaches were used during grip strength tests, histology validation,

immunostaining analysis, CK analysis, and muscle electrophysiology. For each experiment, sample size reflects the number of independent biological replicates and was provided in the figure legend.

Plasmids and cloning

The pSpCas9(BB)-2A-GFP (PX458) plasmid contained the human codon optimized *Sp*Cas9 gene with 2A-EGFP. pSpCas9(BB)-2A-GFP (PX458) was a gift from Feng Zhang (Addgene plasmid # 48138) (Ran et al., 2013). Cloning of sgRNA was done using Bbs I sites. The sgRNAs in this study, listed in Table 2.2, were selected using prediction of crispr.mit.edu. sgRNA sequences were cloned into PX458, then tested in tissue culture using HEK 293 and 10T½ cells, as previously described (Long et al., 2018).

The AAV TRISPR-sgRNAs-CK8e-GFP plasmid contained three sgRNAs driven by the U6, H1 or 7SK promoters and GFP driven by the CK8e regulatory cassette. TRISPR backbone cloning system relies on two consecutive steps of the Golden Gate Assembly (New England Biolabs). Details of the assembly were previously described (Amoasii et al., 2017).

Human iPSCs maintenance and nucleofection

Human iPSCs were cultured in mTeSR^{TM}1 media (STEMCELL Technologies) and passaged approximately every 4 days (1:12 to 1:18 split ratio depending on the cell lines). One hour before nucleofection, iPSCs were treated with 10 μM ROCK inhibitor (Y-27632) and dissociated into single cells using Accutase (Innovative Cell Technologies, Inc.). 1 x 10^6 iPSCs were mixed with 5 μg of PX458-sgRNA-2A-GFP plasmid and nucleofected using the P3

Primary Cell 4D-Nucleofector X kit (Lonza) according to manufacturer's protocol. After nucleofection, iPSCs were cultured in mTeSR™1 media supplemented with 10 μM ROCK inhibitor and changed to mTeSR™1 media the next day. Three days post-nucleofection, media were changed into mTeSR™1 media supplemented with 10 μM ROCK inhibitor and 100 μg/ml Primosin (InvivoGen) one hour before FACS sorting. GFP(+) and (-) cells were sorted by FACS and subjected to T7E1 assay. Single clones derived from GFP(+) iPSCs were picked and sequenced.

Human iPSC-CMs differentiation

Human iPSCs were cultured in mTeSR™1 media for 3 to 4 days until they reached 90-95% confluence. To differentiate the iPSCs into cardiomyocytes, the cells were cultured in CDM3-C media for 2 days, followed by CDM3-WNT media for 2 days, followed by BASAL media for 6 days, followed by SELECTIVE media for 10 days and lastly by BASAL media for 2 to 6 days. Then, the cardiomyocytes were dissociated using TrypLE™ Express media (Gibco) and re-plated at 2 x 10^6 cells per well in a 6-well dish. The contents of the differentiation medium can be found in Table 2.3.

Mice

Mice were housed in a barrier facility with a 12-hour light/dark cycle and maintained on standard chow (2916 Teklad Global). ΔEx44 DMD mice were generated in the C57/BL6J background using the CRISPR/Cas9 system. Two sgRNAs specific to the intronic regions surrounding exon 44 of the mouse *Dmd* locus were cloned into vector PX458 (Addgene

plasmid #48138) using the primers from Table 2.2. For the in vitro transcription of sgRNA, T7 promoter sequence was added to the sgRNA template by PCR using the primers from Table 2.2. The gel purified PCR products were used as template for in vitro transcription using the MEGAshortscript T7 Kit (Life Technologies). sgRNA were purified by MEGAclear kit (Life Technologies) and eluted with nuclease-free water (Ambion). The concentration of guide RNA was measured by a NanoDrop instrument (Thermo Scientific). Injection procedures were performed as described previously (Long et al., 2016). ΔEx44 DMD mice were backcrossed with C57/BL6J mice for more than three generations. ΔEx44 DMD mice and WT littermates were genotyped using primers encompassing the targeted region from Table 2.2. Tail biopsies were digested in 100 µl of 25 mM NaOH, 0.2 mM EDTA (pH 12) for 20 min at 95 °C. Tails were briefly centrifuged followed by addition of 100 µl of 40 mM Tris·HCl (pH 5) and mixed to homogenize. Two milliliters of this reaction was used for subsequent PCR reactions with the primers in Table 2.2, followed by gel electrophoresis.

Genomic DNA isolation, PCR amplification and T7E1 analysis of PCR products

Genomic DNA of mouse 10T½ fibroblasts, mouse C2C12 myoblasts, human HEK 293 cells and human iPSCs was isolated using DirectPCR (cell) lysis reagent (VIAGEN) according to manufacturer's protocol. Genomic DNA of mouse muscle tissues was isolated using GeneJET genomic DNA purification kit (Thermo Fisher Scientific) according to manufacturer's protocol. Genomic DNA was PCR-amplified using GoTaq DNA polymerase (Promega) or with primers. PCR products were gel purified and subcloned into pCRII-TOPO vector (Invitrogen) according to the manufacturer's protocol. Individual clones were picked, and the

DNA was sequenced. Primer sequences are listed in Table 2.2. Mismatched duplex DNA was obtained by denaturing/renaturing of 25 µl of the genomic PCR product using the following conditions: 95 ºC for 5 min, 95 ºC to 85 ºC (-2.0 ºC /seconds), 85 ºC to 25 ºC (-0.1ºC /seconds), hold at 4 ºC. Then 25 µl of the mismatched duplex DNA was incubated with 2.7 µl of 10X NEB buffer 2 and 0.3 µl of T7E1 (New England BioLabs) at 37 ºC for 90 minutes. The T7E1 digested PCR product was analyzed by 2% agarose gel electrophoresis.

AAV vector production

AAVs were prepared by Boston Children's Hospital Viral Core as previously described (Grieger et al., 2006). AAV vectors were purified by discontinuous iodixanol gradients (Cosmo Bio, AXS-1114542-5), then concentrated with Millipore Amicon filter unit (UFC910008, 100KDa). AAV Titers were determined by quantitative real-time PCR assays. Briefly, 4 µl of the AAV vector was treated with DNase I (NEB M0303S) and 2M NaOH, followed by neutralization. The mixture was serial diluted, and qPCRs were performed with the primers listed in Table 2.3. The number of copies was determined by a standard curve made by serial dilutions of the transgene plasmid.

AAV9 delivery to ΔEx44 DMD mice

Before AAV9 injections, the ΔEx44 DMD mice were anesthetized. For intramuscular injection, the TA muscle of P12 male ΔEx44 DMD mice was injected with 50 µl of AAV9 (1×10^{12} vg/ml) preparations or with saline solution. For intraperitoneal injection, the P4 ΔEx44 DMD mice were injected using an ultrafine needle (31 gauge) with 80 µl of AAV9 preparations

with a dosage of 5×10^{13} vg/kg of AAV-Cas9 and a corresponding ratio of AAV-G6 indicated in the figure legend or with saline solution.

Dystrophin Western blot analysis

For Western blot of iPSC-CMs, 2 x 10^6 cardiomyocytes were harvested and lysed with lysis buffer (10% SDS, 62.5 mM Tris pH6.8, 1 mM EDTA, and protease inhibitor). For Western blot of skeletal or heart muscles, tissues were crushed into fine powder using a liquid nitrogen-frozen crushing apparatus. Cell or tissue lysates were passed through a 25G syringe and then a 27G syringe, 10 times each one. Protein concentration was determined by BCA assay and 50 μg of total protein was loaded onto a 4-20% acrylamide gel. Gels were run at 100V 15min, and switched to 200V for 45 minutes followed by 1 hour 20 min transfer to a PVDF membrane at 100V at 4ºC. The blot was incubated with mouse anti-dystrophin antibody (MANDYS8, Sigma-Aldrich, D8168), mouse anti-Cas9 antibody (Clone 7A9, Millipore, MAC133), or rabbit anti-GFP antibody (Invitrogen, A-11122) at 4ºC overnight, then with goat anti-mouse HRP antibody or goat anti-rabbit HRP antibody (Bio-Rad Laboratories) at room temperature for 1 hour. The blot was developed using Western Blotting Luminol Reagent (Santa Cruz, sc-2048). The loading control was determined by blotting with mouse anti-vinculin antibody (Sigma-Aldrich, V9131).

Amplicon deep-sequencing analysis

PCR of genomic DNA and cDNA from muscles was performed using primers designed against the respective target region and the top 10 off-target sites. A second round of PCR was used to

add Illumina flow cell binding sequences and target specific barcodes on the 5' end of the primer sequence. All primer sequences are listed in Table 2.4 and 2.5. Before sequencing, DNA libraries were analyzed using a Bioanalyzer High Sensitivity DNA Analysis Kit (Agilent). Library concentration was then determined by qPCR using a KAPA Library Quantification Kit for Illumina platforms. The resulting PCR products were pooled and sequenced with 300 bp paired-end reads on an Illumina MiSeq instrument. Samples were demultiplexed according to assigned barcode sequences. FASTQ format data was analyzed using the CRISPResso software package version 1.0.8.

Histological analysis of muscles

Skeletal muscles from WT and ΔEx44 DMD mice were individually dissected and cryo-embedded in a 1:2 volume mixture of Gum Tragacanth powder (Sigma-Aldrich) to Tissue Freezing Medium (TFM) (Triangle Bioscience). All embeds were snap frozen in isopentane heat extractant supercooled to -155^{o}C. Resulting blocks were stored at -80^{o}C prior to sectioning. Eight-micron transverse sections of skeletal muscle, and frontal sections of heart were prepared on a Leica CM3050 cryostat and air-dried prior to staining on the same day. H&E staining was performed according to established staining protocols (Long et al., 2016) and dystrophin immunohistochemistry was performed using MANDYS8 monoclonal antibody (Sigma-Aldrich) with modifications to manufacturer's instructions. In brief, cryostat sections were thawed and rehydrated/delipidated in 1% triton/phosphate-buffered-saline, pH 7.4 (PBS). Following delipidation, sections were washed free of Triton, incubated with mouse IgG blocking reagent (M.O.M. Kit, Vector Laboratories), washed, and sequentially equilibrated

with MOM protein concentrate/PBS, and MANDYS8 diluted 1:1800 in MOM protein concentrate/PBS. Following overnight primary antibody incubation at 4°C, sections were washed, incubated with MOM biotinylated anti-mouse IgG, washed, and detection completed with incubation of Vector fluorescein-avidin DCS. Nuclei were counterstained with propidium iodide (Molecular Probes) prior to cover slipping with Vectashield.

Isolated EDL muscle preparation and electrophysiology stimulation

Muscle preparation was performed as described previously (Long et al., 2016). Briefly, the muscles were surgically isolated from 4-week-old mice and mounted on Grass FT03.C force transducers connected to Powerlab 8/SP data acquisition unit (AD Instruments, Colorado Springs, CO), bathed in physiological salt solution at 37°C, and gassed continuously with 95% O_2-5% CO_2. After calibration, muscles were adjusted to initial length at which the passive force was 0.5 grams and then stimulated with two platinum wire electrodes to establish optimal length (Lo) for obtaining maximal isometric tetanic tension step by step following the protocol (at 150 Hz for 2 s). Specific force (mN/mm2) was calculated to normalize contraction responses to tissue cross-sectional area.

Statistics

All data are presented as mean ± S.E.M. One-way ANOVA was performed followed by Newman-Keuls post hoc test for multiple comparisons. Unpaired two-tailed Student's t-tests were performed for comparison between the respective two groups (wild-type and ΔEx44 DMD mice, wild-type and ΔEx44 DMD-AAV9 treated mice, and ΔEx44 DMD control and

ΔEx44 DMD-AAV9 treated mice). Data analyses were performed with statistical software (GraphPad Prism Software, San Diego, CA, USA). P values less than 0.05 were considered statistically significant.

Tables

Table 2.2 Primer sequences for exon targeting and generation of ΔEx44 DMD mouse model.

Purpose of the primers	ID	Sequence (5'-3')
Primers for sgRNA targeting exon 43	Ex43-gRNA#1-DMD-Top	CACCGTTTTAAAATTTTTATATTA
	Ex43-gRNA#1-DMD-Bot	AAACTAATATAAAAATTTTAAAAC
	Ex43-gRNA#2-DMD-Top	CACCGTTTTATATTACAGAATATAA
	Ex43-gRNA#2-DMD-Bot	AAACTTATATTCTGTAATATAAAAC
	Ex43-gRNA#3-DMD-Top	CACCGTATGTGTTACCTACCCTTGT
	Ex43-gRNA#3-DMD-Bot	AAACACAAGGGTAGGTAACACATAC
	Ex43-gRNA#4-DMD-Top	CACCGTACAAGGACCGACAAGGGT
	Ex43-gRNA#4-DMD-Bot	AAACACCCTTGTCGGTCCTTGTAC
Primers for sgRNA targeting exon 45	Ex45-gRNA#5-Top	CACCGCGCTGCCCAATGCCATCCTG
	Ex45-gRNA#5-Bot	AAACCAGGATGGCATTGGGCAGCGC
	Ex45-gRNA#6-Top	CACCGCTTACAGGAACTCCAGGA
	Ex45-gRNA#6-Bot	AAACTCCTGGAGTTCCTGTAAGC
	Ex45-gRNA#7-Top	CACCGAGGAACTCCAGGATGGCATT
	Ex45-gRNA#7-Bot	AAACAATGCCATCCTGGAGTTCCTC
	Ex45-gRNA#8-Top	CACCGCGCTGCCCAATGCCATCC
	Ex45-gRNA#8-Bot	AAACGGATGGCATTGGGCAGCGC
Primers for T7E1 assay	mDmd-T7E1-Ex45-F	CTAACATAAAAGGTGTCTTTCTATC
	mDmd-T7E1-Ex45-R	GGCAATCCCTCATGATTTTTAGCAC
	DMD-T7E1-Ex45-F	GTCTTTCTGTCTTGTATCCTTTGG
	DMD-T7E1-Ex45-R	AATGTTAGTGCCTTTCACCC
Primers for sgRNA targeting Dmd exon 44 to generate the ΔEx44 DMD model	mDmd-In44-2-Top	CACCGGTAGTTCTGAATCAGGAGGA
	mDmd-In44-2-Bot	AAACTCCTCCTGATTCAGAACTACC
	mDmd-In44-6-Top	CACCGTATGTTGGAACCAGTCCAGA
	mDmd-In44-6-Bot	AAACTCTGGACTGGTTCCAACATAC
Primers for in vitro transcription of sgRNA	Exon 44_T7-In44-2-F	GAATTGTAATACGACTCACTATAGGGGTAGTTCTGAATCAGGAGGA
	Exon 44_T7-In44-6-F	GAATTGTAATACGACTCACTATAGGGTATGTTGGAACCAGTCCAGA
	Exon 44_T7-Rv	AAAAGCACCGACTCGGTGCCAC
Primers for genotyping of ΔEx44 DMD model	Geno dE44-F	GCTGAGGGGGAGACAGTAGA
	Geno dE44-R	TCAGAAGGCATTTTGTCAAT

Table 2.3 Media for iPSC-CMs differentiation.

CDM3	
RPMI-1640 (Gibco 11875-093)	500mL
CDM3 Supplement: - 4.224g L-ascorbic acid-2-phosphate - 10g recombinant human albumin - 200mL H_2O	5mL

CDM3-C	
CDM3	100mL
4, 5, or 6 **µ**M CHIR99021-HCl (12mM).	33.3, 41.6, or 50 µL

CDM3-WNT	
CDM3	100mL
2 uM WNT-C59 (10mM)	20 µL

SELECTIVE	
RPMI-1640 -glucose (Gibco 11879-020)	500mL
B27 Supplement (Thermo Fisher Scientific 17504044)	10mL

BASAL	
RPMI-1640 (Gibco 11875-093)	500mL
B27 Supplement (Thermo Fisher Scientific 17504044)	10mL

Table 2.4 Sequence of primers to titer AAV.

Purpose of the primers	ID	Sequence (5'-3')
AAV-Trispr	CO388-GFP-F	AGAACGGCATCAAGGTGAAC
	CO389-GFP-R	GAACTCCAGCAGGACCATGT
AAV-CK8e-Cas9	CO460-spCas9-F	CGGCTTCATCAAGAGACAGC
	CO461-spCas9-R	TTCACTTCCCGGATCAGCTT

Table 2.5 Sequence of primers for on and off target genomic amplicon deep sequencing.

Sites	ID	Sequence (5'->3')	Product (bps)	miSeq-with Adaptor
E45G6 Target	mDmd-Ex45G6-Ontarget-DS-F1	CCCTGAGCTGAAGTGAGAGG	404	TCGTCGGCAGCGTCAGATGTGTATAAGAGACAGCCCTGAGCTGAAGTGAGAGG
	mDmd-Ex45G6-Ontarget-DS-R2	ACCTCTTTCTCCTTTCTGCCAG		GTCTCGTGGGCTCGGAGATGTGTATAAGAGACAGACCTCTTTCTCCTTTCTGCCAG
E45G6 OT1	E45G6OT1-DS-F1-YLM	CTGCCCCAACAAGAGCATTCTAAG	374	TCGTCGGCAGCGTCAGATGTGTATAAGAGACAGCTGCCCCAACAAGAGCATTCTAAG
	E45G6OT1-DS-R1-YLM	AGCCACTGTTTAACTTGCAGTCAC		GTCTCGTGGGCTCGGAGATGTGTATAAGAGACAGAGCCACTGTTTAACTTGCAGTCAC
E45G6 OT2	E45G6OT2-DS-F1-YLM	CTTTCCTCCTCCACCCTCACAG	356	TCGTCGGCAGCGTCAGATGTGTATAAGAGACAGCTTTCCTCCTCCACCCTCACAG
	E45G6OT2-DS-R1-YLM	TCCTGTTACATGTCCCCGACAC		GTCTCGTGGGCTCGGAGATGTGTATAAGAGACAGTCCTGTTACATGTCCCCGACAC
E45G6 OT3	E45G6OT3-DS-F1-YLM	CTCAGAGAGTCGATGGAACTCCTG	442	TCGTCGGCAGCGTCAGATGTGTATAAGAGACAGCTCAGAGAGTCGATGGAACTCCTG
	E45G6OT3-DS-R1-YLM	TCCTATGGGGTCAATTTCTGCACA		GTCTCGTGGGCTCGGAGATGTGTATAAGAGACAGTCCTATGGGGTCAATTTCTGCACA
E45G6 OT4	E45G6OT4-DS-F1-YLM	GGTTCTCAAAATGCCCTGTTGTGA	487	TCGTCGGCAGCGTCAGATGTGTATAAGAGACAGGGTTCTCAAAATGCCCTGTTGTGA
	E45G6OT4-DS-R1-YLM	TCTCCTGGAGGGGTGAAAGAAAAG		GTCTCGTGGGCTCGGAGATGTGTATAAGAGACAGTCTCCTGGAGGGGTGAAAGAAAAG
E45G6 OT5	E45G6OT5-DS-F1-YLM	TGTGGGACTGCTAGAAAGTTTGGA	440	TCGTCGGCAGCGTCAGATGTGTATAAGAGACAGTGTGGGACTGCTAGAAAGTTTGGA
	E45G6OT5-DS-R2-YLM	GATCCCCGCCTGGAGTTTATTAGT		GTCTCGTGGGCTCGGAGATGTGTATAAGAGACAGGATCCCCGCCTGGAGTTTATTAGT
E45G6 OT6	E45G6OT6-DS-F2-YLM	TGGACAAAGGAGCAAACAAAAGCT	413	TCGTCGGCAGCGTCAGATGTGTATAAGAGACAGTGGACAAAGGAGCAAACAAAAGCT
	E45G6OT6-DS-R2-YLM	TTTATGGACAGTTGAGGTGCCAGA		GTCTCGTGGGCTCGGAGATGTGTATAAGAGACAGTTTATGGACAGTTGAGGTGCCAGA
E45G6 OT7	E45G6OT7-DS-F1-YLM	AAGGGACAGCTCAAAGACCTTCTT	398	TCGTCGGCAGCGTCAGATGTGTATAAGAGACAGAAGGGACAGCTCAAAGACCTTCTT
	E45G6OT7-DS-R1-YLM	ACTTCAAACGCACTGTCACATCAG		GTCTCGTGGGCTCGGAGATGTGTATAAGAGACAGACTTCAAACGCACTGTCACATCAG
E45G6 OT8	E45G6OT8-DS-F1-YLM	TCTGAAGAAGCCCTTGGTCATTCA	459	TCGTCGGCAGCGTCAGATGTGTATAAGAGACAGTCTGAAGAAGCCCTTGGTCATTCA
	E45G6OT8-DS-R1-YLM	ATCCTCTACACGTAACAGGAAGCC		GTCTCGTGGGCTCGGAGATGTGTATAAGAGACAGATCCTCTACACGTAACAGGAAGCC
E45G6 OT9	E45G6OT9-DS-F1-YLM	GAAGGCAGTCAAGCAGATTGGATC	414	TCGTCGGCAGCGTCAGATGTGTATAAGAGACAGGAAGGCAGTCAAGCAGATTGGATC
	E45G6OT9-DS-R2-YLM	ACTAGCAGCCTTTGGATGAAGACA		GTCTCGTGGGCTCGGAGATGTGTATAAGAGACAGACTAGCAGCCTTTGGATGAAGACA
E45G6 OT10	E45G6OT10-DS-F2-YLM	ATGACGACGACGACAATGTTGATG	445	TCGTCGGCAGCGTCAGATGTGTATAAGAGACAGATGACGACGACGACAATGTTGATG
	E45G6OT10-DS-R2-YLM	CCTCAAAGCCTTCTTGAAGGAAGC		GTCTCGTGGGCTCGGAGATGTGTATAAGAGACAGCCTCAAAGCCTTCTTGAAGGAAGC

Table 2.6 Sequence of primers for on target cDNA amplicon deep sequencing.

RT-Site	ID	Sequence (5'->3')	Product (bps)	miSeq-with Adaptor
E45G6 RT-DS	mDmd-E4346-RT-DS-F1	AGGTGAAAGTACAGGAAGCCGT	370	TCGTCGGCAGCGTCAGATGTGTATAAGAGACAGAGGTGAAAGTACAGGAAGCCGT
	mDmd-E4346-RT-DS-R1	CTGCTGCTCATCTCCAAGTGGA		GTCTCGTGGGCTCGGAGATGTGTATAAGAGACAGCTGCTGCTCATCTCCAAGTGGA

CHAPTER THREE

GENERATION OF THREE DUCHENNE MUSCULAR DYSTROPHY MOUSE MODELS WITH HUMANIZED DELETION OF DYSTROPHIN EXON 43, EXON 45, OR EXON 52

Abstract

Duchenne muscular dystrophy (DMD), which affects 1 in 5,000 male births, is one of the most common genetic disorders of children. This disease is caused by an absence or deficiency of dystrophin protein in striated muscle. The major DMD deletion "hot spots" are found between exon 6 to 8, and exons 45 to 53. Here, we create three DMD mouse models that can be used to test a variety of DMD exon skipping and reframing strategies, including CRISPR/Cas9, oligonucleotides, small molecules that promote exon skipping or exon reframing. Micro dystrophin and other cell-based therapies can also be tested in these animal models. Several strategies were tested and validated in patient-derived iPS cells for restoring the reading frame of exon 43, exon 45, and exon 52 deletion.

Results

*Δ*Ex43, Δ*Ex45, and Δ*Ex52 DMD mouse models recapitulate muscle dystrophy phenotype.*

To investigate CRISPR/Cas9-mediated exon skipping and reframing in vivo, three mimics of the human "hot spot" regions were generated in three mouse models by deleting the exon 43, exon 45, and exon 52, respectively, using CRISPR/Cas9 system directed by 2 single

guide RNAs (sgRNA) (Figure 3.1, panel A). sgRNAs targeting 5' end and 3' end of *Dmd* exon 43, exon 45, and exon 52 were designed and validated. C57BL/6 zygotes were co-injected with in vitro transcribed Cas9 mRNA and in vitro transcribed sgRNAs, and then re-implanted into pseudo-pregnant females.

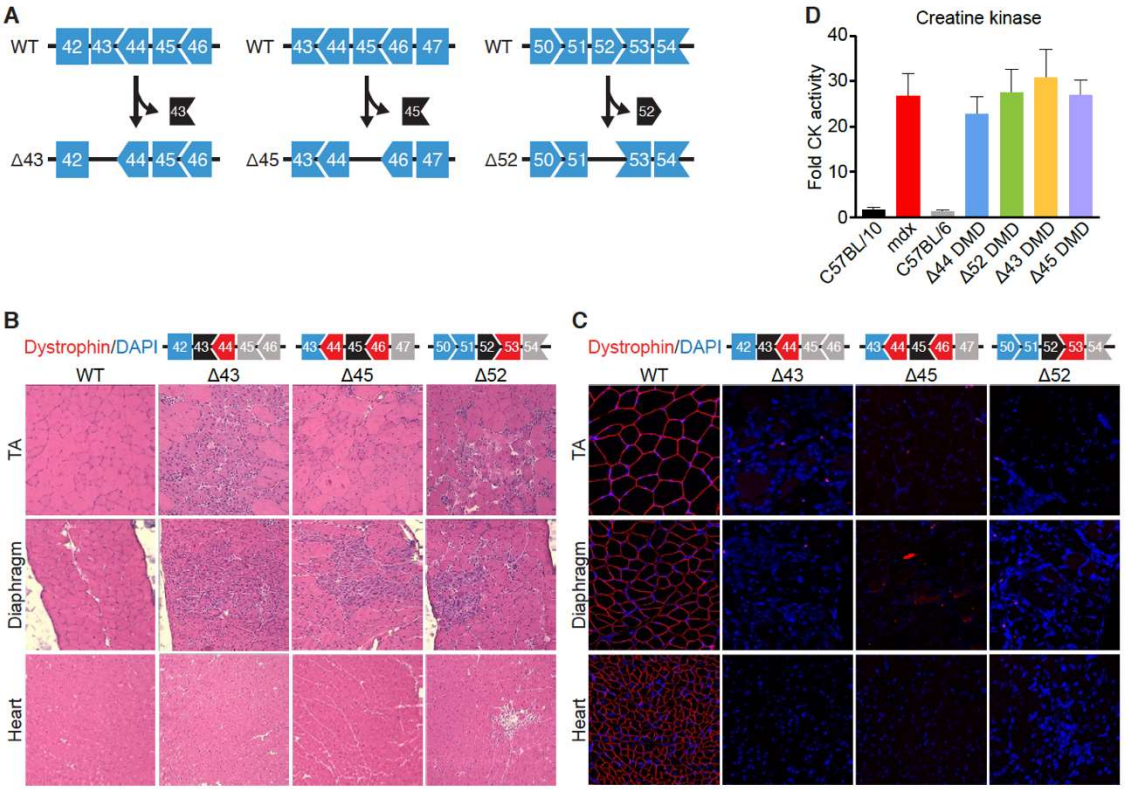

Figure 3.1 Generation and characterization of mice with a DMD exon 43, 45, and 52 deletion. (A) CRISPR/Cas9 editing strategy used for generation of exon 43, 45, and 52 deleted mice. (B) H&E staining of TA, diaphragm and heart. Note extensive inflammatory infiltrate and centralized myonuclei in ΔEx43, ΔEx45, and ΔEx52 DMD mice. (C) Dystrophin staining of TA, diaphragm and heart of WT and ΔEx43, ΔEx45, and ΔEx52 DMD mice. Dystrophin is shown in red. Nuclei are marked by DAPI stain in blue. (D) Serum creatine kinase (CK), a marker of muscle damage and membrane leakage, was measured in WT (C57BL/6 and C57BL/10), mdx, ΔEx44, ΔEx43, ΔEx45, and ΔEx52 DMD mice.

The deletion of *Dmd* exon 43, exon 45, and exon 52 was confirmed by DNA genotyping. Mice lacking exon 43, exon 45, or exon 52 showed pronounced dystrophic muscle changes in 1-month old mice (Figure 3.1, panel B). The deletion of these exons placed the dystrophin gene out of frame leading to the absence of dystrophin protein in skeletal muscle and heart (Figure 3.1, panel C). Serum analysis of the Δ43, Δ45, and Δ52 DMD mice shows a significant increase of creatine kinase (CK) level, which is a sign of muscle damage (Figure 3.1, panel D). Taken together, dystrophin protein expression, muscle histology, and serum creatine kinase level validated dystrophic phenotype of the ΔEx43, ΔEx45, and ΔEx52 DMD mouse models.

Identification of optimal sgRNAs for CRISPR/Cas9 correction of DMD exon 43, exon 45, and exon 52 deletions.

Skipping or reframing of exon 44, exon 46, and exon 53 would apply to a DMD patient group of ~18%. To restore the ORF of the DMD patient with exon 43, exon 45, or exon 53 deletion, we applied single guide RNA to disrupt the splicing junction of exon 44, exon 46, and exon 53 respectively, which results in reframing of the exon downstream of the deleted exon and restoration of the protein reading frame (Figure 3.2, panel A). To test sgRNA efficiency within these regions, we designed sgRNAs to target the splicing junctions of exon 44, exon 46 or exon 53 (Table 3). We then validated the cleavage efficiency of these gRNAs in both mouse 10T1/2 or mouse N2a cells or human 293 cells. By T7E1 assay, we demonstrated that 1 exon 44 sgRNA and 2 exon 46 sgRNAs and 2 exon 53 sgRNA efficiently cause DNA cleavage at Dmd exon target locus in mouse cells (Figure 3.2, panel B). By T7E1 assay, we

demonstrated that 7 exon 44 sgRNA and 2 exon 46 sgRNAs and 9 exon 53 sgRNA efficiently cause DNA cleavage at DMD exon target locus in human cells (Figure 3.2, panel C).

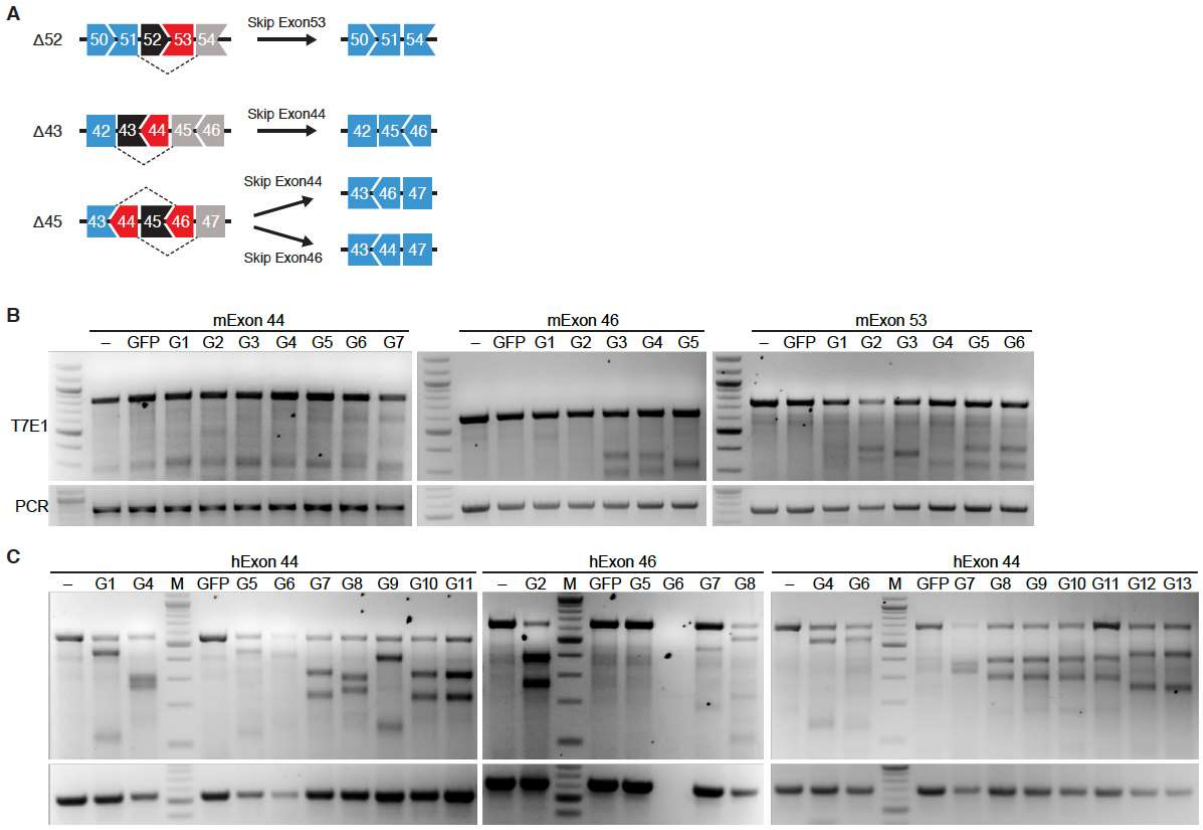

Figure 3.2 (A) CRISPR/Cas9 correction strategy of DMD exon 43, exon 45, and exon 52 deletions. (B) T7E1 assay using mouse 10T½ transfected with plasmids that express SpCas9 and exon 44, exon 46 or exon 53 sgRNAs show cleavage of the *Dmd* locus at the target sites. PCR indicates the undigested PCR product. (C) T7E1 assay using human 293 cells transfected with plasmids that express SpCas9 and exon 44, exon 46 or exon 53 sgRNAs show cleavage of the *Dmd* locus at the target sites. PCR indicates the undigested PCR product.

DMD iPSC-derived cardiomyocytes express dystrophin after CRISPR/Cas9 mediated genome editing by exon skipping and exon reframing.

We then generated iPSCs from DMD patients (TX16) that have deletion of exon 52 and an isogenic iPSC line with deletion of exon 43 (ΔEx43 DMD). Exon 44 editing sgRNAs were tested on ΔEx43 DMD iPSCs, and dystrophin protein expression restoration were validated by Western blot analysis and immunostaining of iPSC-derived cardiomyocytes (Figure 3.3, panel A and C). We also tested exon 53 editing sgRNAs on TX16 patient derived iPSCs. The restoration of dystrophin in these TX16 DMD patient iPSCs was confirmed by Western blot analysis and immunostaining of iPSC-derived cardiomyocytes (Figure 3.3, panel B and C).

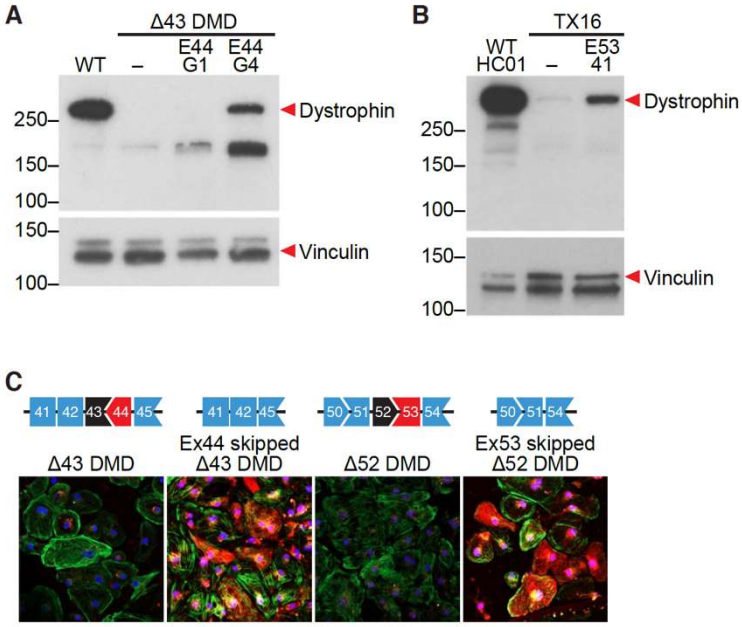

Figure 3.3 (A) Western blot analysis shows restoration of dystrophin expression in exon 44-edited (E44) ΔEx43 iPSC-CMs with sgRNAs (G) 1 and 4, as indicated. Vinculin is loading control. WT/HC01, iPSC-CMs from a healthy control. The second lane is unedited ΔEx43 patient iPSC-CMs. (B) Western blot analysis shows restoration of dystrophin expression in exon 53-edited (E53) ΔEx52 iPSC-CMs (TX16) with sgRNAs (G) 4, as

indicated. Vinculin is loading control. WT/HC01, iPSC-CMs from a healthy control. The second lane is unedited ΔEx52 patient iPSC-CMs. (C) Immunostaining shows restoration of dystrophin expression in exon 44-edited and exon 53-edited ΔEx43 and ΔEx52 iPSC-CMs. Dystrophin is shown in red. Cardiac troponin I is shown in green. Nuclei are marked by DAPI stain in blue.

Materials and Methods

Study Approval

All experimental procedures involving animals in this study were reviewed and approved by the University of Texas Southwestern Medical Center's Institutional Animal Care and Use Committee.

Plasmids

The pSpCas9(BB)-2A-GFP (PX458) plasmid containing the human codon optimized SpCas9 gene with 2A-EGFP and the backbone of sgRNA was purchased from Addgene (Plasmid #48138). Cloning of sgRNA was done using Bbs I sites. The AAV TRISPR-CK8-GFP plasmid containing three sgRNAs driven by U6, H1 or 7SK promoter and GFP driven by CK8 promoter.

Human iPSCs maintenance and nucleofection

Human iPSCs were cultured in mTeSR^{TM}1 media (STEMCELL Technologies) and passaged approximately every 4 days (1:12 to 1:18 split ratio depending on the cell lines). One hour before nucleofection, iPSCs were treated with 10 μM ROCK inhibitor (Y-27632) and dissociated into single cells using Accutase (Innovative Cell Technologies, Inc.). 1 x 10^6 iPSCs

were mixed with 5 μg of PX458-sgRNA-2A-GFP plasmid and nucleofected using the P3 Primary Cell 4D-Nucleofector X kit (Lonza) according to manufacturer's protocol. After nucleofection, iPSCs were cultured in mTeSR™1 media supplemented with 10 μM ROCK inhibitor and changed to mTeSR™1 media the next day. Three days post-nucleofection, media were changed into mTeSR™1 media supplemented with 10 μM ROCK inhibitor and 100 μg/ml Primosin (InvivoGen) one hour before FACS sorting. GFP(+) and (-) cells were sorted by FACS and subjected to T7E1 assay. Single clones derived from GFP(+) iPSCs were picked and sequenced.

Human iPSC-CMs differentiation

Human iPSCs were cultured in mTeSR™1 media for 3 to 4 days until they reached 90-95% confluence. To differentiate the iPSCs into cardiomyocytes, the cells were cultured in CDM3-C media for 2 days, followed by CDM3-WNT media for 2 days, followed by BASAL media for 6 days, followed by SELECTIVE media for 10 days and lastly by BASAL media for 2 to 6 days. Then, the cardiomyocytes were dissociated using TrypLE™ Express media (Gibco) and re-plated at 2 x 10^6 cells per well in a 6-well dish. The contents of the differentiation medium can be found in Table 2.3.

Genomic DNA isolation, PCR amplification and T7E1 analysis of PCR products

Genomic DNA of mouse 10T½ fibroblasts, mouse C2C12 myoblasts, human HEK 293 cells and human iPSCs was isolated using DirectPCR (cell) lysis reagent (VIAGEN) according to manufacturer's protocol. Genomic DNA of mouse muscle tissues was isolated using

GeneJET genomic DNA purification kit (Thermo Fisher Scientific) according to manufacturer's protocol. Genomic DNA was PCR-amplified using GoTaq DNA polymerase (Promega) or with primers. PCR products were gel purified and subcloned into pCRII-TOPO vector (Invitrogen) according to the manufacturer's protocol. Individual clones were picked, and the DNA was sequenced. Primer sequences are listed in Table 3.

Mismatched duplex DNA was obtained by denaturing/renaturing of 25 µl of the genomic PCR product using the following conditions: 95 ºC for 5 min, 95 ºC to 85 ºC (-2.0 ºC /seconds), 85 ºC to 25 ºC (-0.1ºC /seconds), hold at 4 ºC. Then 25 µl of the mismatched duplex DNA was incubated with 2.7 µl of 10X NEB buffer 2 and 0.3 µl of T7E1 (New England BioLabs) at 37 ºC for 90 minutes. The T7E1 digested PCR product was analyzed by 2% agarose gel electrophoresis.

Dystrophin Western blot analysis

For Western blot of iPSC-CMs, 2 x 10^6 cardiomyocytes were harvested and lysed with lysis buffer (10% SDS, 62.5 mM Tris pH6.8, 1 mM EDTA, and protease inhibitor). Cell or tissue lysates were passed through a 25G syringe and then a 27G syringe, 10 times each one. Protein concentration was determined by BCA assay and 50 µg of total protein was loaded onto a 4-20% acrylamide gel. Gels were run at 100V 15min, and switched to 200V for 45 minutes followed by 1 hour 20 min transfer to a PVDF membrane at 100V at 4ºC. The blot was incubated with mouse anti-dystrophin antibody (MANDYS8, Sigma-Aldrich, D8168), mouse anti-Cas9 antibody (Clone 7A9, Millipore, MAC133), or rabbit anti-GFP antibody (Invitrogen, A-11122) at 4ºC overnight, then with goat anti-mouse HRP antibody or goat anti-

rabbit HRP antibody (Bio-Rad Laboratories) at room temperature for 1 hour. The blot was developed using Western Blotting Luminol Reagent (Santa Cruz, sc-2048). The loading control was determined by blotting with mouse anti-vinculin antibody (Sigma-Aldrich, V9131).

CRISPR/Cas9-mediated exon deletion in mice

Two single-guide RNA (sgRNA) specific intronic regions surrounding exon 43, exon 45, or exon 52 sequence of the mouse *Dmd* locus were cloned into vector pX458 using the primers from Table 3. For the in vitro transcription of sgRNA, T7 promoter sequence was added to the sgRNA template by PCR using the primers from Table 3. The gel purified PCR products were used as template for in vitro transcription using the MEGAshortscript T7 Kit (Life Technologies). sgRNA were purified by MEGAclear kit (Life Technologies) and eluted with nuclease-free water (Ambion). The concentration of guide RNA was measured by a NanoDrop instrument (Thermo Scientific).

Genotyping of Δ43, Δ45, and Δ52 DMD mice

Δ43, Δ45, and Δ52 DMD mice were genotyped using primers encompassing the targeted region from Table 3. Tail biopsies were digested in 100 μL of 25 mM NaOH, 0.2 mM EDTA (pH 12) for 20 min at 95 °C. Tails were briefly centrifuged followed by addition of 100 μL of 40 mM Tris·HCl (pH 5) and mixed to homogenize. Two microliters of this reaction was used for subsequent PCR reactions with the primers below, followed by gel electrophoresis.

Histological analysis of muscles

Skeletal muscles from WT, Δ43 DMD, Δ45 DMD, and Δ52 DMD mice were individually dissected and cryo-embedded in a 1:2 volume mixture of Gum Tragacanth powder (Sigma-Aldrich) to Tissue Freezing Medium (TFM) (Triangle Bioscience). All embeds were snap frozen in isopentane heat extractant supercooled to -155ºC. Resulting blocks were stored at -80ºC prior to sectioning. Eight-micron transverse sections of skeletal muscle, and frontal sections of heart were prepared on a Leica CM3050 cryostat and air-dried prior to staining on the same day. H&E staining was performed according to established staining protocols (Long et al., 2016) and dystrophin immunohistochemistry was performed using MANDYS8 monoclonal antibody (Sigma-Aldrich) with modifications to manufacturer's instructions. In brief, cryostat sections were thawed and rehydrated/delipidated in 1% triton/phosphate-buffered-saline, pH 7.4 (PBS). Following delipidation, sections were washed free of Triton, incubated with mouse IgG blocking reagent (M.O.M. Kit, Vector Laboratories), washed, and sequentially equilibrated with MOM protein concentrate/PBS, and MANDYS8 diluted 1:1800 in MOM protein concentrate/PBS. Following overnight primary antibody incubation at 4ºC, sections were washed, incubated with MOM biotinylated anti-mouse IgG, washed, and detection completed with incubation of Vector fluorescein-avidin DCS. Nuclei were counterstained with propidium iodide (Molecular Probes) prior to cover slipping with Vectashield.

Table 3 Primer sequences

Purpose of the primers	ID	Sequence (5'-3')	Purpose of the primers	ID	Sequence (5'-3')
Primers for sgRNA targeting exon 44	hDMD-E44g5-bottom	aaacGCAGGCGATTTGACAGATCTC	Primers for sgRNA targeting exon 53	mDmd-E53g3-bottom	aaacGTTCTGCAGCTGTTCTTGAAC
	hDMD-E44g5-top	CACCGAGATCTGTCAAATCGCCTGC		mDmd-E53g3-top	CACCGTTCAAGAACAGCTGCAGAAC
	hDMD-E44g6-top	CACCGACAGATCTGTTGAGAAATGG		mDmd-E53g4-bottom	aaacTTAACATTTCATTCAACTGTC
	hDMD-E44g6-bottom	aaacCCATTTCTCAACAGATCTGTC		mDmd-E53g4-top	CACCGACAGTTGAATGAAATGTTAA
	hDMD-E44g7-bottom	aaacGAGAATTGGGAACATGCTAAC		mDmd-E53g5-bottom	aaacTTGTGTTGAATCCTTTAACAC
	hDMD-E44g7-top	CACCGTTAGCATGTTCCCAATTCTC		mDmd-E53g5-top	CACCGTGTTAAAGGATTCAACACAA
	hDMD-E44g8-bottom	aaacTTTGTATTTAGCATGTTCCC		mDmd-E53g6-bottom	aaacGCCATTGTGTTGAATCCTTTC
	hDMD-E44g8-top	CACCGGGAACATGCTAAATACAAA		mDmd-E53g6-top	CACCGAAAGGATTCAACACAATGGC
	hDMD-E44g9-top	CACCGTTGACAGATCTGTTGAGAAA	Primers for sgRNA targeting Dmd exon 43 to generate the ΔEx43 DMD model	mDmd-Ex43-N1-Top	caccgaagtgagttccaggacagcc
	hDMD-E44g9-bottom	aaacTTTCTCAACAGATCTGTCAAC		mDmd-Ex43-N1-Bottom	aaacGGCTGTCCTGGAACTCACTTc
	hDMD-E44g10-bottom	aaacATTCTCAGGAATTTGTGTCTC		mDmd-Ex43-N2-Top	caccgTTATTAGTACTAACTCAGAA
	hDMD-E44g10-top	CACCGAGACACAAATTCCTGAGAAT		mDmd-Ex43-N2-Bottom	aaacTTCTGAGTTAGTACTAATAAc
	hDMD-E44g11-bottom	aaacAATTCTCAGGAATTTGTGTC		mDmd-Ex43-N3-Top	caccgtagtactaataaaagtagtc
	hDMD-E44g11-top	CACCGACACAAATTCCTGAGAATT		mDmd-Ex43-N3-Bottom	aaacGACTACTTTTATTAGTACTAc
	mDmd-E44g1-bottom	aaacATAATTTGAAAACATGGATGC		mDmd-Ex43-C1-Top	caccgATGTTGAAATACACTGCTCT
	mDmd-E44g1-top	CACCGCATCCATGTTTTCAAATTAT		mDmd-Ex43-C1-Bottom	aaacAGAGCAGTGTATTTCAACATc
	mDmd-E44g2-bottom	aaacTTTTTCAACTGATCTGTCGAC		mDmd-Ex43-C2-Top	caccgGTAAATATCAACTTCTAAAT
	mDmd-E44g2-top	CACCGTCGACAGATCAGTTGAAAAA		mDmd-Ex43-C2-Bottom	aaacATTTAGAAGTTGATATTTACc
	mDmd-E44g3-bottom	aaacGTTTTCAGGATTTTGTGTCTC		mDmd-Ex43-C3-Top	caccggtatttccctatttttaatg
	mDmd-E44g3-top	CACCGAGACACAAAATCCTGAAAAC		mDmd-Ex43-C3-Bottom	aaacCATTAAAAATAGGGAAATACc
	mDmd-E44g4-bottom	aaacGAAAACTGGGAACATGCTAAC	Primers for sgRNA targeting Dmd exon 45 to generate the ΔEx45 DMD model	mDmd-Exon45-5-G1-top	CACCGaactaatatatccaaatact
	mDmd-E44g4-top	CACCGTTAGCATGTTCCCAGTTTTC		mDmd-Exon45-5-G1-bot	AAACAGTATTTGGATATATTAGTT C
	mDmd-E44g5-bottom	aaacAGTTTTCAGGATTTTGTGTC		mDmd-Exon45-5-G2-top	CACCGttaaacatagaaacatccttg
	mDmd-E44g5-top	CACCGACACAAAATCCTGAAAACT		mDmd-Exon45-5-G2-bot	AAACCAAGGATGTTCTATGTTTAA C
	mDmd-E44g6-bottom	aaacTTTGTATTTAGCATGTTCCC		mDmd-Exon45-5-G3-top	CACCGaatcgaatttgtcttgaga
	mDmd-E44g6-top	CACCGGGAACATGCTAAATACAAA		mDmd-Exon45-5-G3-bot	AAACTCTCAAGAGCAAATTCGATT C
	mDmd-E44g7-bottom	aaacTAAGATACCATTTGTATTTAC		mDmd-Exon45-3-G4-top	CACCGagtttgtgctaaaaatcatg
	mDmd-E44g7-top	CACCGTAAATACAAATGGTATCTTA		mDmd-Exon45-3-G4-bot	AAACCATGATTTTTAGCACAAACT C
Primers for sgRNA targeting exon 46	hDMD-E46g5-bottom	aaacGGCTAGAAGAACAAAGAATC		mDmd-Exon45-3-G5-top	CACCGgctttacccagctgaatcac
	hDMD-E46g5-top	CACCGATTCTTTTGTTCTTCTAGCC		mDmd-Exon45-3-G5-bot	AAACGTGATTCAGCTGGGTAAAGC C
	hDMD-E46g6-bottom	aaacACCATAAAACAAATTCATTTC		mDmd-Exon45-3-G6-top	CACCGaattttcacagcattgctta
	hDMD-E46g6-top	CACCGAAATGAATTTGTTTTATGGT		mDmd-Exon45-3-G6-bot	AAACTAAGCAATGCTGTGAAAATT C
	hDMD-E46g7-top	CACCGTGAATTTGTTTTATGGTTGG	Primers for sgRNA targeting Dmd exon 52 to generate the ΔEx52 DMD model	mDmd-Ex52-N1-Top	CACCGatatatcttaaatgatgtat
	hDMD-E46g7-bottom	aaacCCAACCATAAAACAAATTCAC		mDmd-Ex52-N1-bottom	AAACATACATCATTTAAGATATATC
	hDMD-E46g8-bottom	aaacTGACTTGCTCAAGCTTTTCTC		mDmd-Ex52-N2-Top	CACCGaataataatgctgtttgatg
	hDMD-E46g8-top	CACCGAGAAAAGCTTGAGCAAGTCA		mDmd-Ex52-N2-bottom	aaacCATCAAACAGCATTATTATTc
	mDmd-E46g1-top	CACCGAATTTTGTTATTCTTAATAC		mDmd-Ex52-N3-Top	CACCGGATAGTTAGAAATGACTCCA
	mDmd-E46g1-bottom	aaacGTATTAAGAATAACAAAATTC		mDmd-Ex52-N3-bottom	AAACTGGAGTCATTTCTAACTATCC
	mDmd-E46g2-bottom	aaacGCCACAAAACAAATTCATTTC		mDmd-Ex52-C1-Top	CACCGtctttaatgtctgtctacta
	mDmd-E46g2-top	CACCGAAATGAATTTGTTTTGTGGC		mDmd-Ex52-C1-Bottom	aaacTAGTAGACAGACATTAAAGAc
	mDmd-E46g3-bottom	aaacAGTGGAGTAATAGCAATGTTC		mDmd-Ex52-C2-Top	caccgtgcaatttcatagtatattt
	mDmd-E46g3-top	CACCGAACATTGCTATTACTCCACT		mDmd-Ex52-C2-Bottom	aaacAAATATACTATGAAATTGCAc
	mDmd-E46g4-top	CACCGAGCTGCTGCTCATCTCCAAG		mDmd-Ex52-C3-Top	caccgccaagttaatcaaattgttc
	mDmd-E46g4-bottom	aaacCTTGGAGATGAGCAGCAGCTC		mDmd-Ex52-C3-Bottom	aaacGAACAATTTGATTAACTTGGc
	mDmd-E46g5-top	CACCGAGAACAACTTGAACAAGTCA	Primers for in vitro transcription of sgRNAs	IVTT7-mDmd-E43-N1-F	gaattgTAATACGACTCACTATAGGGaagtgagttccaggacagcc
	mDmd-E46g5-bottom	aaacTGACTTGTTCAAGTTGTTCTC		IVTT7-mDmd-E43-N2-F	gaattgTAATACGACTCACTATAGGGTTATTAGTACTAACTCAGAA
Primers for sgRNA targeting exon 53	hDMD-E53g7-bottom	aaacACTGATTCTGAATTCTTTCAC		IVTT7-mDmd-E43-N3-F	gaattgTAATACGACTCACTATAGGGtagtactaataaaagtagtc
	hDMD-E53g7-top	CACCGTGAAAGAATTCAGAATCAGT		IVTT7-mDmd-E43-C1-F	gaattgTAATACGACTCACTATAGGGATGTTGAAATACACTGCTCT
	hDMD-E53g8-bottom	aaacTCAGAACCGGAGGCAACAGTC		IVTT7-mDmd-E43-C2-F	gaattgTAATACGACTCACTATAGGGGTAAATATCAACTTCTAAAT
	hDMD-E53g8-top	CACCGACTGTTGCCTCCGGTTCTGA		IVTT7-mDmd-E43-C3-F	gaattgTAATACGACTCACTATAGGGgtatttccctatttttaatg
	hDMD-E53g9-top	CACCGTACAAGAACACCTTCAGAAC		IVTT7-mDmd-E52-N1-F	gaattgTAATACGACTCACTATAGGGatatatcttaaatgatgtat
	hDMD-E53g9-bottom	aaacGTTCTGAAGGTGTTCTTGTAC		IVTT7-mDmd-E52-N2-F	gaattgTAATACGACTCACTATAGGGaataataatgctgtttgatg
	hDMD-E53g10-bottom	aaacCCGGTTCTGAAGGTGTTCTTC		IVTT7-mDmd-E52-N3-F	gaattgTAATACGACTCACTATAGGGGATAGTTAGAAATGACTCCA
	hDMD-E53g10-top	CACCGAAGAACACCTTCAGAACCGG		IVTT7-mDmd-E52-C1-F	gaattgTAATACGACTCACTATAGGGtctttaatgtctgtctacta
	hDMD-E53g11-bottom	aaacGAGGCAACAGTTGAATGAAAC		IVTT7-mDmd-E52-C2-F	gaattgTAATACGACTCACTATAGGGtgcaatttcatagtatattt
	hDMD-E53g11-top	CACCGTTTCATTCAACTGTTGCCTC		IVTT7-mDmd-E52-C3-F	gaattgTAATACGACTCACTATAGGGccaagttaatcaaattgttc
	hDMD-E53g12-top	CACCGTGTTAAAGGATTCAACACAA		T7-Rv	AAAAGCACCGACTCGGTGCCAC
	hDMD-E53g12-bottom	aaacTTGTGTTGAATCCTTTAACAC	Primers for genotyping of DMD mouse models	mDmd-Ex43-geno-F1	agatgtggtaacgcacacct
	hDMD-E53g13-bottom	aaacGCCATTGTGTTGAATCCTTTC		mDmd-Ex43-geno-R1	tctgcagccgaatacttca
	hDMD-E53g13-top	CACCGAAAGGATTCAACACAATGGC		mDmd-Ex45-geno-F1	TGCAAAATAGATCGGTGCAA
	mDmd-E53g1-top	CACCGTGAAAGAATTCAGATTCAGT		mDmd-Ex45-geno-R2	TAGCATGCATTTGGCTTCAG
	mDmd-E53g1-bottom	aaacACTGAATCTGAATTCTTTCAC		mDmd-Ex52-geno-F1	agggaatctgctgtccttga
	mDmd-E53g2-bottom	aaacCATCCCACTGAATCTGAATTC		mDmd-Ex52-geno-R1	tggaggttagatttcacaactgt
	mDmd-E53g2-top	CACCGAATTCAGATTCAGTGGGATG			

CHAPTER FOUR

IDENTIFICATION OF A MULTIPOTENT TWIST2-EXPRESSING CELL POPULATION IN THE ADULT HEART

Acknowledgement

Parts of this chapter, including figures, have been reproduced, with or without modifications, from my previous published work (Min et al., 2018).

Abstract

Twist transcription factors function as ancestral regulators of mesodermal cell fates in organisms ranging from Drosophila to mammals. Through lineage tracing of Twist2 (Tw2)-expressing cells with tamoxifen-inducible Tw2-CreERT2 and tdTomato (tdTO) reporter mice, a unique cell population that progressively contributes to cardiomyocytes (CMs), endothelial cells, and fibroblasts in the adult heart were discovered. Clonal analysis confirmed the ability of Tw2-derived $tdTO^+$ (Tw2-$tdTO^+$) cells to form CMs in vitro. Within the adult heart, Tw2-$tdTO^+$ CMs accounted for ∼13% of total CMs, the majority of which resulted from fusion of Tw2-$tdTO^+$ cells with existing CMs. Tw2-$tdTO^+$ cells also contribute to cardiac remodeling after injury. We conclude that Tw2-$tdTO^+$ cells participate in lifelong maintenance of cardiac function, at least in part through de novo formation of CMs and fusion with preexisting CMs, as well as in the genesis of other cellular components of the adult heart.

Introduction

In the previous chapters, I discussed the CRISPR gene editing in Duchenne muscular dystrophy, that the primary focus is to correct dystrophin gene in both skeletal and cardiac muscles. In this chapter, I will switch topic to another project that I have been working on during my PhD study, which is focusing on the role of Tw2-derived cells in adult cardiac regeneration and maintenance under homeostasis and injury.

Adult mammalian hearts have limited capacity for self-renewal. In the adult mouse, new cardiomyocytes (CMs) are produced at a rate of 1.3–4% per year (Malliaras et al., 2013). In humans, only ~1% of CMs renew each year before age 20 y, declining later in life to 0.4%/y (Senyo et al., 2013). Upon myocardial injury, such as myocardial infarction (MI), the rate of CM turnover increases but is insufficient to offset CM loss, resulting in contractile demise and eventual heart failure (Bergmann et al., 2009; Bergmann et al., 2015; Hsieh et al., 2007; Sutton and Sharpe, 2000). Studies combining genetic lineage tracing and radioactive isotope labeling revealed that the few myocytes that are generated after birth arise largely from the proliferation of existing CMs (Bergmann et al., 2009; Kimura et al., 2015; Mollova et al., 2013; Senyo et al., 2013), whereas resident c-kit^{+} cardiac progenitor cells (CPCs) were originally reported to contribute significantly to CM renewal (Beltrami et al., 2003). Recent genetic lineage-tracing studies question these conclusions by showing only a minimal contribution of ckit^{+}CPCs to CM renewal in the adult heart both during homeostasis and after injury (Sultana et al., 2015; van Berlo et al., 2014; van Berlo and Molkentin, 2014). Although the contribution of c-kit^{+} cells to adult CMs appears minimal, a low level of renewal activity from CPCs is detectable,

especially during cardiac remodeling after injury (Hsieh et al., 2007). In this regard, other types of CPCs have been identified in mice and humans based on the expression of specific cell-surface markers or cellular phenotypes; these include resident $Sca1^+$ CPCs, cardiac side population (SP) cells, $WT1^+$ epicardial-derived cells, Islet1 $(Isl1)^+$ CPCs, endothelial derived CPCs, and $W8B2^+$ CPCs (Anversa et al., 2013; Bearzi et al., 2007; Beltrami et al., 2003; Ellison et al., 2013; Fioret et al., 2014; Laugwitz et al., 2008; Noseda et al., 2015; Oh et al., 2003; Pfister et al., 2005; Smart et al., 2011; Uchida et al., 2013; Zhang et al., 2015). Although most of these CPCs have been reported to contribute to CM self-renewal to various extents, there is no consensus as to the set of markers that specifically identify CPCs, nor is there an understanding of the potential lineage relationships among the CPC populations. Members of the Twist family of basic helix–loop–helix transcription factors function as ancestral regulators of mesodermal cell fates in organisms ranging from Drosophila to mammals (Baylies and Bate, 1996; Borkowski et al., 1995; Cripps et al., 1998; Currie and Bate, 1991). In adult Drosophila, Twist expression is restricted to muscle precursors, which are similar to muscle stem cells in vertebrates (Figeac et al., 2007) and are required for the formation of the adult musculature (Cripps and Olson, 1998). There are two Twist genes in vertebrates, Twist1 (Tw1) and Twist2 (Tw2), which are highly homologous and evolutionarily conserved (Castanon and Baylies, 2002). It has been shown that Twist overexpression can revert the terminal differentiation status of skeletal myotubes to undifferentiated myoblasts (Mastroyiannopoulos et al., 2013). Tw2 global-knockout mice failed to thrive and died by postnatal day (P) 15. Before death, homozygous mutant mice were underweight and frail and showed signs of impaired movement and wasting. The mutant mice also showed notable skin abnormalities and severe fat

deficiency. A cardiac phenotype was not observed in Tw2 global-knockout mice by P15, possibly due to redundancy with its close family member Tw1 (Šošić et al., 2003). Recently, we discovered an interstitial myogenic progenitor, marked by the expression of Tw2, which gives rise to type IIb/x skeletal muscle fibers (Liu et al., 2017). Tw1 has also been shown to promote epithelial–mesenchymal transition (EMT), metastasis, and tumor stemness in many cancer models (Beck et al.; Schmidt et al., 2015b; Yang et al., 2004). Collectively, these studies support the premise that Twist expression influences the stem cell state as well as cell-fate determination. Within the developing heart, Tw1 controls proliferation, migration, and differentiation of the cardiac cushions (Shelton and Yutzey, 2008; VanDusen and Firulli, 2012), but the potential involvement of Twist genes in the adult mouse heart has not been explored. Here, by lineage tracing using inducible Tw2-CreERT2 and tdTomato (tdTO) reporter mice, we discovered a Tw2-tdTO$^+$ cell population that contributes to a subset of CMs as well as endothelial cells (ECs) and fibroblasts. Intriguingly, this cell population fuses with preexisting CMs and, to a lesser extent, gives rise to new CMs de novo. Our findings reveal a unique population of interstitial heart cells that contributes to cardiac homeostasis and regeneration.

Results

Tw2-tdTO$^+$ Cells Contribute to CMs in the Adult Heart

To explore the role of Tw2 in the adult heart, we first examined its expression in the adult mouse myocardium by immunostaining. Tw2 protein was detected in interstitial cells throughout the adult heart but not in CMs at 2–17 mo of age (Figure 4.1, panel A and B).

Consistent with these findings, Tw1 and Tw2 mRNA transcripts were readily detected in non-CM populations but not in CM populations separated by Langendorff perfusion of the adult ventricles (Figure 4.1, panel C).

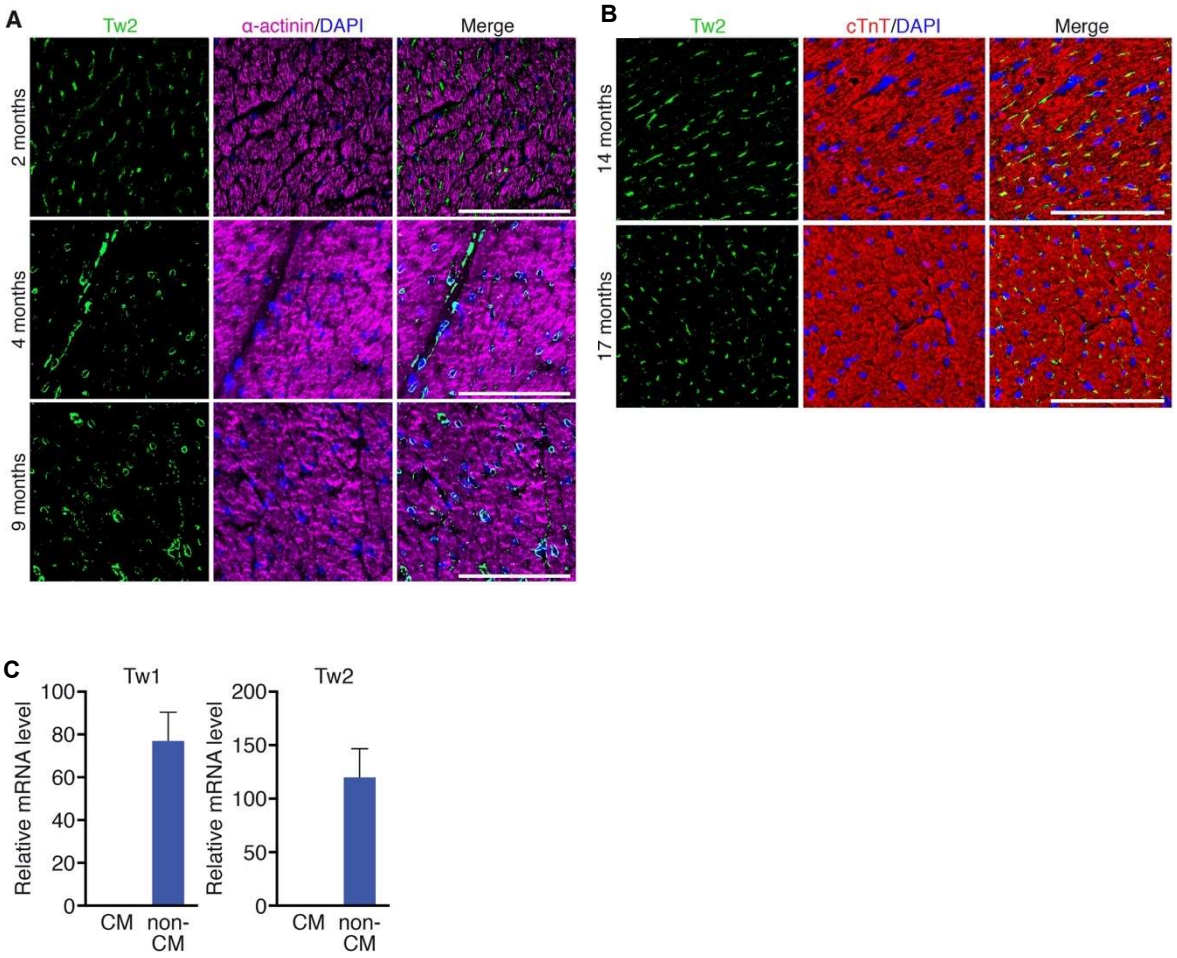

Figure 4.1 (A) Immunostaining of Tw2 (green) and α-actinin (violet) proteins on heart sections of 2-, 4- and 9-month old wild-type mice. Scale bar: 100 um. (B) Immunostaining of Tw2 (green) and cTnT (red) proteins on heart sections of 14- and 17-month old wild-type mice. Scale bar: 100 um. (C) Expression of Tw1 and Tw2 transcripts in cardiomyocyte (CM) and non-CM enriched populations in mouse adult heart, as detected by realtime RT-PCR (n=3).

To further assess the potential contribution of Tw2-expressing cells to adult tissues, we generated tamoxifen (TMX)-inducible Tw2-CreERT2; R26-tdTO reporter mice (Liu et al., 2017) in which Tw2-expressing cells and their derivatives were terminally labeled with tdTO. Following treatment of 8-wk-old Tw2-CreERT2; R26-tdTO mice with TMX on three alternative days, we monitored tdTO labeling as a marker for Tw2-expressing cells in the heart at various time points (Figure 4.2, panel A). At 10 d post-TMX treatment we observed tdTO labeling of interstitial cells but rarely of CMs in the adult heart ventricles (Figure 4.2, panel B and C).

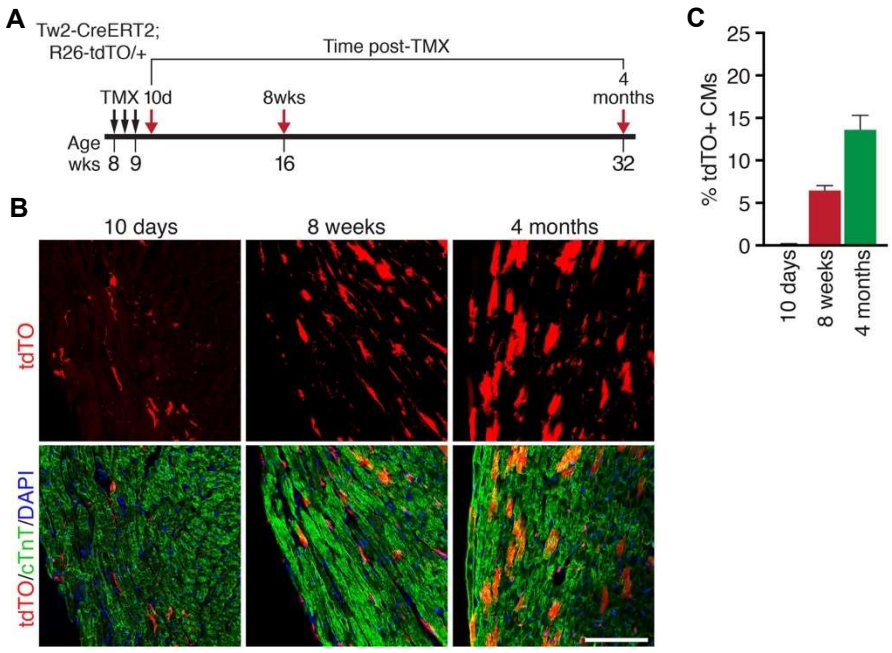

Figure 4.2 (A) Schematic of TMX treatment. Tw2-CreERT2; R26-tdTO mice were injected with 1mg of TMX on 3 alternative days at 8 weeks of age. Mice were analyzed at 10 days, 8 weeks, and 4 months following the first TMX injection. (B) Progressive tdTO labeling of CMs at the indicated time points following TMX treatment. Sections were co-stained with cTnT (green) to detect CMs. Scale bar: 100 um. (C) Percentage of Tw2-tdTO+ CMs in ventricles was quantified and averaged at the indicated time points. n=3 mice for each time point.

Colocalization of tdTO labeling and Tw2 protein was also observed in interstitial cells at 10 d post-TMX treatment (Figure 4.3, panel A). In addition, tdTO-labeled CMs were significantly more abundant in atria than in ventricles at 10 d post-TMX treatment (Figure 4.3, panel B–D). By 8 wk post-TMX treatment strong tdTO labeling was observed in the CM population in both ventricles and atria as well as in the interventricular septum (Figure 4.2, panel B and Figure 4.3, panel D). The number of $tdTO^+$ CMs continued to increase for up to 4 mo (Figure 4.2, panel B), when ∼13% of CMs in the ventricles were labeled by tdTO (Figure 4.2, panel C).

No $tdTO^+$ labeling was detected in the hearts of Tw2-CreERT2; R26-tdTO mice without TMX treatment even at 9 mo of age, indicating that there was no leakiness of the reporter (Figure 4.4, panel A). To determine whether the contribution of Tw2-$tdTO^+$ cells to CMs is age dependent, we performed TMX treatment on 7-moold Tw2-CreERT2; R26-tdTO mice (Figure 4.4, panel B). At 3 and 9 mo post-TMX treatment, only non-CMs were labeled by Tw2-tdTO in these mice (Figure 4.4, panel C). This is in contrast to the observation that in young adult (8-wk-old) mice both CMs and non-CMs were labeled by Tw2-tdTO (Figure 4.2, panel B). These findings suggest that Tw2- $tdTO^+$ cells contribute to ventricular CMs in young adult mice at 2 mo of age but lose this ability by 7 mo of age. Furthermore, in comparison with the Tw2-tdTO labeling in CMs of young adult mice (Figure 4.2, panel A and B), our observations in older mice (Figure 4.4, panel B and C) indicate that tdTO labeling in CMs at 4 mo post-TMX treatment is not due to Tw2 expression in adult CMs. In addition to labeling CMs, ∼7.5% of non-CMs were Tw2- $tdTO^+$

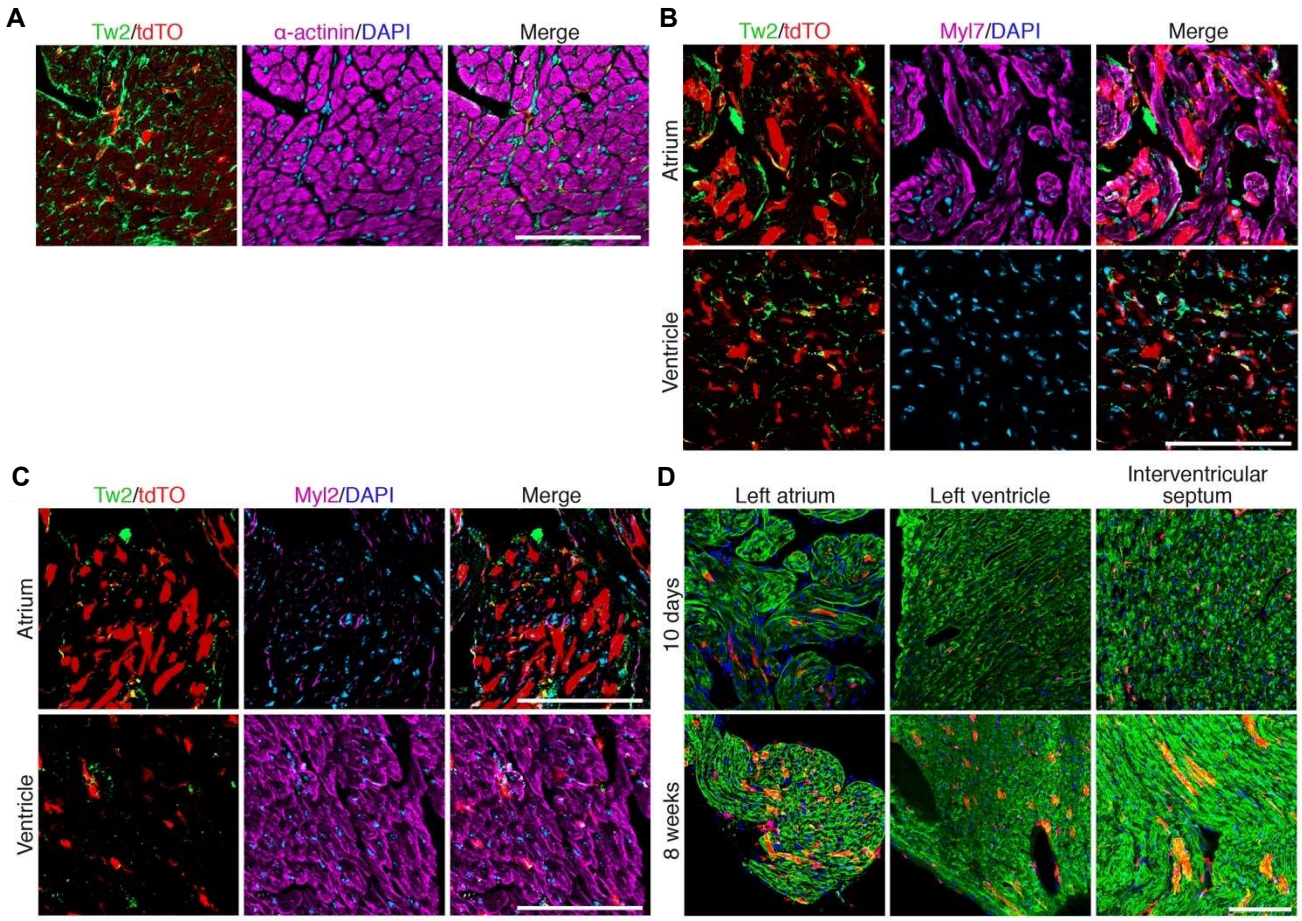

Figure 4.3 (A) Tw2 antibody immunostaining (green) and tdTO labeling on heart sections of Tw2-CreERT2; R26-tdTO mice at 10 days post TMX treatment. Scale bar: 100 um. (B) Tw2 antibody immunostaining (green) and tdTO labeling in atrium and ventricle at 10 days post-TMX treatment. Sections were co-immnuostained with anti-Myl7, an atrial marker (violet). Scale bar: 100 um. (C) Tw2 antibody immunostaining (green) and tdTO labeling in atrium and ventricle at 10 days post-TMX treatment. Sections were co-immnuostained with anti-Myl2, a ventricular marker (violet). Scale bar: 100 um. (D) tdTO labeling in left atrium, left ventricle and interventricular septum at 10 days and 8 weeks post-TMX treatment. Sections were immunostained with cTnT. Scale bar: 100 um.

in adult ventricles at 10 d post-TMX treatment and by 4 mo post-TMX treatment ~20.3% of total non-CMs were Tw2-tdTO^{+} (Figure 4.4, panel D), indicating a substantial contribution of Tw2-tdTO^{+} cells to lineages other than CMs. Specifically, Tw2-tdTO–labeled ECs and fibroblasts but not smooth muscle cells, as evidenced by costaining with cell-specific markers at 10 d post-TMX treatment (Figure 4.5, panel A). At 8 wk post-TMX treatment, tdTO labeling continued to be observed in ECs and fibroblasts, suggesting that Tw2 tdTO^{+} cells gradually contribute to these cell lineages.

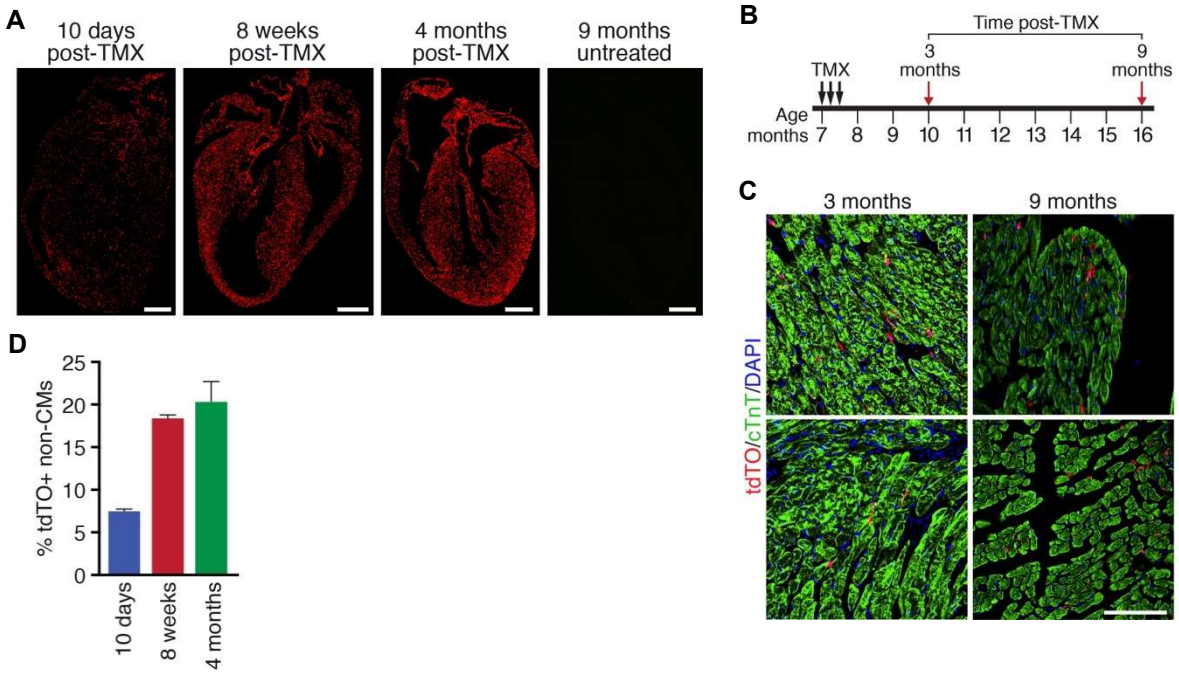

Figure 4.4 (A) Whole heart imaging at various time points post-TMX treatment. Right panel shows absence of tdTO signal in heart of Tw2-CreERT2; R26-tdTO mice without TMX treatment. Scale bar: 100 um. (B) Schematic of TMX treatment on aged Tw2-CreERT2; R26-tdTO mice. (C) Hearts from aged Tw2-CreERT2; R26-tdTO mice at the indicated times post-TMX were co-stained with cTnT (green). Scale bar: 100 um. (D) Percentage of tdTO+ non-CMs was quantified and averaged at indicated time points. n= 3 mice for each time point. Data are expressed as mean ± SEM.

Differentiation Potential of Tw2-tdTO$^+$ Cells in Vitro.

To study their differentiation potential in vitro, Tw2-tdTO$^+$ cells were isolated together with other non-CMs from ventricles of adult Tw2- CreERT2; R26-tdTO/+ mice at 10 d post-TMX treatment. Tw2-tdTO$^+$ cells in regular culture medium spontaneously differentiated into fibroblasts, as indicated by the expression of DDR2, a fibroblast marker (Figure 4.5, panel B). Under culture conditions that favor EC formation, Tw2-tdTO$^+$ cells differentiated into ECs and expressed the EC marker CD31 (Figure 4.5, panel B). Tw2-tdTO$^+$ cells differentiated into CMs when maintained in CM induction medium, as identified by the expression of the CM marker cardiac troponin T (cTnT) (Figure 4.5, panel B). Some of the differentiated CMs began beating after 2 wk of culture (Figure 4.5, panel C). These results are consistent with the cardiogenic potential of Tw2-tdTO$^+$ cells in vivo. Given our prior findings that Tw2-tdTO$^+$ cells within the interstitial region of skeletal muscle can form skeletal muscle and bone cells under appropriate conditions (Liu et al., 2017), we also exposed Tw2-tdTO$^+$ cells isolated from the heart to culture conditions that favor the formation of myotubes and osteoblasts. However, we observed no myotube or osteoblast formation, suggesting that the potential fates of Tw2-tdTO$^+$ cells differ depending on the tissue niche and/or lineage of origin.

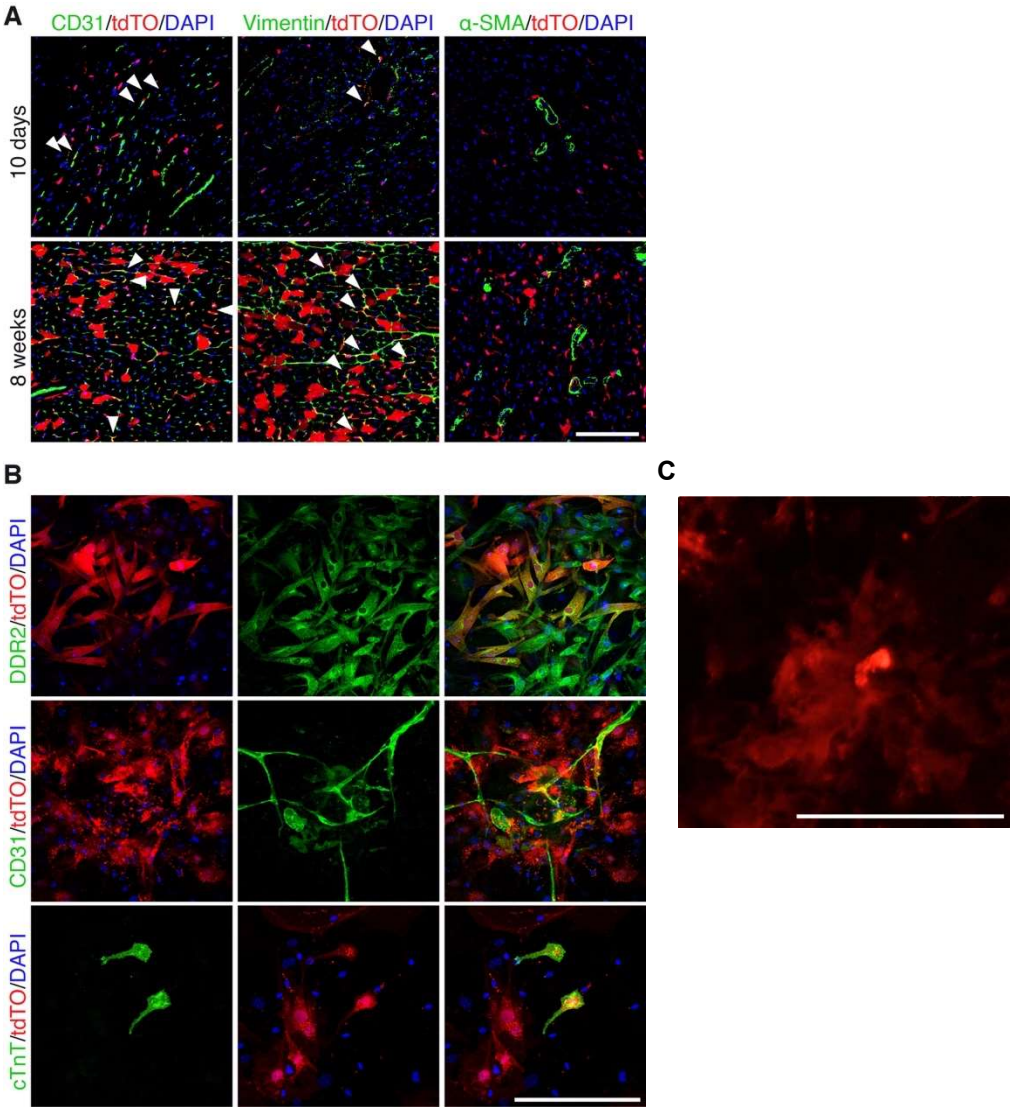

Figure 4.5 Tw2-tdTO+ cells express markers of fibroblasts and endothelial cells, but not smooth muscle cells. (A) Ventricles from 10 days (upper panel) and 8 weeks (lower panel) post-TMX treatment were immunostained with antibodies against CD31, vimentin or smooth muscle α-actin (α-SMA). White arrowheads indicate co-localization with tdTO signals. Scale bar: 100 um. (B) Ventricles from 10 days post-TMX treatment were dissociated and the non-CM-enriched population was cultured for a week, and immunostained with antibodies against DDR2, CD31 or cTnT. Scale bar: 100 um. (C) Image from video of Tw2-tdTO+ cells that differentiated into beating CMs in culture. Scale bar: 100 um.

Tw2-tdTO$^+$ Cells Contribute to CMs by both Fusion and de Novo Differentiation.

The progressive labeling of CMs in the young adult heart (Figure 4.2, panel B) could result from either de novo generation of CMs from Tw2-tdTO$^+$ cells or fusion of Tw2-tdTO$^+$ cells with existing CMs. To distinguish between these possibilities, we generated Tw2-CreERT2; ROSA26-mT/mG/$^+$ reporter mice by breeding the Tw2-CreERT2 mice with Rosa26-mT/mG mice. The R26-mT/mG mice harbor a membrane Tomato (mT) cassette and a polyA signal flanked by two loxP sites at the Rosa26 locus, followed by a membrane eGFP (mG) cassette (Muzumdar et al., 2007). In the absence of Cre activity, every cell in the Tw2-CreERT2; R26-mT/mG reporter mice expresses mT but not mG. Upon Cre activation by TMX, the mT cassette is excised, resulting in mG expression and loss of mT expression. Therefore, if a Tw2-expressing interstitial cell fuses with an existing CM, both the mT and mG signal will be present (Figure 4.6). In contrast, if a Tw2-expressing cell differentiates de novo into a CM, that CM would be mG$^+$ and mT$^-$ (Figure 4.6).

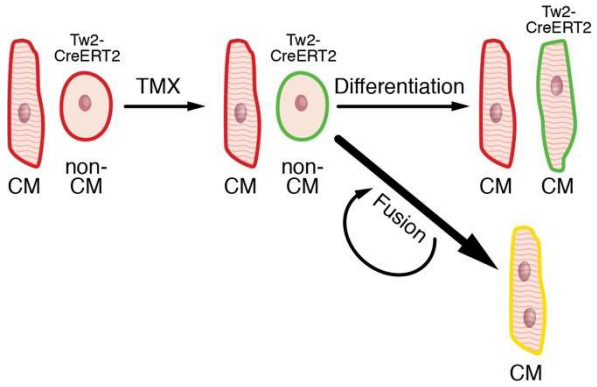

Figure 4.6 Schematic of using Tw2-CreERT2; R26-mT/mG/+ mice to distinguish between fusion and differentiation events. CM denotes cardiomyocytes, non-CM represents non-cardiomyocytes. Upon TMX treatment of Tw2-CreERT2; R26-mT/mG/+ mice, a CM with a yellow membrane represents fusion of a non-CM to a CM. On the other hand, a CM with a green membrane represents de novo differentiation of a non-CM to a CM.

To activate Cre expression, Tw2-CreERT2; R26-mTmG mice were treated with three doses of TMX at 8 wk of age and were kept on a TMX-containing diet for 14 wk. Two weeks before the hearts were harvested, the TMX diet was removed (Figure 4.7, panel A). As shown in Figure 4.7, panel B, the majority of mG^+ CMs retained mT expression, indicating fusion of Tw2-mG^+ interstitial cells with existing mT^+ CMs. To a lesser extent, we observed mG^+ CMs without mT expression, indicating de novo formation of CMs from a Tw2-mG^+ interstitial cell (Figure 4.7, panel B). All mG^+ non-CMs were mT^- , validating the fidelity of the labeling strategy (Figure 4.7, panel B). To quantify the frequency of differentiation versus fusion events, hearts from Tw2-CreERT2; R26-mT/mG mice were dissociated by Langendorff perfusion, and CMs of ventricles were plated in culture. mG^+ /mT^- and mG^+ /mT^+ CMs were imaged and quantified (Figure 4.7, panel C). Among the mG^+ CMs, 11% had lost mT expression, indicating that they were derived from de novo differentiation, whereas 89% of mG^+ CMs were derived from fusion, as they retained mT expression. We further quantified the number of nuclei in the fusion-derived mG^+ /mT^+ CMs and found that 99.3% of mT and mG double-positive cells had more than one nucleus, with 69.2% having two nuclei and 30.1% having three or more nuclei per cell (Figure 4.7, panel D). The percentage of cells with three or more nuclei was 6.9-fold higher in mG^+ /mT^+ CMs than in mG^- / mT^+ cells. These results suggest that the majority of Tw2-mG^+ cells fuse with CMs in young adult mice and that a small subset of these Tw2-mG^+ can differentiate into CMs.

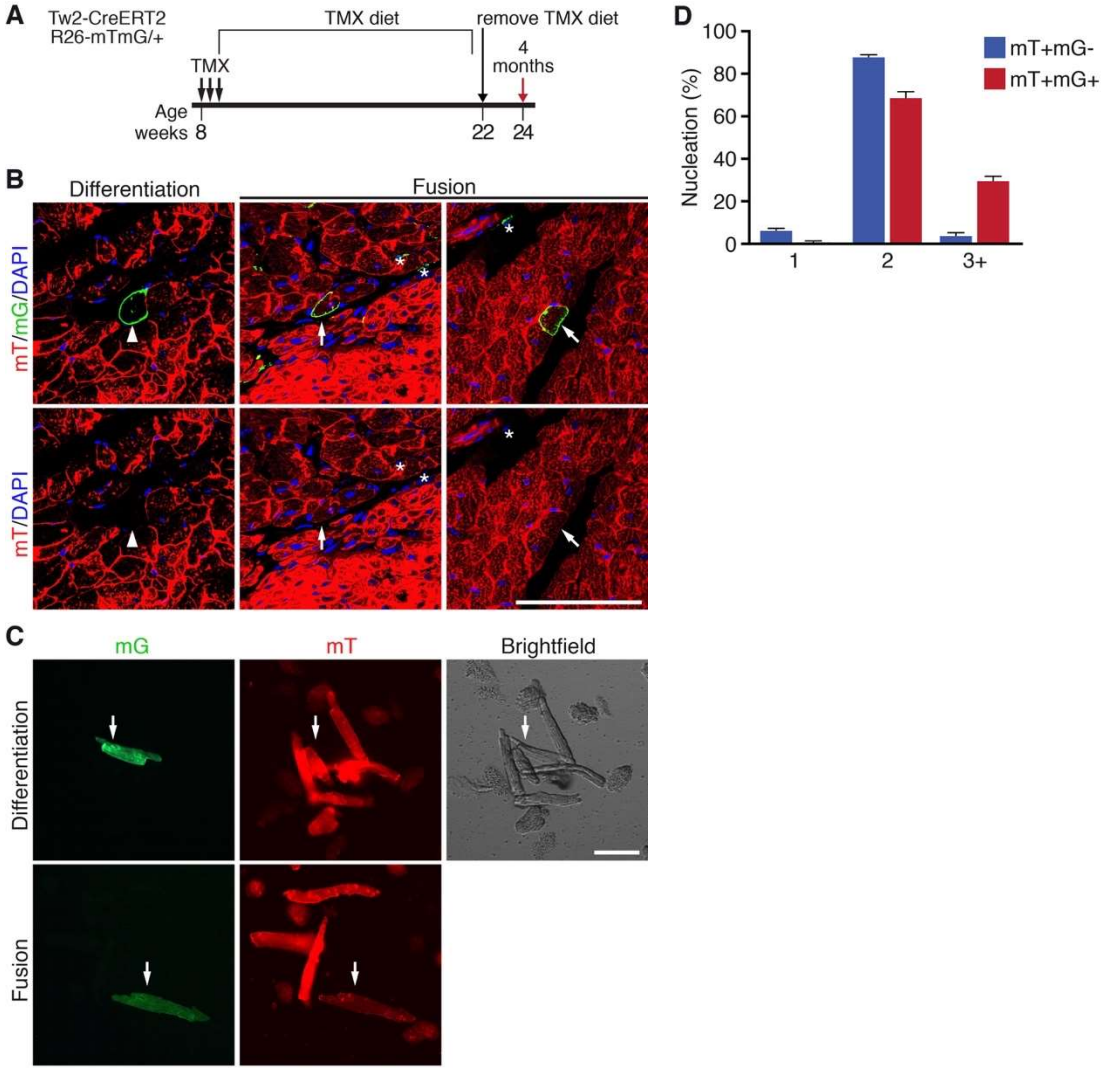

Figure 4.7 (A) Schematic of TMX treatment of Tw2-CreERT2; R26-mT/mG mice. (B) Representative images of differentiation and fusion events detected in hearts of Tw2-CreERT2; R26-mT/mG mice. In the left panels, the mG+ CMs no longer express the mT signal, indicating de-novo CM formation (white arrow head). In the middle panels, the Tw2-mG+ CMs are mT negative (white asterisks). In the right panels, the Tw2-mG+ CMs retain mT expression, indicating that Tw2-mG+ non-CMs fused with existing CMs (white arrow). Nuclei were stained with DAPI (blue). Scale bar: 100 um. (C) CMs from ventricles of the Tw2-CreERT2; R26-mT/mG mice were dissociated and plated in culture. Upper panels show a de novo CM that is mG+ but mT-, and the bottom panels show evidence of a fusion event in which the CM is mG and mT double positive. Scale bar: 100 um. (D) Percent of cells that contain 1, 2 or greater than 3 nuclei among all mT+ and mG- CMs or mT+ and mG+ CMs. n=3 mice. Data in D are expressed as mean ± SEM.

Cardiogenic Potential of Single Tw2-tdTO$^+$ Cells.

The finding that a small but significant number of CMs were derived de novo from Tw2-tdTO$^+$ cells suggests that Tw2-tdTO$^+$ cells in the adult heart include a potential cardiogenic population. To determine whether single Tw2-tdTO$^+$ cells can differentiate into CMs, we performed clonal analysis of Tw2-tdTO$^+$ cells. Briefly, Tw2- CreERT2; R26-tdTO/$^+$ mice were treated with TMX at 8 wk of age as described in Figure 4.2, panel A. Ten days after the first dose of TMX, cells from the heart ventricle were dissociated, and Tw2- tdTO$^+$ interstitial cells were isolated by FACS (Figure 4.8, panel A). To avoid contamination of CMs in the isolation, we stained cells with the mitochondrial dye Mitoview 633, which preferentially labels CMs because of their high mitochondria content. Single clones of Tw2-tdTO$^+$ interstitial cells, identified as tdTO$^+$ and Mitoview 633^{low}, were sorted into individual wells on 96-well plates and were cocultured with murine embryonic fibroblasts (MEFs) (Figure 4.8, panel A-C). Tw2-tdTO$^+$ clones were then cultured for 3 wk in growth medium before being switched to differentiation medium to induce cardiogenesis (Figure 4.8, panel C). CMs derived from individual Tw2-tdTO$^+$ clones were identified by immunostaining for cTnT and were captured by high-throughput confocal microscopy. Of 4,512 Tw2-tdTO$^+$ clones, 43 were positive for cTnT staining (Figure 4.8, panel C), while other clones were negative for cTnT (Figure 4.8, panel D), demonstrating that 0.95% of the Tw2-tdTO$^+$ single clones differentiate into CMs in vitro. Taken together with the in vivo observations, these findings suggest that a subset of Tw2-tdTO$^+$ cells has the potential to differentiate into CMs.

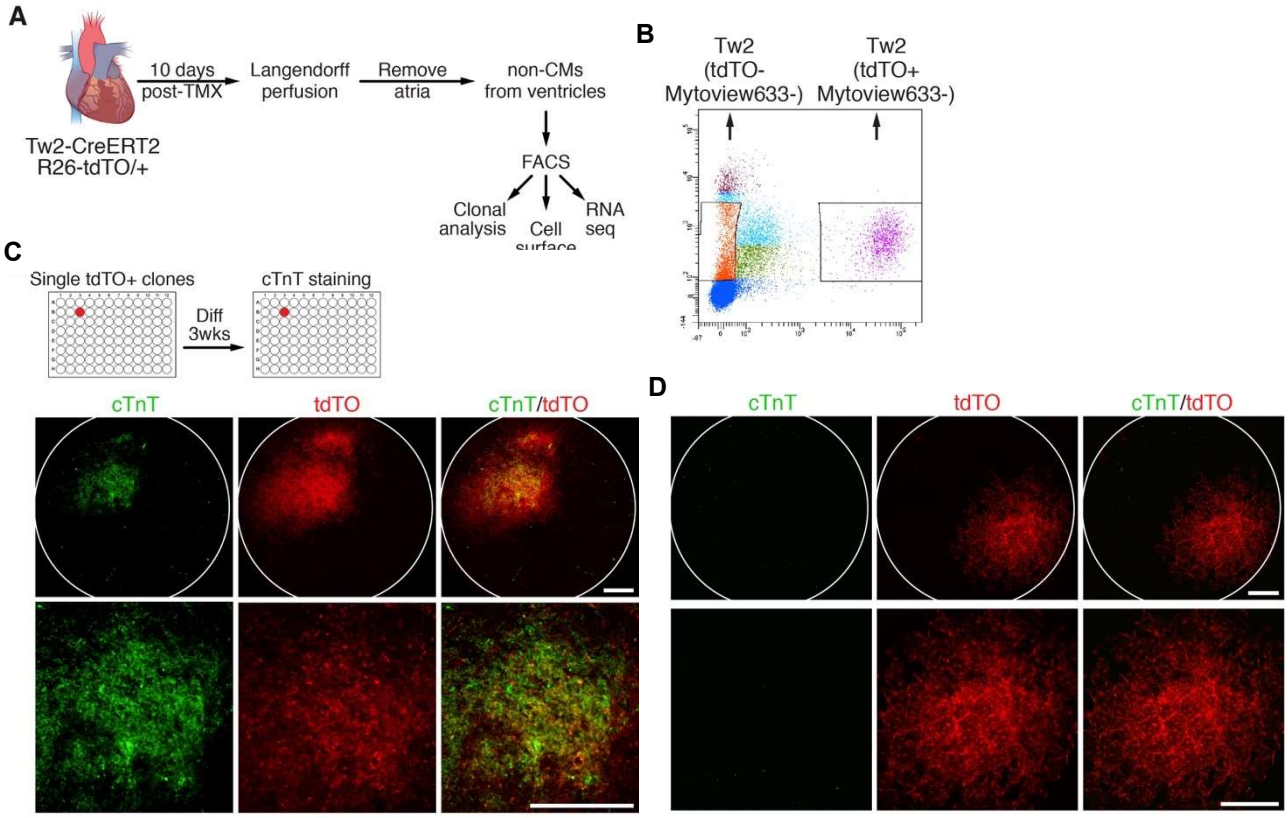

Figure 4.8 (A) Schematic of analyzing Tw2-tdTO+ cells in vitro. Following Langendorf perfusion and FACS isolation, Tw2-tdTO+ cells from ventricles were subjected to cell-surface marker analysis and RNA-seq. In addition, single Tw2-tdTO+ clones were plated on 96-well plates for clonal analysis. (B) FACS plot showing isolation of Tw2-tdTO+ (tdTO+; Mitoview 633^{low}) and Tw2-tdTO- (tdTO- Mitoview 633^{low}) cell populations from ventricles of Tw2-CreERT2; R26-tdTO mice at 10 days post-TMX treatment. (C) Representative images of a well conaining cTnT+ cells from clonal analysis. The images were acquired using an INCell high throughput confocal microscope under a 4X lens. Bottom panels show magnified images. Scale bar: 100 um. (D) Representative images of a well containing cTnT negative cells from clonal analysis. The images were acquired using an INCell high throughput confocal microscope under 4X lens. Bottom panels show magnified images. Scale bar: 100 um.

Molecular Signature of Tw2-tdTO$^+$ Cells.

To further define the molecular identity of Tw2-tdTO$^+$ cells, we examined by FACS analysis the expression of cell-surface markers on Tw2-tdTO$^+$ cells freshly isolated from 8-wk-old Tw2-CreERT2; R26-tdTO/$^+$ mice at 10 d post-TMX treatment (Figure 4.8, panel A). Tw2-tdTO$^+$ cells were identified as tdTO$^+$ and Mitoview 633^{low} cells (Figure 4.8, panel B). FACS analysis revealed that the CPC marker c-kit was expressed in 10.2% of Tw2-tdTO$^+$ cells, while Sca1 was expressed in 2.3% of the cells. In addition, consistent with the in vivo findings, 10.4% of the Tw2-tdTO$^+$ cells expressed the EC marker CD31, and 39.1% of them were identified as fibroblasts by CD90$^+$ and CD31$^-$ surface maker staining (Figure 4.9, panel A). To confirm the fidelity of the FACS analysis, we immunostained Tw2-tdTO$^+$ cells for cTnT and Twist at 10 d post-TMX treatment and found that 97.8% of the Tw2-tdTO$^+$ cells were Twist$^+$ and 99.93% were cTnT$^-$ (Figure 4.9, panel B). Furthermore, 93.8% of the Tw2-tdTO$^+$ cells expressed the mesenchymal stem cell (MSC) marker CD105, while other MSC markers, such as CD73, CD44, and CD29, were expressed at varying levels in Tw2-tdTO$^+$ cells (Figure 4.9, panel A). Multicolor FACS analysis using an MSC antibody panel revealed that 1.2% of the Tw2-tdTO$^+$ cells expressed the consensus MSC markers CD105, CD29, and Sca-1 but not CD45 (Figure 4.9, panel C). MSCs have the potential to differentiate into CMs both in vitro and in vivo (Makino et al., 1999; Toma et al., 2002). Therefore, it is possible that the cardiogenic population of Tw2-tdTO$^+$ cells represents a subset of resident MSCs.

A

Markers	Cell population	Percent in tdTO+ non-CMS
CD105	MSC, ECs	93.8
CD73	MSC	50.2
CD44	MSC	9.7
CD29	MSC	6.6
c-kit	HSC,MPP, CMP	10.2
Sca1	MSC, HSC	2.3
Sca1+/pdgfra+	Cardiogenic population in Sca1+	1.5
CD31	ECs	10.4
CD90+/CD31-	Fibroblasts	39.1
cTnT	CM	0.07
Twist		97.8

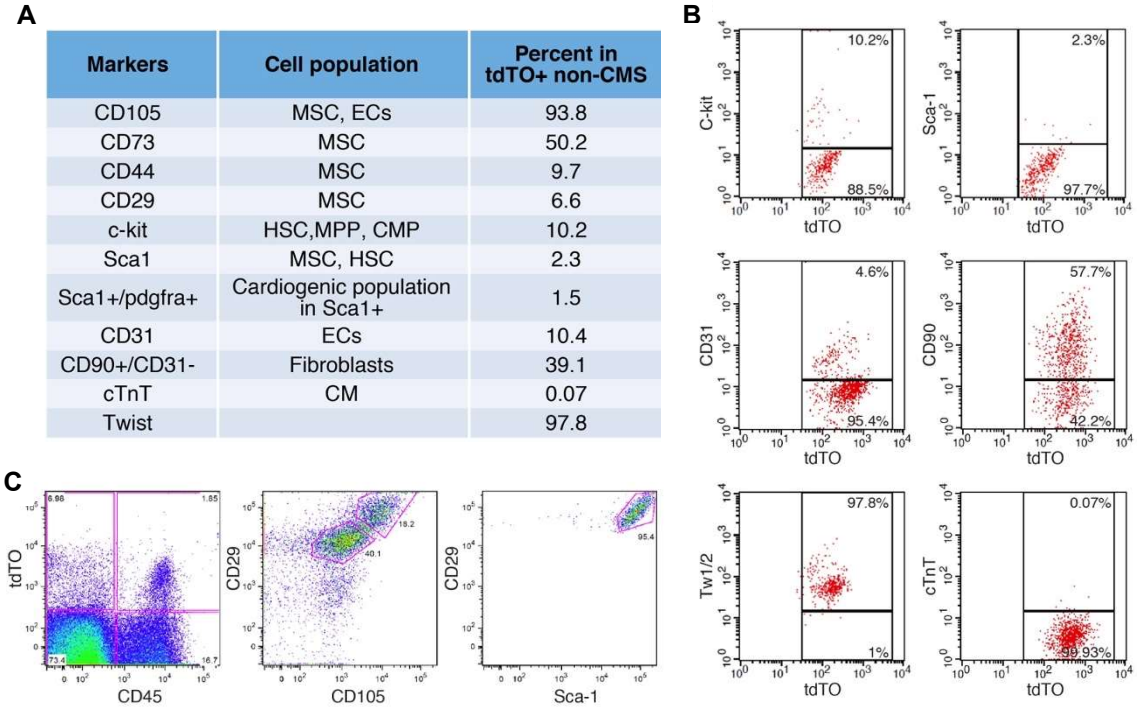

Figure 4.9 (A) Summary of cell marker expression of Tw2-tdTO+ cells by FACS analysis. (B) FACS analysis for expression of Twist, cTnT, CD31, and CD90 was performed on Tw2-tdTO+ cells isolated from ventricles of Tw2-CreERT2; R26-tdTO mice at 10 days post-TMX treatment. (C) FACS plot showing multi-color MSC panel analysis of Tw2-tdTO+ cells isolated from ventricles of Tw2-CreERT2; R26-tdTO mice at 10 days post-TMX treatment. CD45-, CD29+, CD105+, and Sca-1+ mark MSC population.

We also quantified the contribution of Tw2-tdTO$^+$ cells to ECs and fibroblasts over time by FACS analysis. At 10 d postTMX treatment, 3.1% of the Tw2-tdTO$^+$ cells were identified as ECs, and the number increased to 33.4% at 4 mo post-TMX treatment (Figure 4.10, panel A). In addition, Tw2-tdTO$^+$ cells accounted for 6.4% of all cardiac fibroblasts at 10 d, and the population increased to 38.1% at 4 mo post-TMX treatment (Figure 4.10, panel B). We conclude that Tw2-tdTO$^+$ cells contribute to a substantial proportion of ECs and

fibroblasts in the heart. However, since 3.1% of ECs and 6.4% of cardiac fibroblasts are labeled by tdTO at 10 d post-TMX treatment, we cannot exclude the possibility that Tw2 is expressed in a small population of ECs and fibroblasts which give rise to more ECs and fibroblasts over time.

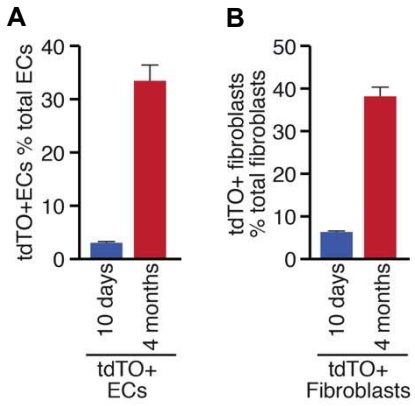

Figure 4.10 (A) Quantification of Tw2-tdTO+ ECs as a percentage of total cardiac ECs at 10 days and 4 months post-TMX treatment as determined by FACS analysis. n=3 mice for each time point. (B) Quantification of Tw2-tdTO+ fibroblasts as a percentage of total cardiac fibroblasts at 10 days and 4 months post-TMX treatment as determined by FACS analysis. n=3 mice for each time point. Data in A and B are expressed as mean ± SEM.

Single-Cell RNA Sequencing of Tw2$^+$ Cells.

To determine whether Tw2-tdTO$^+$ cells are a homogenous or heterogeneous cell population, we performed single-cell RNA-sequencing (scRNA-seq) on the Tw2-tdTO$^+$ cells. Tw2-tdTO$^+$ cells were isolated by FACS based on the expression of tdTO from ventricles of Tw2-CreERT2; R26-tdTO/$^+$ mice at 10 d post-TMX treatment. Graphic clustering based on transcriptional similarities revealed four main clusters of 232 Tw2-tdTO$^+$ cells, indicating that they are a heterogeneous population (Figure 4.11, panel A). Each cluster exhibited distinct gene-expression patterns (Figure 4.11, panel B), which could be categorized as ECs, fibroblasts, immune cells, and smooth muscle cells based on the top 10 marker genes. Further clustering using MSC cell markers revealed that a small population of Tw2-tdTO$^+$ cells

expresses MSC marker genes, correlating with the results of FACS analysis (Figure 4.9, panel A and C and Figure 4.11, panel C).

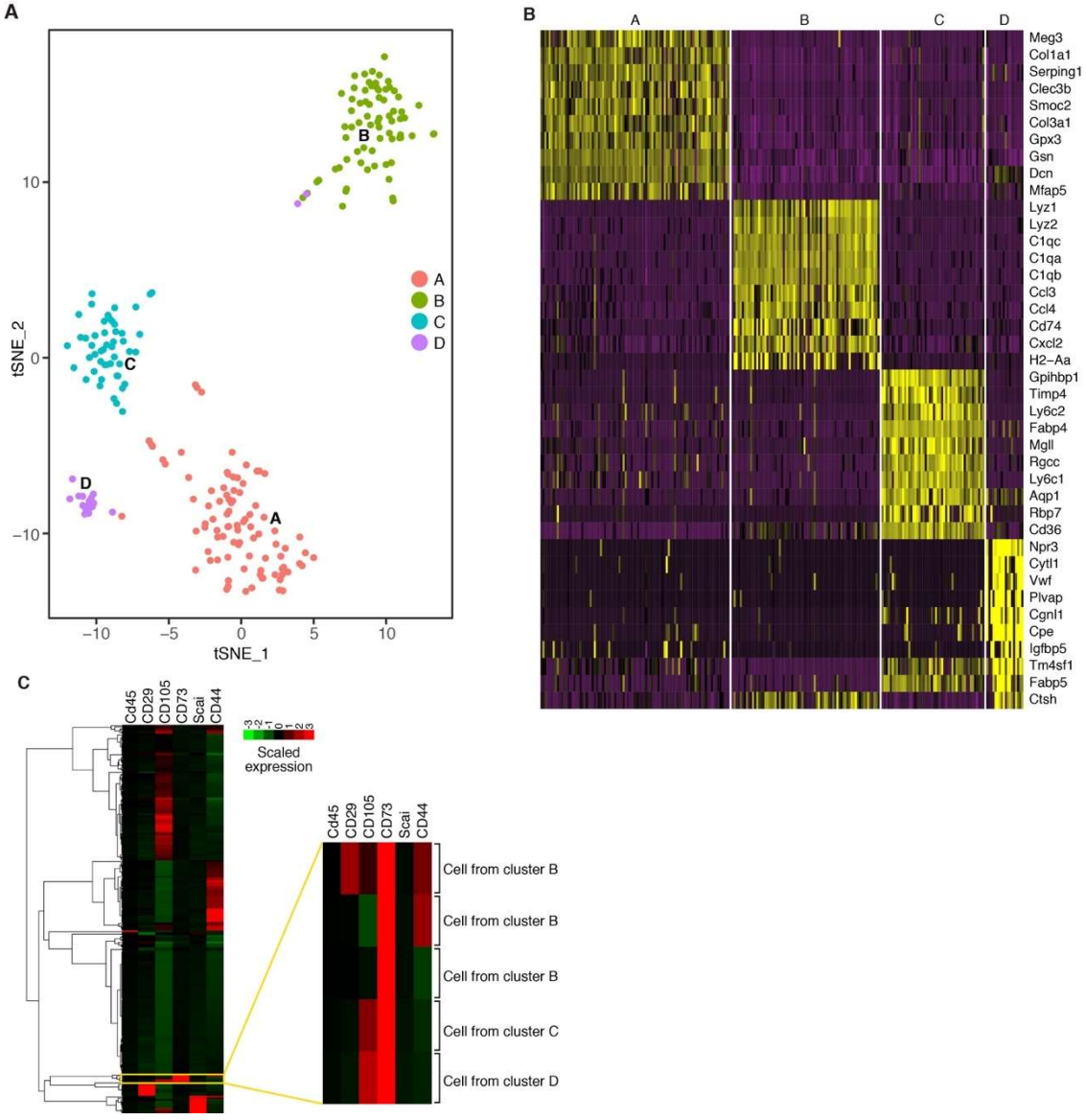

Figure 4.11 Single cell RNA-seq of Tw2-tdTO+ cells. (A) tSNE plot of the Tw2-tdTO+ cells. Each cluster is alphabetically labeled and color coded. (B) Heat map of the 5 clusters with top 10 enriched marker genes, as identified by single cell RNA-seq. (C) Heat map showing the expression of 6 MSC marker genes in each of the single Tw2-tdTO+ cells.

To determine the molecular signature of Tw2-tdTO^{+} cells, we performed unbiased transcriptome profile analysis by RNA-seq. Tw2-tdTO^{+} and Tw2-tdTO^{-} cells were isolated by FACS based on the expression of tdTO from ventricles of Tw2-CreERT2; R26- tdTO/$^{+}$ mice at 10 d post-TMX treatment (Figure 4.8, panel A). Transcriptome analysis revealed that Tw2-tdTO^{+} cells and Tw2- tdTO^{-} cells displayed highly distinct gene-expression patterns (Figure 4.12, panel A). Bioinformatics analysis identified 3,365 genes that were differentially expressed between the two populations, with 1,502 genes being enriched in Tw2-tdTO^{+} cells and 1,863 genes being down-regulated (Figure 4.12, panel A). A list of the top 20 enriched genes in Tw2-tdTO^{+} cells is shown in Fig. 5B, including the known Tw2 target genes Ctgf, Htr2b, and Sox9, the EMT regulators Foxc1, Foxc2, and Tgfb2, and Fgf2, an upstream regulator of Tw2 (Figure 4.12, panel B). Sixteen gene-expression clusters were assigned according to the hierarchy correlations of the differentially expressed genes (Figure 4.12, panel A). These clusters were functionally annotated using Gene Ontology (GO) analysis and compared using clusterProfiler (Figure 4.12, panel C). Clusters 2–7 represent the enriched genes in the Tw2-tdTO^{+} cells, and clusters 9–15 represent the enriched genes in the Tw2-tdTO^{-} cells. Clusters for enriched genes in Tw2-tdTO^{+} cells were grouped into several GO biological functions (Figure 4.12, panel C). Angiogenesis-, mesenchymal tissue development-, and epithelial cell proliferation-related genes were enriched in clusters 2 and 4. In addition, cluster 4 includes genes involved in epithelial cell migration. These results are consistent with the known functions of Tw2 in these pathways. Cluster 3 represents kidney morphogenesis- and renal developmental-related genes, which is consistent with reports showing that Tw1 activation is a common mechanism in the pathophysiology of a wide range of chronic renal

diseases (Grande et al., 2015; Lovisa et al., 2015). Ribosomal RNA processing- and ribosome biogenesisrelated genes were represented in clusters 4 and 7. Enriched genes in the Tw2-tdTO^{-} cells correlated with immune cell activation, migration, and proliferation pathways, as depicted in clusters 9, 10, 12, and 14 (Figure 4.12, panel C). Ingenuity Pathway Analysis (IPA) also revealed that genes with enriched expression in Tw2-tdTO^{+} cells were involved in EIF2 signaling, mTOR signaling, embryonic stem cell pluripotency, EMT, and cancer metastasis, consistent with the known functions of Tw2 in these pathways (Figure 4.13, panel A). GO analysis revealed similar pathways for genes with enriched expression in Tw2-tdTO^{+} cells (Figure 4.13, panel B).

Comparison of Cardiac and Skeletal Muscle Tw2^{+} Cells.

Within adult skeletal muscle, Tw2 marked an interstitial myogenic progenitor population that contributes to type IIb/x myofibers (Liu et al., 2017). To determine the similarity of Tw2-tdTO^{+} cells in heart and skeletal muscle, we compared the transcriptome of these two cell populations and found that they were significantly different by principal component analysis (PCA) (Figure 4.12, panel D). Whereas 380 genes were enriched in Tw2-tdTO^{+} cells from both heart and skeletal muscle, 1,123 genes were enriched only in cardiac Tw2-tdTO^{+} cells, and 2,133 genes were expressed only in Tw2-tdTO^{+} cells from skeletal muscle (Figure 4.12, panel E). These results are consistent with our in vitro differentiation assays and indicate that Tw2-tdTO^{+} cells from the heart and skeletal muscle are largely distinct populations derived from different origins. Interestingly, IPA analysis of the 380 genes that were coexpressed in the two Tw2-tdTO^{+} populations revealed that they are involved in pathways associated with stemness,

such as cancer metastasis, embryonic stem cell pluripotency, and cardiogenesis (Figure 4.13, panel C). Since Tw2-tdTO^{+} cells have fusogenic potential, we looked for known muscle cell fusionrelated genes, such as myomaker and myomixer in the Tw2- tdTO^{-} and Tw2-tdTO^{+} populations. No significant differences in expression of myomaker and myomixer were detected between the two populations (Figure 4.13, panel D).

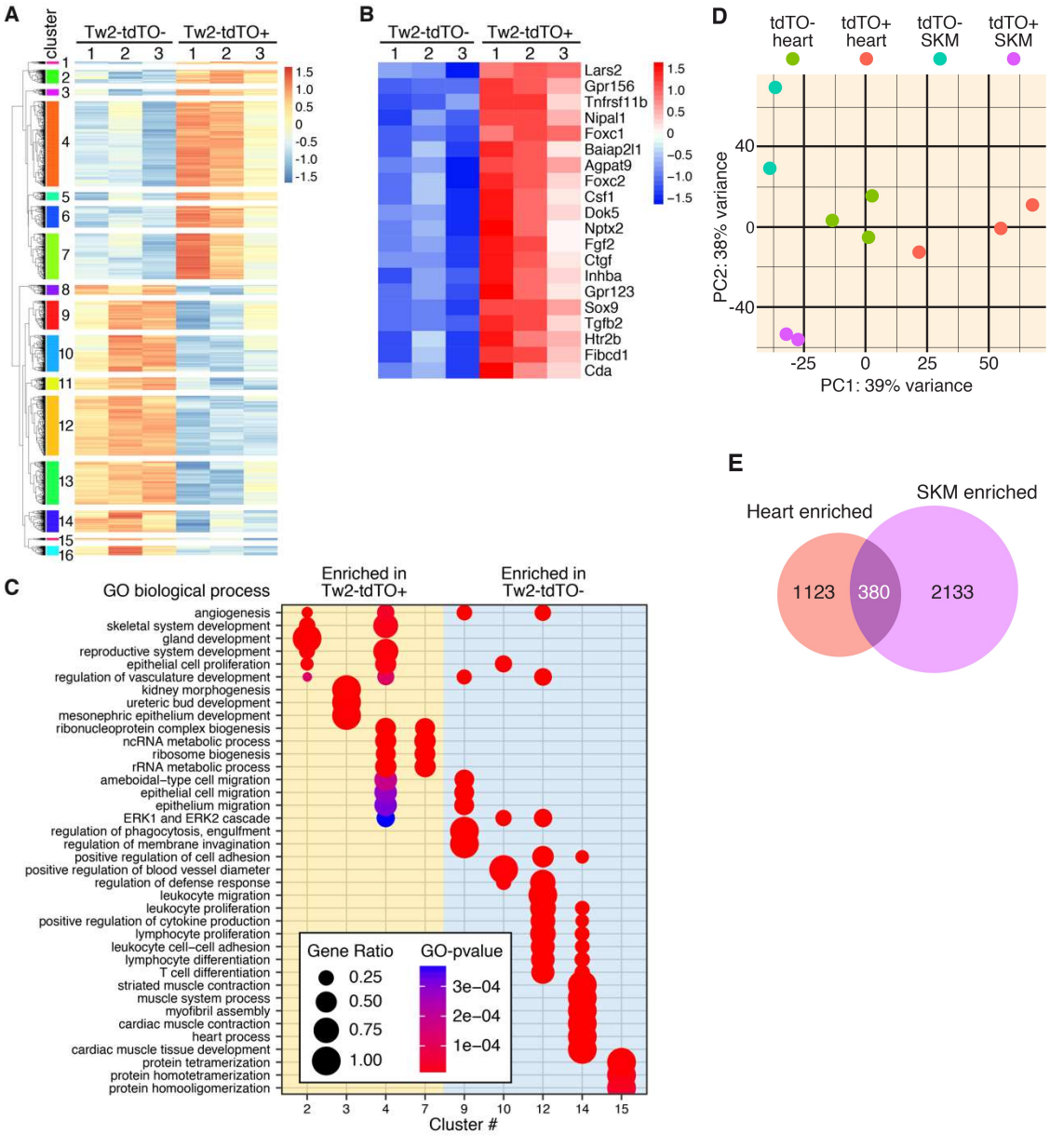

Figure 4.12 Transcriptome analysis of Tw2-tdTO+ cells in adult heart. (A) Heat map of 3,365 genes in freshly sorted Tw2-tdTO+ and Tw2-tdTO- cells in the heart as identified by RNA-seq. Cells were isolated by FACS from ventricles of Tw2-CreERT2; R26-tdTO mice at 10 days post-TMX treatment. n=3 for each sample. Sixteen clusters of genes were identified and indicated on the left panel. (B) Top 20 most enriched genes in Tw2-tdTO+ cells, as identified by RNA-seq. (C) The GO enrichment by differentially expressed genes in Tw2-tdTO+ and Tw2-tdTO- cells analyzed using clusterProfiler R package. GeneRatio, the size of the circle, corresponds to the number of genes enriched for a particular GO term. Enrichment term is represented by colored dots (red indicates high enrichment and blue indicates low enrichment). (D) Principle Component Analysis (PCA) of Tw2-tdTO+ and Tw2-tdTO- cells in skeletal muscle (SKM) and hearts from Tw2-CreERT2; R26-tdTO mice identified by RNA-seq. (E) Venn diagram indicates overlapping genes and differentially expressed genes between Tw2-tdTO+ cells in heart and SKM, respectively.

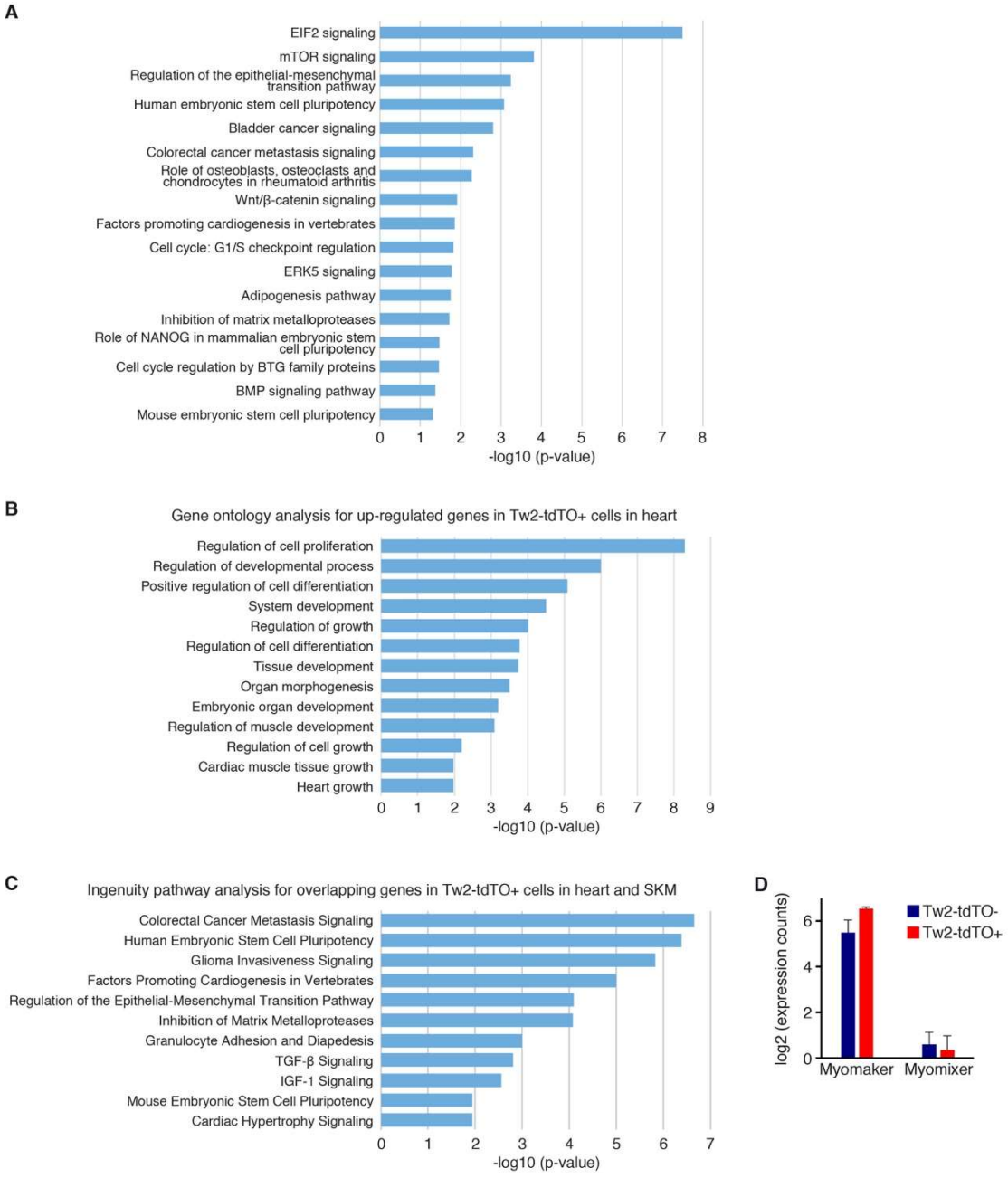

Figure 4.13 RNA-seq analysis of Tw2-tdTO+ cells. (A) IPA analysis of genes enriched in Tw2-tdTO+ cells relative to Tw2-tdTO- cells. (B) GO analysis of up-regulated genes in Tw2-tdTO+ cells compared to Tw2-tdTO- interstitial cells. (C) IPA analysis of the 380 overlapping genes in Tw2-tdTO+ cells in heart and skeletal muscle (SKM). (D) Myomaker and myomixer expression profile in Tw2-tdTO+ and Tw2-tdTO- cells.

Tw2-tdTO$^+$ Cells Contribute to Cardiac Remodeling After Myocardial Infarction.

Our results showed that Tw2-tdTO$^+$ cells give rise to CMs in the young adult heart. To determine whether Tw2- tdTO$^+$ cells contribute to cardiac remodeling after injury, we performed permanent ligation of the left anterior descending (LAD) artery to induce MI in 9-wk-old Tw2-CreERT2;R26- tdTO mice that had been treated with TMX 1 wk before surgery, as schematized in Figure 4.14, panel A. One week post-MI, Tw2-tdTO$^+$ cells were strongly activated at the infarct and border zones of infarcted hearts (Figure 4.14, panel B), and there were more Tw2-tdTO$^+$ CMs in the remote zone following MI than in mice treated with sham surgery (Figure 4.14, panel B and Figure 4.15, panel A). We also performed transient LAD artery ligation followed by release of the ligation to induce ischemia–reperfusion (I/R) injury and observed similar accumulation of Tw2-tdTO$^+$ interstitial cells and CMs at 1 wk postinjury (Figure 4.14, panel B). Injury-induced Tw2-tdTO$^+$ interstitial cells expressed markers of ECs (CD31) or of fibroblasts (Vimentin) in the infarct zone, border zone, and remote zone of MI or I/R hearts (Figure 4.14, panel C and Figure 4.15, panel B). More Tw2-tdTO$^+$ cells differentiated into ECs than into fibroblasts after injury (Figure 4.14, panel C and D). Tw2-tdTO$^+$ ECs were more abundant in the infarct and border zones than in the remote zone (Figure 4.14, panel C and D). Tw2-tdTO$^+$ cells continued to accumulate in the infarct zone of MI or I/R hearts at 2 wk postinjury (Figure 4.15, panel C). Together, these results indicate that Tw2-tdTO$^+$ cells participate in cardiac remodeling during injury.

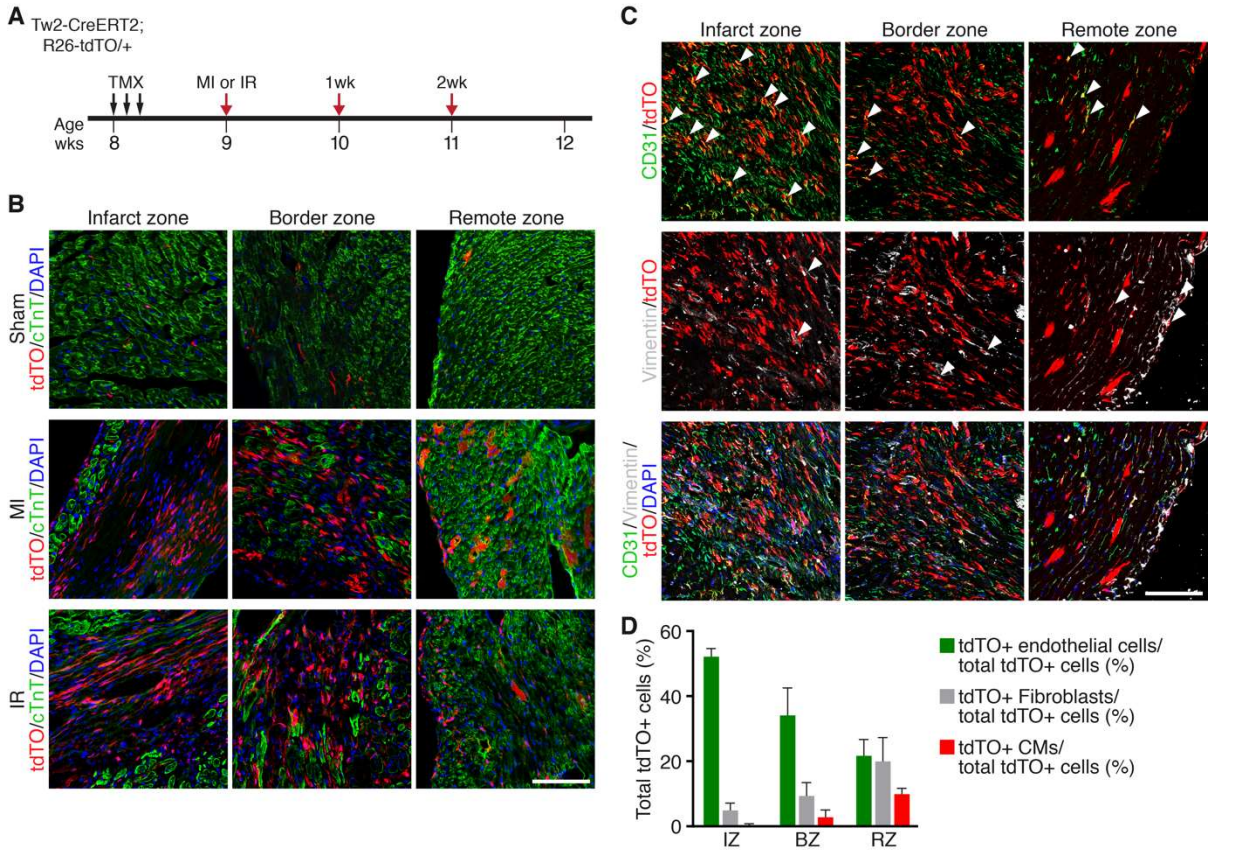

Figure 4.14 Tw2-tdTO+ cells contribute to cardiac remodeling after MI. (A) Schematic of TMX treatment and LAD ligation to induce MI or IR on Tw2-CreERT2; R26-tdTO mice. (B) Different areas of the heart after MI and IR were immunostained with cTnT (green). Infarct zone in the left panels, border zone in the middle panels, and remote zone in the right panels after 1 week of MI. Scale bar: 100 um. (C) Different areas of the heart after 1 week of MI were co-stained with vimentin (grey) and CD31 (green). White arrowheads indicate co-localization with tdTO signals. Infarct zone in the left panels, border zone in the middle panels, and remote zone in the right panels after 1 week of MI. Scale bar: 100 um. (D) Quantification of tdTO+ ECs, fibroblasts, and CMs as a percentage of total of total tdTO+ cells in the infarct zone (IZ), boarder zone (BZ) and remote zone (RZ) of the heart after 1 week of MI. n=3. Data is expressed as mean ± SEM.

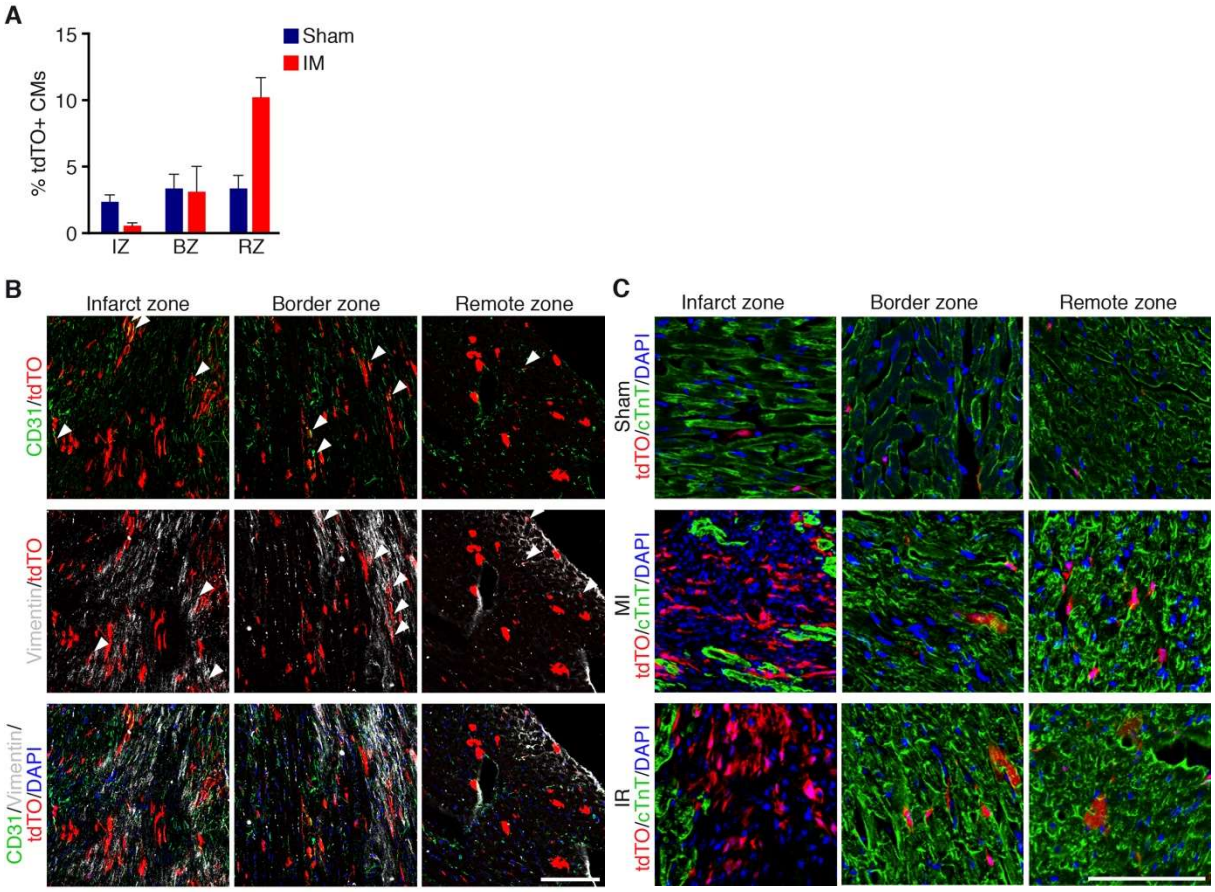

Figure 4.15 Tw2-tdTO+ cells during myocardial injury after MI and I/R. (A) Quantification of the Tw2-tdTO+ CMs in infarct zone (IZ), boarder zone (BZ) and remote zone (RZ) after sham and MI injury. (B) Different areas of the heart after 1 week of IR were co-immnuostained with vimentin (grey) and CD31 (green). Infarct zone in the left panels, border zone in the middle panels, and remote zone in the right panels after 1 week of IR. Scale bar: 100 um. (C) Immunostaining of different areas of the heart after MI. Infarct zone in the left panels, border zone in the middle panels, and remote zone in the right panels after 2 weeks of MI and I/R. cTnT marks cardiomyocytes in green. Scale bar: 100 um.

Discussion

Using genetic lineage tracing, we identified a previously unrecognized population of cardiogenic cells in the adult heart marked by the expression of Tw2. Tw2-tdTO$^+$ cells can contribute to CMs, ECs, and fibroblasts in vivo and in vitro (Figure 4.16). We did not exclude the possibility that the population of Tw2- tdTO$^+$ cells contains a subset of ECs and fibroblasts before 10 d post-TMX treatment, thus continuously giving rise to subsequent EC and fibroblast populations. Although the majority of Tw2- tdTO$^+$ cells contribute to CMs via fusion, a small subset of Tw2- tdTO$^+$ cells can differentiate into CMs in vivo and in vitro, confirming their cardiogenic potential. Tw2-tdTO$^+$ cells are activated in response to MI and I/R injury. Tw2-tdTO$^+$ cells appear to represent a subset of MSCs and are distinct from other CPCs that have been reported to give rise to CMs, including Sca1$^+$, c-kit$^+$, SPs, and endothelial-derived CPCs.

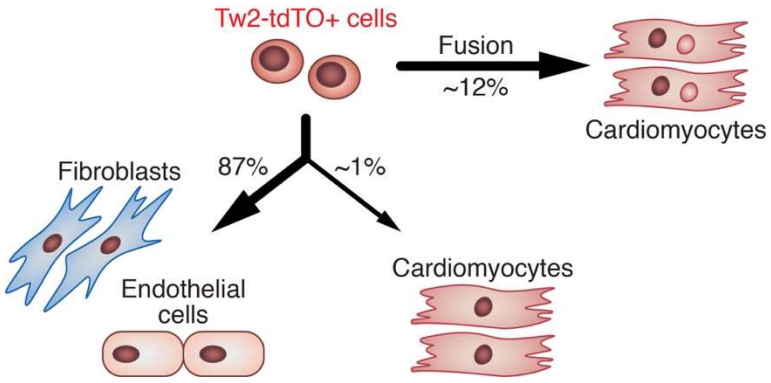

Figure 4.16 Model for the role of Tw2-tdTO+ cells in heart maintenance. In the adult heart, Tw2-tdTO+ cells can give rise to cardiomyocytes and maintain a group of fibroblasts and endothelial cells. Tw2-tdTO+ cells contribute to cardiomyocytes mainly by fusion.

Comparison with Other CPCs.

There is intense debate in the field as to whether adult CPCs exist and make functional contributions to the adult heart (Leri et al., 2015; van Berlo et al., 2014; van Berlo and Molkentin, 2014). Sca1-derived cells have been reported to make a substantial and lasting contribution to CMs during normal aging (Uchida et al., 2013). These cells are a source for CM renewal rather than fusion. $Sca1^+$ cells were further subdivided based on marker gene expression, among which the $PDGFR\alpha^+$/ $Sca1^+$ subgroup displayed both cardiogenic potential and clonogenicity (Noseda et al., 2015). In addition, ECs retain cardiogenic potential in specific areas of the adult heart (Fioret et al., 2014). Endothelial-derived CPCs express GATA4 and Sca1, and the majority of $Sca1^+$ CPCs are derived from cells with endothelial characteristics, indicating substantial overlap between these CPC populations (Fioret et al., 2014). Tw2- $tdTO^+$ cells from the adult heart share similarities with these cells in terms of cardiogenic potential and clonogenicity. However, based on FACS analysis, less than 3% of Tw2-$tdTO^+$ cells express Sca1 and Sca1/PDGFRα, and only 10% are $CD31^+$. In addition, our study shows that Tw2-$tdTO^+$ cells contribute to 13% of CMs after 4 mo of lineage tracing, which is a higher level than reported by lineage tracing with other CPC markers (Uchida et al., 2013; van Berlo et al., 2014). These results indicate that Tw2-$tdTO^+$ cells are distinct from $Sca1^+$, c-kit^+, and EC-derived CPCs. Our study also showed that Tw2-$tdTO^+$ cells are a heterogeneous population, as assessed by FACS analysis and scRNA-seq. These results indicated that there is a potential subpopulation within the Tw2- $tdTO^+$ population that contributes to specific cell types. MSCs have been shown to differentiate into CMs both in vitro (Makino et al., 1999) and in vivo (Toma et al., 2002). In humans, a novel population of

MSCs marked by expression of W8B2 has been found in adult atrial appendages (Zhang et al., 2015). These W8B2$^+$ CPCs are clonogenic, are capable of selfrenewal in culture, and can give rise to several cell lineages within the heart, including CMs, ECs, and smooth muscle cells (Zhang et al., 2015). It will be interesting to examine whether Tw2-tdTO$^+$ cells also exist in humans and whether there is overlap between Tw2- tdTO$^+$ cells and W8B2$^+$ CPCs.

Fusion and Ploidy.

While adult CMs are generally multinucleated, the potential contributions of fusion versus nuclear division without cytokinesis to this phenomenon are not fully understood. A recent study reported transient membrane fusion events in the zebrafish heart (Sawamiphak et al., 2017). Fusion between CMs and resident cells or CMs within the adult heart has not been characterized in mice, possibly due to the lack of knowledge of the cell types and/or markers for this event. Our findings show that resident Tw2-tdTO$^+$ cells can fuse with existing CMs during normal aging in mice. Interestingly, fusion of Tw2-tdTO$^+$ cells with CMs occurs only in young adult but not in aged mice. Cell fusion can provide specific proteins or change gene expression of CMs during aging. It would be interesting to understand the downstream gene-expression differences between the Tw2-tdTO$^+$ cells in 2-mo-old and 7-moold mouse hearts, which may provide insights into the potential mechanism for CM maintenance under homeostasis in young and old adult hearts. Cell fusion can offer substantial beneficial effects in the setting of heart disease. For example, transplanted bone marrow cells have been shown to fuse with CMs to rescue them from apoptosis and restore cardiac function following ischemic injury (Garbade et al., 2005; Nygren et al., 2004; Yang et al., 2012). Thus, enhancing cell fusion may provide a means of preserving CMs following MI. Since Tw2 tdTO$^+$ cells are

activated following MI, they might play a role in maintaining CM survival and/or function after injury.

Twisting Cell Fate.

Twist proteins can influence cell-fate decisions by inhibiting lineage-specific transcription factors, such as MyoD in the muscle lineage (Gong and Li, 2002). Twist proteins can also reverse the terminal differentiation of myotubes and promote their proliferation to become undifferentiated myoblasts (Hjiantoniou et al., 2008; Liu et al., 2017). RNA-seq analysis confirmed that Tw2 overexpression inhibits myogenesis and activates genes involved in cell-cycle regulation, cancer metastasis, many signaling pathways, and EMT (Liu et al., 2017). Generating heart-specific Tw2 and/or Tw1 conditional-knockout mice would reveal the cardiac lineage contribution of Twist proteins. In addition, Twist has been reported to inhibit chondrogenesis (Reinhold et al., 2006) and osteogenesis (Bialek et al., 2004) but to promote adipogenesis (Isenmann et al., 2009). Similar results were observed when Twist proteins were overexpressed in human bone marrow MSCs. MSCs overexpressing Tw1 and Tw2 showed a higher proliferation rate and extended life span and maintained an immature mesenchymal precursor phenotype (Isenmann et al., 2009). In this study, Tw2 was used as a marker for lineage tracing in the heart. However, given the involvement of Twist proteins in differentiation of several MSC lineages, it is conceivable that Tw2 plays a role in regulating cardiac lineage and CM homeostasis in adult mice.

Materials and Methods

Mouse Lines

Tw2-CreERT2 mice were previously described (33). R26-tdTO [(ROSA)26Sortm14(CAG-tdTomato) , stock no. 007914], and ROSA26-mT/mG [(ROSA)26Sortm4(ACTB-tdTomato,-EGFP)Luo/J, stock no. 007576)] mice were obtained from the Jackson Laboratory. Both male and female adult mice were used in the studies. Mice were maintained on a mixed genetic background. Mice were maintained in 12-h light:dark cycles (light: 6:00 AM to 6:00 PM) at 22 °C. Animal work described in this paper was approved by and conducted under the oversight of the University of Texas Southwestern Institutional Animal Care and Use Committee.

Primary Cultures

Tw2-CreERT2;R26-tdTO mice were treated with TMX at 8 wk of age. At 10 d after the first dose of TMX, a pool of cardiac cells from ventricles (the atria were removed) was isolated using Langendorff perfusion. Cells were then further separated by gravity and a BSA gradient into CM-enriched and non–CM-enriched populations. Staining with Mitoview 633 (Biotium) was performed on the non-CM population, which was then sorted on a BD Aria cell sorter based on tdTO and Mitoview633 signals. Tw2-TdTO$^+$ cells and Tw2-TdTO$^-$ cells were harvested for subsequent culturing, staining, clonal analysis, or RNA-seq analysis. Tw2-tdTO$^+$ cells were isolated by FACS sorting as the tdTO$^+$ and Mitoview 633low population. Cells were maintained in cardiac stem cell maintenance medium (catalog no. SCM101; Millipore). For CM differentiation, cells were switched to cardiomyocyte differentiation medium (catalog no.

SCM102; Millipore). For EC differentiation, cells were cultured in EGM-2 BulletKit EC growth medium (catalog no. CC-3162; Lonza). For culturing fibroblasts, cell were maintained in DMEM and 10% FBS.

TMX Treatment

Mice were randomly divided into treatment groups while satisfying the criterion that the average body weight in each group would be about the same. TMX (Sigma-Aldrich) was dissolved at 10 mg/mL in a mixture of sesame oil and ethanol (9:1) and was administered by i.p. injection as schematized in the figures. Tw2-CreERT2; R26-mTmG mice were placed on TMX-containing diet (250 mg/kg) (Harlan Laboratories) immediately following TMX injection.

Histology and Immunohistochemistry

For immunohistochemistry, hearts were harvested and fixed in 4% paraformaldehyde at 4 °C for 1 h. Tissues were then switched to 10% sucrose/PBS overnight followed by 18% sucrose/PBS at 4 °C overnight before they were frozen, embedded, and sectioned. For immunostaining, slides were rinsed three times in PBS and blocked in 10% goat serum for 20 min followed by three rinses in PBS. This was followed by overnight incubation with primary antibodies (see Table 4 for antibody information). The following day, slides were washed three times in PBS and incubated with anti-mouse and anti-rabbit secondary antibodies conjugated to Alexa Fluor 488 or 555 (1:400 dilution; Invitrogen) for 1 h at room temperature. Slides were washed three times in PBS and mounted in VECTASHIELD containing DAPI (Vector

Laboratories). For a list of primary antibodies, please refer to Table 4. Following isolation, mononuclear cells were resuspended in PBS/2% BSA at 1 × 106 cells/50 μL, aliquoted into 100 μL per tube, and incubated on ice for 1 h with Fc blocking agent and one of the following fluorophoreconjugated antibodies: CD73-Alexa Fluor 488 rat IgG2A (1:50), CD44-APC rat IgG2B (1:50), CD117-APC rat IgG2B (1:50), CD31-APC rat IgG2A (1:50), CD90.2-APC rat IgG2A (1:50), Ly-6A/E-APC-Cy7 rat IgG2A (1:20) (all from BD Biosciences-Pharmingen), CD105-APC rat IgG2A (1:50; BioLegend), pdgfraAlexa Fluor 488 goat IgG (1:50; R&D Systems), CD45-PerCP rat IgG2B (1:20; R&D Systems), CD29-APC hamster IgG (1:20; eBioscience), or CD105/EndoglinCFS rat IgG2A (1:20; R&D Systems). Isotype-specific controls were also performed on these cells. Unstained cells isolated from Cre^{+} and Cre^{-} mice were used as unstained controls. Cells were analyzed on a FACSCalibur (BD) flow cytometer, and FACS data were analyzed using FlowJo Software (Tree Star). For a list of primary antibodies, please refer to Table 4. Immunostaining of Cultured Cells. Cells grown on plates or chamber slides were fixed with 4% paraformaldehyde at room temperature for 15 min and subsequently permeabilized with 0.3% Triton X-100/PBS. Cells were blocked in 10% goat serum diluted in 0.1% Triton X-100/PBS at room temperature for 1 h. Primary antibodies were diluted in 1% goat serum/0.1% TritonX-100 and were incubated at room temperature for 2 h (See Table 4 for antibody information). Cells were washed, and secondary antibodies were diluted in 1% goat serum/0.1%Triton X-100 and were incubated at room temperature for 1 h. After washing with PBS, coverslips were mounted on glass slides with VectoLab Mounting Medium (with DAPI) (Vector Laboratories).

Clonal Analysis

MEFs were used as feeder cells for clonal analysis. One day before FACS sorting, confluent MEFs were treated with 8 μg/mL of mitomycin C for 2.5 h at 37 °C to inhibit cell proliferation. Cells were then washed twice with PBS followed by trypsinization. MEFs were then seeded into 96-well plates at a density of 1.5 × 106 cells per plate in DMEM/10% FBS/penicillin and streptomycin and were allowed to attach overnight at 37 °C. Two hours before sorting, the medium was replaced with cardiac stem cell maintenance medium (catalog no. SCM101; Millipore). Single clones of Tw2-tdTO^{+} cells were sorted by FACS onto 96-well plates coated with MEFs, were cocultured for 3 wk in cardiac stem cell maintenance medium, and then were switched to CM differentiation medium (catalog no. SCM102; Millipore) to promote CM differentiation. Cells were then stained with cTnT and Hoechst. Highthroughput imaging was performed using an IN Cell Analyzer 600 Cell Imaging System (GE Healthcare Life Sciences).

Adult MI and I/R

Mice (8–12 wk old) were anesthetized with 2.4% isoflurane and placed in a supine position on a heating pad (37 °C). Animals were intubated with a 19-gauge stump needle and were ventilated with room air using a MiniVent mouse ventilator (Hugo Sachs Elektronik; stroke volume, 250 μL; respiratory rate, 210 breaths/min). Via left thoracotomy between the fourth and fifth ribs, the LAD artery was visualized under a microscope and ligated by using a 6–0 PROLENE suture. Regional ischemia was confirmed by visual inspection under a dissecting microscope (Leica) by discoloration of the occluded distal myocardium. For I/R, the ligation was released after 45 min of ischemia, and tissue was allowed to reperfuse as confirmed by

visual inspection. Sham-operated animals underwent the same procedure without occlusion of the LAD artery.

Single-Cell RNA-Seq and Analysis

Tw2-tdTO^{+} and Tw2-tdTO^{-} cells were isolated from 8-wk-old mouse hearts 10 d after TMX treatment using the protocol described in Primary Cultures section above. FACS-sorted cells were washed in PBS with 0.04% BSA and resuspended at a concentration of ∼1,000 cells/μL. Library generation for 10× Genomics v2 chemistry was performed following the Chromium Single Cell 3′ Reagents Kit v2 User Guide: CG00052 Rev B. Sequencing was performed on an Illumina NextSeq 500 sequencing platform using the 75-cycle kit. On average more than 500,000 reads per cell were sequenced. Fastq files were generated using cellranger mkfastq and were mapped to the mm10 genome using cellranger count with standard parameters. For cluster identification, R package Seurat (https://www.nature.com/articles/nbt.3192) was used. Briefly, the data matrices were imported into R and were processed with the Seurat R package version 1.2.1. A minimum cutoff of 200 genes per cell and a maximum cutoff of 5,000 genes per cell were used for this dataset. In addition, cells in which >25% of total reads aligned to the mitochondrial genome were removed. After data filtering, PCA was performed using highly variable genes. The first eight principal components were used to find clusters with the resolution parameter set to 1.0. Identified clusters were visualized with t-distributed statistical neighbor embedding (tSNE) plots. Marker genes for each cluster were identified using the FindMarkers function in Seurat. The scRNA-seq data have been deposited in the Gene

Expression Omnibus database under the ID code GSE118411 (https://www.ncbi.nlm.nih.gov/geo/query/acc.cgi?acc=GSE118411).

RNA-Seq and Real-Time RT-PCR Analysis

Cells were resuspended in 1 mL of TRIzol and homogenized using 20-gauge needles. Following chloroform extraction, the supernatant was mixed with an equal volume of 75% ethanol and loaded on RNeasy minicolumns (Qiagen). Total RNA was isolated according to the manufacturer's instructions (Qiagen). RNA quality was verified by the Agilent 2100 Bioanalyzer, and RNA-seq was performed using an Illumina HiSeq 2500 by the University of Texas Southwestern Genomics and Microarray Core Facility. For real-time RT-PCR analysis, total RNA was extracted from sorted cells with TRIzol (Invitrogen) following the manufacturer's instructions. cDNA was synthesized using SuperScript III reverse transcriptase (Invitrogen), and the expression of selected genes was analyzed by real-time RT-PCR using Taqman probes. Analysis of RNA-Seq Data. Quality assessment of the RNA-seq data was performed using the NGS-QC-Toolkit (v2.3.3) (journals.plos.org/plosone/article?id=10.1371/journal.pone.0030619). Reads with more than 30% nucleotides with phred quality scores less than 20 were removed from further analysis. Quality-filtered reads were then aligned to the mouse reference genome GRCm38 (mm10) using the Tophat2 (v 2.0.0) aligner using default settings except for –library-type = fr-firststrand. Aligned reads were counted using featurecount (v1.4.6) (https://academic.oup.com/bioinformatics/article/30/7/923/232889) per gene ID. Differential gene-expression analysis was done using the R package DEseq2 (v 1.6.3). Cutoff values of absolute fold change >1.5 and a false-discovery rate ≤0.05

were then used to select for differentially expressed genes between sample group comparisons. Normalized gene-count values were averaged within groups for heat map generation and were clustered using the R package clusterProfiler (v3.6.0).

GO Analysis

The Database for Annotation, Visualization and Integrated Discovery (DAVID) (v6.8) gene functional annotation and classification tool [PubMed ID (PMID):19131956, PMID:19033363] was used to annotate the list of differentially expressed genes with respective GO terms and to perform GO enrichment analysis for biological function category. The enrichGO function in clusterProfiler (v3.6.0) was used to perform GO enrichment analysis for each cluster. GO groups were selected for significance by using a P value cutoff of 1%.

Pathway Analysis

Significant pathway enrichment analysis was performed using IPA (Ingenuity Systems). Statistically significant biological pathways were then identified by using a P value cutoff of 0.05.

Statistical Analysis

All statistical analyses were performed using GraphPad Prism 7 (GraphPad Software). Data are presented as mean ± SEM. Differences between groups were tested for statistical significance by using the unpaired two-tailed Student's t test. $P < 0.05$ was considered significant. For analysis of multiple groups, we utilized the Holm–Sidak correction for multiple

comparisons with a false-discovery rate of 0.05. The number of biological (nontechnical) replicates for each experiment is indicated

Table 4. Description of antibodies used in Chapter 4

Primary antibodies	Manufacturer	Catalog#	Antibody	Dilution (frozen sections)	Dilution (isolated cells)	Dilution (Flow cytometry)
Twist2	Abcam	Ab66031	Rabbit polyclonal	1:200		1:50
Twist2	Sigma	WH0117581M1	Mouse monoclonal	1:50		
cTnI	Abcam	Ab47003	Rabbit polyclonal	1:100		
cTnT	Invitrogen	MA5-12960	Mouse monoclonal	1:200	1:200	
a-actinin	Abcam	Ab90776	Rabbit polyclonal	1:200		
CD31	BD Biosciences	553370	Mouse monoclonal	1:100	1:200	
vimentin	Sigma	V2258	Mouse monoclonal	1:100		
a-SMA	Sigma	A2547	Mouse monoclonal	1:200		
DDR2	Sigma	SAB1302555	Rabbit polyclonal		1:200	
CD105	BioLegend	120413	CD105-APC Rat IgG2A			1:50
CD73	BD Biosciences	561545	CD73-Alexa Fluor 488 Rat IgG2A			1:50
CD44	BD Biosciences	561862	CD44-APC Rat IgG2B			1:50
c-kit	BD Biosciences	553356	CD117-APC Rat IgG2B			1:50
pdfgra	R&D Systems	FAB1062G	pdgfra-Alexa Fluor 488 Goat IgG			1:50
CD31	BD Biosciences	551262	CD31-APC Rat IgG2A			1:50
CD90.2	BD Biosciences	561974	CD90.2-APC Rat IgG2A			1:50
CD45	R&D Systems	967208	CD45-PerCP Rat IgG2B			1:20
CD29	eBioscience	17-0291-82	CD29-APC Hamster IgG			1:20
Sca-1	BD Bioscience	560654	Ly-6A/E-APC-Cy7 Rat IgG2A			1:20
CD105	R&D Systems	967207	CD105/Endoglin-CFS Rat IgG2A			1:20
Isotype Controls	Manufacturer	Catalog#		Dilution (Flow cytometry)		
PerCP Rat IgG2B	R&D Systems	967114	Rat IgG2B-PerCP Isotype Control	1:20		
APC Hamster IgG	eBioscience	17-4888	Armenian Hamster IgG-APC Isotype Control	1:20		
APC-Cy7 Rat IgG2A	BD Bioscience	552770	Rat IgG2a-APC-Cy7 Isotype Control	1:20		
CFS Rat IgG2A	R&D Systems	965715	Rat IgG2A-CFS Isotype Control	1:20		
APC Rat IgG2B	BD Biosciences	553991	Rat IgG2b-APC Isotype Control	1:50		
APC Rat IgG2A	BD Biosciences	553932	Rat IgG2a-APC Isotype Control	1:50		
Alexa Fluor 488 Goat IgG	R&D Systems	IC108G	Goat IgG-Alexa Fluor 488 Isotype Control	1:50		
Alexa Fluor 488 Rat IgG2	BD Biosciences	557676	Rat IgG2a-Alexa Fluor® 488 Isotype Control	1:50		
Secondary antibodies	Manufacturer	Catalog#		Dilution (frozen sections)	Dilution (isolated cells)	Dilution (Flow cytometry)
Alexa Fluor 488	Life Technologies	A-11029	Goat anti Mouse IgG (H+L)	1:400	1:400	
Alexa Fluor 488	Life Technologies	A-11008	Goat anti-Rabbit IgG (H+L)	1:400	1:400	
Alexa Fluor 647	Life Technologies	A-21236	Goat anti-Mouse IgG (H+L)			1:200
Alexa Fluor 647	Life Technologies	A-32733	Goat anti-Rabbit IgG (H+L)			1:200

CHAPTER FIVE

CONCLUDING REMARKS

Potential advantages of CRISPR gene editing over other Duchenne Muscular Dystrophy therapies

The work in this dissertation shows that CRISPR gene editing can restore dystrophin expression in patient derived iPSCs and DMD mouse models with human mutations. How does gene editing differ from other therapeutic approaches that have been attempted for DMD? First, by eliminating the genetic mutations responsible for the disease, gene editing has the potential in principle to prevent further progression following a single treatment. Second, gene editing can allow the production of normal or nearly normal forms of dystrophin, which likely will maintain maximal function. This depends, of course, on the type of mutation being corrected. Third, the form of dystrophin generated by editing of exon 45, is 3570 amino acids in length by skipping exon 45 and 3,629 amino acids) if corrected by reframing. In contrast, the microdystrophin, which is the optimized truncate form of dystrophin that are currently being tested for gene therapy, are ~116 kDa (1,001 amino acids) and contain the minimal functional domains. Finally, because expression of dystrophin following gene editing originates from the endogenous dystrophin gene, which contains the normal cis-regulatory elements within the native genomic location, the temporospatial expression and the level of expression are normal. This is in contrast with the microdystrophin gene replacement therapy

in which microdystrophin expression depends on the cis-regulatory sequences within the AAV vector.

Future challenges of CRISPR gene editing for DMD

Despite the potential advantages of gene editing as a therapeutic strategy for DMD, this remains an experimental approach in early developmental stages with many unknowns and potential challenges. Perhaps the biggest challenge is the efficiency of body-wide delivery of the gene editing components to all affected muscles and the heart. At present, AAV has provided promising results in mice and dogs, but cost-effective large-scale production of the quantities of AAV that will be needed for treatment of large cohorts of patients will be a challenge. It also remains to be determined whether gene editing will allow long-term maintenance and retention of dystrophin expression over months, years, and even decades. Because cardiomyocytes are thought to be extremely long lived with an estimated turnover rate of only ~1% per year in humans, it seems likely that dystrophin correction will be durable in the heart. Less clear is the turnover rate of adult skeletal muscle fibers, particularly in the setting of DMD. If we assume that gene editing will not fully rescue all muscle fibers, then there will likely be gradual muscle turnover and regeneration via satellite cell recruitment. As new satellite cells fuse with damaged myofibers, perhaps their nuclei will be exposed to the gene editing components within the injured myofibers and will be subsequently edited to allow dystrophin expression, thereby sustaining therapeutic rescue. However, it remains unknown whether satellite cell nuclei will be localized appropriately within a damaged myofiber so as to be exposed to gene editing components throughout life. Gene editing within satellite cells represents a means of maintaining a reservoir of myonuclei with the potential to restore

dystrophin expression in DMD. However, with the exception of one report (Tabebordbar et al., 2016), efficient infection of satellite cells with AAV has not been observed (Arnett et al., 2014). Whether the resistance of satellite cells to AAV-mediated editing reflects the lack of tropism of currently employed serotypes for satellite cells or the inaccessibility of satellite cells, which reside below the basal lamina, to AAV infection is uncertain.

The longevity of expression of Cas9 and sgRNAs from AAV is also unknown, although estimates of AAV half-life indicate sustained expression over many years (Kessler et al., 1996). Because exposure to AAV elicits an immune response, at present only a single dose can be delivered. Thus, if expression is not sustained, subsequent injections with the same AAV serotype seem unlikely to be effective. It may be possible to use plasmapheresis to remove AAV antibodies to allow subsequent injections, or to use different AAV serotypes for subsequent injections, but such efforts remain in early development.

The risk of off-target mutations in the genome has been raised as a safety concern for gene editing in vivo, although there have been no documented examples of such mutations having deleterious effects in mice. Another theoretical concern for gene editing is the consequence of long-term expression of Cas9 throughout the body. Might this increase the likelihood of off-target effects or other pathological sequelae? To date, there has been no evidence for off-target mutagenesis in animals treated with AAV9-Cas9 and sgRNAs. Nevertheless, the possibility of a deleterious off-target mutation within a rogue cell somewhere in the body during a person's lifespan cannot easily be ruled out. To minimize possible off-target effects in nonmuscle tissues, we and others have used muscle-specific cis-regulatory elements to drive expression of Cas9, thus restricting expression to muscle and preventing

expression in the liver or kidney, which are known to accumulate AAV (Amoasii et al., 2017; Bengtsson et al., 2017; Lau and Suh, 2017). Moreover, because muscle tissues are permanently postmitotic, possible oncogenic off-target effects in these tissues are likely to be insignificant.

There are several immunological considerations with respect to restoration of dystrophin expression by gene editing. As a foreign bacterial protein, Cas9 is likely to evoke an immune response, although studies to date have not observed this to be significant. As in any gene replacement therapy, the possibility of immune rejection of the protein being replaced is a concern. In the case of DMD, patients typically contain a small number of dystrophin-positive revertant fibers that arise because inaccurate splicing allows exon skipping and dystrophin expression. Because of these fibers, the immune system of DMD patients has been exposed to dystrophin, which may mitigate immune rejection of dystrophin-expressing cells following gene editing. In addition, DMD patients are typically treated with corticosteroids, which may also diminish possible adverse immune reactions.

Conclusions and Future Perspectives

While we have focused in this dissertation on the potential application of gene editing to DMD, the lessons learned from these studies will undoubtedly be applicable to other monogenic disorders of muscle. Indeed, a study on facioscapulohumeral muscular dystrophy showed that CRISPR/dCas9 fused with a transcriptional repressor represses the expression of Double homeobox 4 (DUX4), a potent transcription factor that activates various genes that lead to oxidative stress and muscle atrophy (Himeda et al., 2016). CRISPR/Cas9-mediated genome editing has also been shown to successfully correct genomic mutations by HDR in

iPSCs derived from limb-girdle muscular dystrophy patients (Turan et al., 2016). Another report used CRISPR/Cas9-mediated NHEJ DNA repair to excise the entire region of expanded CTG/CAG repeats, thereby removing the pathogenic hallmarks of myotonic dystrophy (van Agtmaal et al., 2017).

It is remarkable to realize that CRISPR was only described about five years ago as a possible gene editing tool for mammalian cells and has already advanced into initial clinical studies. Despite the challenges and uncertainties of the CRISPR/Cas9 system, this technology has opened up new opportunities for correcting monogenic neuromuscular diseases, and there will undoubtedly be many unforeseen advances and applications of this technology in the years to come.

BIBLIOGRAPHY

Aartsma-Rus, A., Van Deutekom Judith, C.T., Fokkema Ivo, F., Van Ommen Gert-Jan, B., and Den Dunnen Johan, T. (2006). Entries in the Leiden Duchenne muscular dystrophy mutation database: An overview of mutation types and paradoxical cases that confirm the reading-frame rule. Muscle & Nerve *34*, 135-144.

Adkar, S.S., Willard, V.P., Brunger, J.M., Shiao, K.T., Gersbach, C.A., and Guilak, F. (2016). 318. Targeted genome editing of human induced pluripotent stem cells using CRISPR/CAS9 to generate a knock-in type II collagen reporter for the purification of chondrogenic cells. Molecular Therapy *24*, S128.

Ahn, A.H., and Kunkel, L.M. (1993). The structural and functional diversity of dystrophin. Nature Genetics *3*, 283.

Allen, D., Whitehead, N., and Froehner, S. (2015). Absence of dystrophin disrupts skeletal muscle signaling: roles of Ca2+, reactive oxygen species, and nitric oxide in the development of muscular dystrophy, Vol 96.

Amoasii, L., Hildyard, J.C.W., Li, H., Sanchez-Ortiz, E., Mireault, A., Caballero, D., Harron, R., Stathopoulou, T.-R., Massey, C., Shelton, J.M.*, et al.* (2018). Gene editing restores dystrophin expression in a canine model of Duchenne muscular dystrophy. Science.

Amoasii, L., Long, C., Li, H., Mireault, A.A., Shelton, J.M., Sanchez-Ortiz, E., McAnally, J.R., Bhattacharyya, S., Schmidt, F., Grimm, D.*, et al.* (2017). Single-cut genome editing restores dystrophin expression in a new mouse model of muscular dystrophy. Science translational medicine *9*, eaan8081.

Andrews, J.G., and Wahl, R.A. (2018). Duchenne and Becker muscular dystrophy in adolescents: current perspectives. Adolescent Health, Medicine and Therapeutics *9*, 53-63.

Anversa, P., Kajstura, J., Rota, M., and Leri, A. (2013). Regenerating new heart with stem cells. The Journal of Clinical Investigation *123*, 62-70.

Arnett, A.L.H., Konieczny, P., Ramos, J.N., Hall, J., Odom, G., Yablonka-Reuveni, Z., Chamberlain, J.R., and Chamberlain, J.S. (2014). Adeno-associated viral vectors do not efficiently target muscle satellite cells. Molecular Therapy - Methods & Clinical Development *1*.

Aslesh, T., Maruyama, R., and Yokota, T. (2018). Skipping multiple exons to treat DMD—promises and challenges. Biomedicines *6*, 1.

Barzel, A., Paulk, N.K., Shi, Y., Huang, Y., Chu, K., Zhang, F., Valdmanis, P.N., Spector, L.P., Porteus, M.H., Gaensler, K.M., *et al.* (2015). Promoterless gene targeting without nucleases ameliorates haemophilia B in mice. Nature *517*, 360-364.

Baylies, M.K., and Bate, M. (1996). twist: A myogenic switch in Drosophila. Science *272*, 1481-1484.

Bearzi, C., Rota, M., Hosoda, T., Tillmanns, J., Nascimbene, A., De Angelis, A., Yasuzawa-Amano, S., Trofimova, I., Siggins, R.W., Lecapitaine, N., *et al.* (2007). Human cardiac stem cells. Proceedings of the National Academy of Sciences of the United States of America *104*, 14068-14073.

Beck, B., Lapouge, G., Rorive, S., Drogat, B., Desaedelaere, K., Delafaille, S., Dubois, C., Salmon, I., Willekens, K., Marine, J.-C., *et al.* Different levels of Twist1 regulate skin tumor initiation, stemness, and progression. Cell Stem Cell *16*, 67-79.

Beltrami, A.P., Barlucchi, L., Torella, D., Baker, M., Limana, F., Chimenti, S., Kasahara, H., Rota, M., Musso, E., Urbanek, K., *et al.* (2003). Adult cardiac stem cells are multipotent and support myocardial regeneration. Cell *114*, 763-776.

Bengtsson, N.E., Hall, J.K., Odom, G.L., Phelps, M.P., Andrus, C.R., Hawkins, R.D., Hauschka, S.D., Chamberlain, J.R., and Chamberlain, J.S. (2017). Muscle-specific CRISPR/Cas9 dystrophin gene editing ameliorates pathophysiology in a mouse model for Duchenne muscular dystrophy. Nature Communications *8*, 14454.

Bergmann, O., Bhardwaj, R.D., Bernard, S., Zdunek, S., Barnabé-Heider, F., Walsh, S., Zupicich, J., Alkass, K., Buchholz, B.A., Druid, H., *et al.* (2009). Evidence for cardiomyocyte renewal in humans. Science *324*, 98-102.

Bergmann, O., Zdunek, S., Felker, A., Salehpour, M., Alkass, K., Bernard, S., Sjostrom, Staffan L., Szewczykowska, M., Jackowska, T., dos Remedios, C., *et al.* (2015). Dynamics of cell generation and turnover in the human heart. Cell *161*, 1566-1575.

Bialek, P., Kern, B., Yang, X., Schrock, M., Sosic, D., Hong, N., Wu, H., Yu, K., Ornitz, D.M., Olson, E.N., *et al.* (2004). A Twist code determines the onset of osteoblast differentiation. Developmental Cell *6*, 423-435.

Bladen Catherine, L., Salgado, D., Monges, S., Foncuberta Maria, E., Kekou, K., Kosma, K., Dawkins, H., Lamont, L., Roy Anna, J., Chamova, T., *et al.* (2015). The TREAT-NMD DMD global database: analysis of more than 7,000 Duchenne Muscular Dystrophy mutations. Human Mutation *36*, 395-402.

Bock, C., Kiskinis, E., Verstappen, G., Gu, H., Boulting, G., Smith, Z.D., Ziller, M., Croft, G.F., Amoroso, M.W., Oakley, D.H.*, et al.* (2011). Reference maps of human ES and iPS cell variation enable high-throughput characterization of pluripotent cell lines. Cell *144*, 439-452.

Bonne, G., Rivier, F., and Hamroun, D. (2017). The 2018 version of the gene table of monogenic neuromuscular disorders (nuclear genome). Neuromuscular Disorders *27*, 1152-1183.

Borkowski, O.M., Brown, N.H., and Bate, M. (1995). Anterior-posterior subdivision and the diversification of the mesoderm in Drosophila. Development *121*, 4183-4193.

Bostick, B., Yue, Y., Long, C., and Duan, D. (2008). Prevention of dystrophin-deficient cardiomyopathy in twenty-one-month-old Carrier Mice by Mosaic Dystrophin Expression or Complementary Dystrophin/Utrophin Expression. Circulation Research *102*, 121.

Boulting, G.L., Kiskinis, E., Croft, G.F., Amoroso, M.W., Oakley, D.H., Wainger, B.J., Williams, D.J., Kahler, D.J., Yamaki, M., Davidow, L.*, et al.* (2011). A functionally characterized test set of human induced pluripotent stem cells. Nature Biotechnology *29*, 279.

Bulfield, G., Siller, W.G., Wight, P.A., and Moore, K.J. (1984). X chromosome-linked muscular dystrophy (mdx) in the mouse. Proceedings of the National Academy of Sciences *81*, 1189.

Büning, H., Perabo, L., Coutelle, O., Quadt-Humme, S., and Hallek, M. (2008). Recent developments in adeno-associated virus vector technology. The Journal of Gene Medicine *10*, 717-733.

Cai, W.-F., Huang, W., Wang, L., Wang, J.-P., Zhang, L., Ashraf, M., Wu, S., and Wang, Y. (2016). Induced pluripotent stem cells derived muscle progenitors effectively mitigate muscular dystrophy through restoring the dystrophin distribution. Journal of stem cell research & therapy *6*, 1000361.

Campbell, K.P., and Kahl, S.D. (1989). Association of dystrophin and an integral membrane glycoprotein. Nature *338*, 259.

Carnwath, J.W., and Shotton, D.M. (1987). Muscular dystrophy in the mdx mouse: Histopathology of the soleus and extensor digitorum longus muscles. Journal of the Neurological Sciences *80*, 39-54.

Caron, L., Kher, D., Lee, K.L., McKernan, R., Dumevska, B., Hidalgo, A., Li, J., Yang, H., Main, H., Ferri, G.*, et al.* (2016). A human pluripotent stem cell model of

Facioscapulohumeral Muscular Dystrophy-affected skeletal muscles. Stem Cells Translational Medicine *5*, 1145-1161.

Castanon, I., and Baylies, M.K. (2002). A Twist in fate: evolutionary comparison of Twist structure and function. Gene *287*, 11-22.

Chamberlain, J.S., Metzger, J., Reyes, M., Townsend, D., and Faulkner, J.A. (2007). Dystrophin-deficient mdx mice display a reduced life span and are susceptible to spontaneous rhabdomyosarcoma. The FASEB Journal *21*, 2195-2204.

Chang, N.C., Chevalier, F.P., and Rudnicki, M.A. (2016). Satellite cells in muscular dystrophy: lost in polarity. Trends in Molecular Medicine *22*, 479-496.

Chapman, V.M., Miller, D.R., Armstrong, D., and Caskey, C.T. (1989). Recovery of induced mutations for X chromosome-linked muscular dystrophy in mice. Proceedings of the National Academy of Sciences *86*, 1292.

Charleston, J.S., Schnell, F.J., Dworzak, J., Donoghue, C., Lewis, S., Chen, L., Young, G.D., Milici, A.J., Voss, J., DeAlwis, U.*, et al.* (2018). Eteplirsen treatment for Duchenne muscular dystrophy. Neurology.

Chavez, A., Scheiman, J., Vora, S., Pruitt, B.W., Tuttle, M., P R Iyer, E., Lin, S., Kiani, S., Guzman, C.D., Wiegand, D.J.*, et al.* (2015). Highly efficient Cas9-mediated transcriptional programming. Nature Methods *12*, 326.

Chen, Y., Cao, J., Xiong, M., Petersen, A.J., Dong, Y., Tao, Y., Huang, C.T.-L., Du, Z., and Zhang, S.-C. (2015). Engineering human stem cell lines with inducible gene knockout using CRISPR/Cas9. Cell stem cell *17*, 233-244.

Choi, In Y., Lim, H., Estrellas, K., Mula, J., Cohen, Tatiana V., Zhang, Y., Donnelly, Christopher J., Richard, J.-P., Kim, Yong J., Kim, H.*, et al.* (2016). Concordant but varied phenotypes among Duchenne Muscular Dystrophy patient-specific myoblasts derived using a human iPSC-based model. Cell Reports *15*, 2301-2312.

Cong, L., Ran, F.A., Cox, D., Lin, S., Barretto, R., Habib, N., Hsu, P.D., Wu, X., Jiang, W., Marraffini, L.A.*, et al.* (2013). Multiplex engome engineering using CRISPR/Cas systems. Science *339*, 819.

Cripps, R.M., Black, B.L., Zhao, B., Lien, C.-L., Schulz, R.A., and Olson, E.N. (1998). The myogenic regulatory gene Mef2 is a direct target for transcriptional activation by Twist during Drosophila myogenesis. Genes & Development *12*, 422-434.

Cripps, R.M., and Olson, E.N. (1998). Twist is required for muscle template splitting during adult drosophila myogenesis. Developmental Biology *203*, 106-115.

Currie, D.A., and Bate, M. (1991). The development of adult abdominal muscles in Drosophila: myoblasts express twist and are associated with nerves. Development *113*, 91-102.

Dangain, J., and Vrbova, G. (1984). Muscle development in mdx mutant mice. Muscle & Nerve *7*, 700-704.

Deconinck, A.E., Rafael, J.A., Skinner, J.A., Brown, S.C., Potter, A.C., Metzinger, L., Watt, D.J., Dickson, J.G., Tinsley, J.M., and Davies, K.E. (1997). Utrophin-dystrophin-deficient mice as a model for Duchenne Muscular Dystrophy. Cell *90*, 717-727.

Donsante, A., Miller, D.G., Li, Y., Vogler, C., Brunt, E.M., Russell, D.W., and Sands, M.S. (2007). AAV vector integration sites in mouse hepatocellular carcinoma. Science *317*, 477.

Duan, D. (2015). Duchenne Muscular Dystrophy gene therapy in the canine model. Human Gene Therapy Clinical Development *26*, 57-69.

Echevarría, L., Aupy, P., and Goyenvalle, A. (2018). Exon-skipping advances for Duchenne muscular dystrophy. Human Molecular Genetics, ddy171-ddy171.

Ellison, Georgina M., Vicinanza, C., Smith, Andrew J., Aquila, I., Leone, A., Waring, Cheryl D., Henning, Beverley J., Stirparo, Giuliano G., Papait, R., Scarfò, M.*, et al.* (2013). Adult c-kitpos cardiac stem cells are necessary and sufficient for functional cardiac regeneration and repair. Cell *154*, 827-842.

Fayssoil, A., Nardi, O., Orlikowski, D., and Annane, D. (2009). Cardiomyopathy in Duchenne muscular dystrophy: pathogenesis and therapeutics. Heart Failure Reviews *15*, 103.

Figeac, N., Daczewska, M., Marcelle, C., and Jagla, K. (2007). Muscle stem cells and model systems for their investigation. Developmental Dynamics *236*, 3332-3342.

Fioret, Bryan A., Heimfeld, Jeremy D., Paik, David T., and Hatzopoulos, Antonis K. (2014). Endothelial cells contribute to generation of adult ventricular myocytes during cardiac homeostasis. Cell Reports *8*, 229-241.

Flanigan, K.M., Dunn, D., von Niederhausern, A., Soltanzadeh, P., Gappmaier, E., Howard, M.T., Sampson, J., Mendell, J., Wall, C., King, W.*, et al.* (2009). Mutational spectrum of DMD mutations in dystrophinopathy patients: application of modern diagnostic techniques to a large cohort. Human Mutation *30*, 1657-1666.

Funkquist, B., Haraldsson, I., and Stahre, L. (1980). Primary progressive muscular dystrophy in the dog, Vol 106.

Gao, Q.Q.a.M., E. M. (2015). The dystrophin complex: structure, function, and implications for therapy. In Comprehensive Physiology.

Gapinske, M., Luu, A., Winter, J., Woods, W.S., Kostan, K.A., Shiva, N., Song, J.S., and Perez-Pinera, P. (2018). CRISPR-SKIP: programmable gene splicing with single base editors. Genome Biology *19*, 107.

Garbade, J., Schubert, A., Rastan, A.J., Lenz, D., Walther, T., Gummert, J.F., Dhein, S., and Mohr, F.W. (2005). Fusion of bone marrow-derived stem cells with cardiomyocytes in a heterologous in vitro model. European journal of cardio-thoracic surgery : official journal of the European Association for Cardio-thoracic Surgery *28*, 685-691.

Gaudelli, N.M., Komor, A.C., Rees, H.A., Packer, M.S., Badran, A.H., Bryson, D.I., and Liu, D.R. (2017). Programmable base editing of A•T to G•C in genomic DNA without DNA cleavage. Nature *551*, 464.

Ginjaar, I.B., Kneppers, A.L.J., v d Meulen, J.-D.M., Anderson, L.V.B., Bremmer-Bout, M., van Deutekom, J.C.T., Weegenaar, J., den Dunnen, J.T., and Bakker, E. (2000). Dystrophin nonsense mutation induces different levels of exon 29 skipping and leads to variable phenotypes within one BMD family. European Journal Of Human Genetics *8*, 793.

Gong, X.Q., and Li, L. (2002). Dermo-1, a multifunctional basic helix-loop-helix protein, represses MyoD transactivation via the HLH domain, MEF2 interaction, and chromatin deacetylation. Journal of Biological Chemistry *277*, 12310-12317.

Grady, R.M., Teng, H., Nichol, M.C., Cunningham, J.C., Wilkinson, R.S., and Sanes, J.R. (1997). Skeletal and cardiac myopathies in mice lacking utrophin and dystrophin: A model for Duchenne muscular dystrophy. Cell *90*, 729-738.

Grande, M.T., Sánchez-Laorden, B., López-Blau, C., De Frutos, C.A., Boutet, A., Arévalo, M., Rowe, R.G., Weiss, S.J., López-Novoa, J.M., and Nieto, M.A. (2015). Snail1-induced partial epithelial-to-mesenchymal transition drives renal fibrosis in mice and can be targeted to reverse established disease. Nature Medicine *21*, 989.

Grieger, J.C., Choi, V.W., and Samulski, R.J. (2006). Production and characterization of adeno-associated viral vectors. Nature Protocols *1*, 1412.

Guo, C., Willem, M., Werner, A., Raivich, G., Emerson, M., Neyses, L., and Mayer, U. (2006). Absence of α7 integrin in dystrophin-deficient mice causes a myopathy similar to Duchenne muscular dystrophy. Human Molecular Genetics *15*, 989-998.

Guo, R., Zhu, G., Zhu, H., Ma, R., Peng, Y., Liang, D., and Wu, L. (2015). DMD mutation spectrum analysis in 613 Chinese patients with dystrophinopathy. Journal Of Human Genetics *60*, 435.

Hakim, C.H., Grange, R.W., and Duan, D. (2011). The passive mechanical properties of the extensor digitorum longus muscle are compromised in 2- to 20-mo-old mdx mice. Journal of Applied Physiology *110*, 1656-1663.

Himeda, C.L., Jones, T.I., and Jones, P.L. (2016). CRISPR/dCas9-mediated transcriptional inhibition ameliorates the epigenetic dysregulation at D4Z4 and represses DUX4-fl in FSH Muscular Dystrophy. Molecular Therapy *24*, 527-535.

Hjiantoniou, E., Anayasa, M., Nicolaou, P., Bantounas, I., Saito, M., Iseki, S., Uney, J.B., and Phylactou, L.A. (2008). Twist induces reversal of myotube formation. Differentiation; research in biological diversity *76*, 182-192.

Hoffman, E.P., Brown, R.H., Jr., and Kunkel, L.M. (1987). Dystrophin: The protein product of the duchenne muscular dystrophy locus. Cell *51*, 919-928.

Hou, Z., Zhang, Y., Propson, N.E., Howden, S.E., Chu, L.-F., Sontheimer, E.J., and Thomson, J.A. (2013). Efficient genome engineering in human pluripotent stem cells using Cas9 from Neisseria meningitidis. Proceedings of the National Academy of Sciences *110*, 15644.

Hsieh, P.C.H., Segers, V.F.M., Davis, M.E., MacGillivray, C., Gannon, J., Molkentin, J.D., Robbins, J., and Lee, R.T. (2007). Evidence from a genetic fate-mapping study that stem cells refresh adult mammalian cardiomyocytes after injury. Nat Med *13*, 970-974.

Isenmann, S., Arthur, A., Zannettino, A.C.W., Turner, J.L., Shi, S., Glackin, C.A., and Gronthos, S. (2009). TWIST family of basic helix-loop-helix transcription factors mediate human mesenchymal stem cell growth and commitment. STEM CELLS *27*, 2457-2468.

Jinek, M., Chylinski, K., Fonfara, I., Hauer, M., Doudna, J.A., and Charpentier, E. (2012). A programmable dual-RNA–guided DNA endonuclease in adaptive bacterial immunity. Science *337*, 816.

Jinek, M., Jiang, F., Taylor, D.W., Sternberg, S.H., Kaya, E., Ma, E., Anders, C., Hauer, M., Zhou, K., Lin, S.*, et al.* (2014). Structures of Cas9 endonucleases reveal RNA-mediated conformational activation. Science *343*.

Kessler, P.D., Podsakoff, G.M., Chen, X., McQuiston, S.A., Colosi, P.C., Matelis, L.A., Kurtzman, G.J., and Byrne, B.J. (1996). Gene delivery to skeletal muscle results in sustained expression and systemic delivery of a therapeutic protein. Proceedings of the National Academy of Sciences of the United States of America *93*, 14082-14087.

Kim, E.Y., Page, P., Dellefave-Castillo, L.M., McNally, E.M., and Wyatt, E.J. (2016). Direct reprogramming of urine-derived cells with inducible MyoD for modeling human muscle disease. Skeletal Muscle *6*, 32.

Kim, S., Kim, D., Cho, S.W., Kim, J., and Kim, J.-S. (2014). Highly efficient RNA-guided genome editing in human cells via delivery of purified Cas9 ribonucleoproteins. Genome research *24*, 1012-1019.

Kimura, W., Xiao, F., Canseco, D.C., Muralidhar, S., Thet, S., Zhang, H.M., Abderrahman, Y., Chen, R., Garcia, J.A., Shelton, J.M.*, et al.* (2015). Hypoxia fate mapping identifies cycling cardiomyocytes in the adult heart. Nature *523*, 226-230.

Kole, R., and Krieg, A.M. (2015). Exon skipping therapy for Duchenne muscular dystrophy. Advanced Drug Delivery Reviews *87*, 104-107.

Komor, A.C., Kim, Y.B., Packer, M.S., Zuris, J.A., and Liu, D.R. (2016). Programmable editing of a target base in genomic DNA without double-stranded DNA cleavage. Nature *533*, 420.

Kudoh, H., Ikeda, H., Kakitani, M., Ueda, A., Hayasaka, M., Tomizuka, K., and Hanaoka, K. (2005). A new model mouse for Duchenne muscular dystrophy produced by 2.4Mb deletion of dystrophin gene using Cre-loxP recombination system. Biochemical and Biophysical Research Communications *328*, 507-516.

Kyrychenko, V., Kyrychenko, S., Tiburcy, M., Shelton, J.M., Long, C., Schneider, J.W., Zimmermann, W.-H., Bassel-Duby, R., and Olson, E.N. (2017). Functional correction of dystrophin actin binding domain mutations by genome editing. JCI Insight *2*, e95918.

Lau, C.-H., and Suh, Y. (2017). In vivo genome editing in animals using AAV-CRISPR system: applications to translational research of human disease. F1000Research *6*, 2153.

Laugwitz, K.L., Moretti, A., Caron, L., Nakano, A., and Chien, K.R. (2008). Islet1 cardiovascular progenitors: a single source for heart lineages? Development *135*, 193-205.

Lee, K., Conboy, M., Park, H.M., Jiang, F., Kim, H.J., Dewitt, M.A., Mackley, V.A., Chang, K., Rao, A., Skinner, C.*, et al.* (2017). Nanoparticle delivery of Cas9 ribonucleoprotein and donor DNA in vivo induces homology-directed DNA repair. Nature Biomedical Engineering *1*, 889-901.

Lee, T., Takeshima, Y., Kusunoki, N., Awano, H., Yagi, M., Matsuo, M., and Iijima, K. (2014). Differences in carrier frequency between mothers of Duchenne and Becker muscular dystrophy patients. Journal of Human Genetics *59*, 46-50.

Lefaucheur Jean, P., Pastoret, C., and Sebille, A. (1995). Phenotype of dystrophinopathy in old MDX mice. The Anatomical Record *242*, 70-76.

Lemos, B.R., Kaplan, A.C., Bae, J.E., Ferrazzoli, A.E., Kuo, J., Anand, R.P., Waterman, D.P., and Haber, J.E. (2018). CRISPR/Cas9 cleavages in budding yeast reveal templated insertions and strand-specific insertion/deletion profiles. Proceedings of the National Academy of Sciences *115*, E2040.

Leri, A., Rota, M., Pasqualini, F.S., Goichberg, P., and Anversa, P. (2015). Origin of cardiomyocytes in the adult Heart. Circulation Research *116*, 150-166.

Li, Hongmei L., Fujimoto, N., Sasakawa, N., Shirai, S., Ohkame, T., Sakuma, T., Tanaka, M., Amano, N., Watanabe, A., Sakurai, H.*, et al.* (2015). Precise correction of the dystrophin gene in Duchenne Muscular Dystrophy patient induced pluripotent stem cells by TALEN and CRISPR-Cas9. Stem Cell Reports *4*, 143-154.

Liu, N., Garry, Glynnis A., Li, S., Bezprozvannaya, S., Sanchez-Ortiz, E., Chen, B., Shelton, John M., Jaichander, P., Bassel-Duby, R., and Olson, Eric N. (2017). A Twist2-dependent progenitor cell contributes to adult skeletal muscle. Nature Cell Biology *19*, 202.

Long, C., Amoasii, L., Mireault, A.A., McAnally, J.R., Li, H., Sanchez-Ortiz, E., Bhattacharyya, S., Shelton, J.M., Bassel-Duby, R., and Olson, E.N. (2016). Postnatal genome editing partially restores dystrophin expression in a mouse model of muscular dystrophy. Science (New York, NY) *351*, 400-403.

Long, C., Li, H., Tiburcy, M., Rodriguez-Caycedo, C., Kyrychenko, V., Zhou, H., Zhang, Y., Min, Y.-L., Shelton, J.M., Mammen, P.P.A.*, et al.* (2018). Correction of diverse muscular dystrophy mutations in human engineered heart muscle by single-site genome editing. Science Advances *4*, eaap9004.

Long, C., McAnally, J.R., Shelton, J.M., Mireault, A.A., Bassel-Duby, R., and Olson, E.N. (2014). Prevention of muscular dystrophy in mice by CRISPR/Cas9–mediated editing of germline DNA. Science (New York, NY) *345*, 1184-1188.

Lovisa, S., LeBleu, V.S., Tampe, B., Sugimoto, H., Vadnagara, K., Carstens, J.L., Wu, C.-C., Hagos, Y., Burckhardt, B.C., Pentcheva-Hoang, T.*, et al.* (2015). Epithelial-to-mesenchymal transition induces cell cycle arrest and parenchymal damage in renal fibrosis. Nature Medicine *21*, 998.

Maggio, I., Liu, J., Janssen, J.M., Chen, X., and Gonçalves, M.A.F.V. (2016). Adenoviral vectors encoding CRISPR/Cas9 multiplexes rescue dystrophin synthesis in unselected populations of DMD muscle cells. Scientific Reports *6*, 37051.

Makino, S., Fukuda, K., Miyoshi, S., Konishi, F., Kodama, H., Pan, J., Sano, M., Takahashi, T., Hori, S., Abe, H.*, et al.* (1999). Cardiomyocytes can be generated from marrow stromal cells in vitro. The Journal of Clinical Investigation *103*, 697-705.

Mali, P., Yang, L., Esvelt, K.M., Aach, J., Guell, M., DiCarlo, J.E., Norville, J.E., and Church, G.M. (2013). RNA-guided human genome engineering via Cas9. Science *339*, 823.

Malliaras, K., Zhang, Y., Seinfeld, J., Galang, G., Tseliou, E., Cheng, K., Sun, B., Aminzadeh, M., and Marbán, E. (2013). Cardiomyocyte proliferation and progenitor cell recruitment underlie therapeutic regeneration after myocardial infarction in the adult mouse heart. EMBO Molecular Medicine *5*, 191-209.

Mandai, M., Watanabe, A., Kurimoto, Y., Hirami, Y., Morinaga, C., Daimon, T., Fujihara, M., Akimaru, H., Sakai, N., Shibata, Y.*, et al.* (2017). Autologous induced stem-cell–derived retinal cells for macular degeneration. New England Journal of Medicine *376*, 1038-1046.

Martari, M., Sagazio, A., Mohamadi, A., Nguyen, Q., Hauschka, S.D., Kim, E., and Salvatori, R. (2009). Partial rescue of growth failure in growth hormone (GH)-deficient mice by a single injection of a double-stranded adeno-associated viral vector expressing the GH gene driven by a muscle-specific regulatory cassette. Human Gene Therapy *20*, 759-766.

Mastroyiannopoulos, N.P., Antoniou, A.A., Koutsoulidou, A., Uney, J.B., and Phylactou, L.A. (2013). Twist reverses muscle cell differentiation through transcriptional down-regulation of myogenin. Bioscience reports *33*.

McGreevy, J.W., Hakim, C.H., McIntosh, M.A., and Duan, D. (2015). Animal models of Duchenne muscular dystrophy: from basic mechanisms to gene therapy. Disease Models & Mechanisms *8*, 195-213.

Mendell, J.R., Al-Zaidy, S., Shell, R., Arnold, W.D., Rodino-Klapac, L.R., Prior, T.W., Lowes, L., Alfano, L., Berry, K., Church, K.*, et al.* (2017). Single-dose gene-replacement therapy for spinal muscular atrophy. New England Journal of Medicine *377*, 1713-1722.

Miller Jason, B., Zhang, S., Kos, P., Xiong, H., Zhou, K., Perelman Sofya, S., Zhu, H., and Siegwart Daniel, J. (2016). Non-viral CRISPR/Cas gene editing in vitro and in vivo enabled by synthetic nanoparticle co-delivery of Cas9 mRNA and sgRNA. Angewandte Chemie International Edition *56*, 1059-1063.

Min, Y.-L., Jaichander, P., Sanchez-Ortiz, E., Bezprozvannaya, S., Malladi, V.S., Cui, M., Wang, Z., Bassel-Duby, R., Olson, E.N., and Liu, N. (2018). Identification of a multipotent Twist2-expressing cell population in the adult heart. Proceedings of the National Academy of Sciences 115, E8430-E8439.

Mollova, M., Bersell, K., Walsh, S., Savla, J., Das, L.T., Park, S.-Y., Silberstein, L.E., dos Remedios, C.G., Graham, D., Colan, S.*, et al.* (2013). Cardiomyocyte proliferation contributes to heart growth in young humans. Proceedings of the National Academy of Sciences *110*, 1446-1451.

Mourkioti, F., Kustan, J., Kraft, P., Day, J.W., Zhao, M.-M., Kost-Alimova, M., Protopopov, A., DePinho, R.A., Bernstein, D., Meeker, A.K.*, et al.* (2013). Role of telomere dysfunction in cardiac failure in Duchenne Muscular Dystrophy. Nature cell biology *15*, 895-904.

Müller, M., Lee, C.M., Gasiunas, G., Davis, T.H., Cradick, T.J., Siksnys, V., Bao, G., Cathomen, T., and Mussolino, C. (2016). Streptococcus thermophilus CRISPR-Cas9 systems enable specific editing of the human genome. Molecular Therapy *24*, 636-644.

Muzumdar, M.D., Tasic, B., Miyamichi, K., Li, L., and Luo, L. (2007). A global double-fluorescent Cre reporter mouse. Genesis *45*, 593-605.

Nelson, C.E., Hakim, C.H., Ousterout, D.G., Thakore, P.I., Moreb, E.A., Rivera, R.M.C., Madhavan, S., Pan, X., Ran, F.A., Yan, W.X.*, et al.* (2016). In vivo genome editing improves muscle function in a mouse model of Duchenne muscular dystrophy. Science *351*, 403.

Neri, M., Torelli, S., Brown, S., Ugo, I., Sabatelli, P., Merlini, L., Spitali, P., Rimessi, P., Gualandi, F., Sewry, C.*, et al.* (2007). Dystrophin levels as low as 30% are sufficient to avoid muscular dystrophy in the human. Neuromuscular Disorders *17*, 913-918.

Nishida, K., Arazoe, T., Yachie, N., Banno, S., Kakimoto, M., Tabata, M., Mochizuki, M., Miyabe, A., Araki, M., Hara, K.Y.*, et al.* (2016). Targeted nucleotide editing using hybrid prokaryotic and vertebrate adaptive immune systems. Science *353*.

Noseda, M., Harada, M., McSweeney, S., Leja, T., Belian, E., Stuckey, D.J., Abreu Paiva, M.S., Habib, J., Macaulay, I., de Smith, A.J.*, et al.* (2015). PDGFRa demarcates the cardiogenic clonogenic Sca1+ stem/progenitor cell in adult murine myocardium. Nat Commun *6*.

Nygren, J.M., Jovinge, S., Breitbach, M., Säwén, P., Röll, W., Hescheler, J., Taneera, J., Fleischmann, B.K., and Jacobsen, S.E.W. (2004). Bone marrow–derived hematopoietic cells generate cardiomyocytes at a low frequency through cell fusion, but not transdifferentiation. Nature Medicine *10*, 494.

Oh, H., Bradfute, S.B., Gallardo, T.D., Nakamura, T., Gaussin, V., Mishina, Y., Pocius, J., Michael, L.H., Behringer, R.R., Garry, D.J.*, et al.* (2003). Cardiac progenitor cells from adult myocardium: homing, differentiation, and fusion after infarction. Proceedings of the National Academy of Sciences of the United States of America *100*, 12313-12318.

Ousterout, D.G., Kabadi, A.M., Thakore, P.I., Majoros, W.H., Reddy, T.E., and Gersbach, C.A. (2015). Multiplex CRISPR/Cas9-based genome editing for correction of dystrophin mutations that cause Duchenne Muscular Dystrophy. Nature communications *6*, 6244-6244.

Pastoret, C., and Sebille, A. (1995). mdx mice show progressive weakness and muscle deterioration with age. Journal of the Neurological Sciences *129*, 97-105.

Perez-Pinera, P., Kocak, D.D., Vockley, C.M., Adler, A.F., Kabadi, A.M., Polstein, L.R., Thakore, P.I., Glass, K.A., Ousterout, D.G., Leong, K.W.*, et al.* (2013). RNA-guided gene activation by CRISPR-Cas9–based transcription factors. Nature Methods *10*, 973.

Pfister, O., Mouquet, F., Jain, M., Summer, R., Helmes, M., Fine, A., Colucci, W.S., and Liao, R. (2005). CD31− but Not CD31+ cardiac side population cells exhibit functional cardiomyogenic differentiation. Circulation Research *97*, 52-61.

Qi, X., Dong, L., Liu, C., Mao, L., Liu, F., Zhang, X., Cheng, B., and Xie, C. (2018). Systematic identification of endogenous RNA polymerase III promoters for efficient RNA guide-based genome editing technologies in maize. The Crop Journal *6*, 314-320.

Ran, F.A., Cong, L., Yan, W.X., Scott, D.A., Gootenberg, J.S., Kriz, A.J., Zetsche, B., Shalem, O., Wu, X., Makarova, K.S.*, et al.* (2015). In vivo genome editing using Staphylococcus aureus Cas9. Nature *520*, 186.

Ran, F.A., Hsu, P.D., Wright, J., Agarwala, V., Scott, D.A., and Zhang, F. (2013). Genome engineering using the CRISPR-Cas9 system. Nature Protocols *8*, 2281.

Reinhold, M.I., Kapadia, R.M., Liao, Z., and Naski, M.C. (2006). The Wnt-inducible transcription factor Twist1 inhibits chondrogenesis. Journal of Biological Chemistry *281*, 1381-1388.

Reinig Andrea, M., Mirzaei, S., and Berlau Daniel, J. (2017). Advances in the treatment of Duchenne Muscular Dystrophy: new and emerging pharmacotherapies. Pharmacotherapy: The Journal of Human Pharmacology and Drug Therapy *37*, 492-499.

Rodino-Klapac, L.R., Montgomery, C.L., Bremer, W.G., Shontz, K.M., Malik, V., Davis, N., Sprinkle, S., Campbell, K.J., Sahenk, Z., Clark, K.R.*, et al.* (2010). Persistent expression of FLAG-tagged micro dystrophin in nonhuman primates following intramuscular and vascular delivery. Molecular Therapy *18*, 109-117.

Rooney, J.E., Welser, J.V., Dechert, M.A., Flintoff-Dye, N.L., Kaufman, S.J., and Burkin, D.J. (2006). Severe muscular dystrophy in mice that lack dystrophin and α7 integrin. Journal of Cell Science *119*, 2185.

Ryu, S.-M., Koo, T., Kim, K., Lim, K., Baek, G., Kim, S.-T., Kim, H.S., Kim, D.-e., Lee, H., Chung, E.*, et al.* (2018). Adenine base editing in mouse embryos and an adult mouse model of Duchenne muscular dystrophy. Nature Biotechnology.

Sacco, A., Mourkioti, F., Tran, R., Choi, J., Llewellyn, M., Kraft, P., Shkreli, M., Delp, S., Pomerantz, J.H., Artandi, S.E.*, et al.* (2010). Short telomeres and stem cell exhaustion model Duchenne Muscular Dystrophy in mdx/mTR mice. Cell *143*, 1059-1071.

Salmaninejad, A., Valilou, S.F., Bayat, H., Ebadi, N., Daraei, A., Yousefi, M., Nesaei, A., and Mojarrad, M. (2018). Duchenne muscular dystrophy: an updated review of common available therapies. International Journal of Neuroscience, 1-11.

Sawamiphak, S., Kontarakis, Z., Filosa, A., Reischauer, S., and Stainier, D.Y.R. (2017). Transient cardiomyocyte fusion regulates cardiac development in zebrafish. Nature Communications *8*, 1525.

Schaefer, K.A., Wu, W.-H., Colgan, D.F., Tsang, S.H., Bassuk, A.G., and Mahajan, V.B. (2017). Unexpected mutations after CRISPR–Cas9 editing in vivo. Nature Methods *14*, 547.

Schmidt, F., Beaudouin, J., Börner, K., and Grimm, D. (2015a). 117. AAV-TRISPR 2013; A novel versatile AAV vector kit for combinatorial CRISPR and RNAi expression. Molecular Therapy *23*, S48-S49.

Schmidt, J.M., Panzilius, E., Bartsch, H.S., Irmler, M., Beckers, J., Kari, V., Linnemann, J.R., Dragoi, D., Hirschi, B., Kloos, U.J.*, et al.* (2015b). Stem-cell-like properties and epithelial plasticity arise as stable traits after transient Twist1 activation. Cell Rep *10*, 131-139.

Senyo, S.E., Steinhauser, M.L., Pizzimenti, C.L., Yang, V.K., Cai, L., Wang, M., Wu, T.-D., Guerquin-Kern, J.-L., Lechene, C.P., and Lee, R.T. (2013). Mammalian heart renewal by pre-existing cardiomyocytes. Nature *493*, 433-436.

Sharp, N.J.H., Kornegay, J., Van Camp, S.D., Herbstreith, M.H., Secore, S.L., Kettle, S., Hung, W.Y., Constantinou, C.D., Dykstra, M., Roses, A.*, et al.* (1992). An error in dystrophin mRNA processing in golden retriever muscular dystrophy, an animal homologue of Duchenne muscular dystrophy, Vol 13.

Shelton, E.L., and Yutzey, K.E. (2008). Twist1 function in endocardial cushion cell proliferation, migration, and differentiation during heart valve development. Developmental Biology *317*, 282-295.

Sicinski, P., Geng, Y., Ryder-Cook, A.S., Barnard, E.A., Darlison, M.G., and Barnard, P.J. (1989). The molecular basis of muscular dystrophy in the mdx mouse: a point mutation. Science *244*, 1578.

Smart, N., Bollini, S., Dube, K.N., Vieira, J.M., Zhou, B., Davidson, S., Yellon, D., Riegler, J., Price, A.N., Lythgoe, M.F.*, et al.* (2011). De novo cardiomyocytes from within the activated adult heart after injury. Nature *474*, 640-644.

Smith, B.F., Yue, Y., Woods, P.R., Kornegay, J.N., Shin, J.-H., Williams, R.R., and Duan, D. (2011). An intronic LINE-1 element insertion in the dystrophin gene aborts dystrophin expression and results in Duchenne-like muscular dystrophy in the corgi breed. Laboratory investigation; a journal of technical methods and pathology *91*, 216-231.

Snider, L., Geng, L.N., Lemmers, R.J.L.F., Kyba, M., Ware, C.B., Nelson, A.M., Tawil, R., Filippova, G.N., van der Maarel, S.M., Tapscott, S.J.*, et al.* (2010). Facioscapulohumeral dystrophy: incomplete suppression of a retrotransposed gene. PLoS Genetics *6*, e1001181.

Šošić, D., Richardson, J.A., Yu, K., Ornitz, D.M., and Olson, E.N. (2003). Twist regulates cytokine gene expression through a negative feedback loop that represses NF-κB activity. Cell *112*, 169-180.

Stedman, H.H., Sweeney, H.L., Shrager, J.B., Maguire, H.C., Panettieri, R.A., Petrof, B., Narusawa, M., Leferovich, J.M., Sladky, J.T., and Kelly, A.M. (1991). The mdx mouse diaphragm reproduces the degenerative changes of Duchenne muscular dystrophy. Nature *352*, 536.

Sultana, N., Zhang, L., Yan, J., Chen, J., Cai, W., Razzaque, S., Jeong, D., Sheng, W., Bu, L., Xu, M.*, et al.* (2015). Resident c-kit+ cells in the heart are not cardiac stem cells. Nature Communications *6*, 8701.

Sutton, M.G.S.J., and Sharpe, N. (2000). Left ventricular remodeling after myocardial infarction: pathophysiology and therapy. Circulation *101*, 2981-2988.

Suzuki, K., Tsunekawa, Y., Hernandez-Benitez, R., Wu, J., Zhu, J., Kim, E.J., Hatanaka, F., Yamamoto, M., Araoka, T., Li, Z.*, et al.* (2016). In vivo genome editing via CRISPR/Cas9 mediated homology-independent targeted integration. Nature *540*, 144.

Tabebordbar, M., Zhu, K., Cheng, J.K.W., Chew, W.L., Widrick, J.J., Yan, W.X., Maesner, C., Wu, E.Y., Xiao, R., Ran, F.A.*, et al.* (2016). In vivo gene editing in dystrophic mouse muscle and muscle stem cells. Science *351*, 407.

Takeshima, Y., Yagi, M., Okizuka, Y., Awano, H., Zhang, Z., Yamauchi, Y., Nishio, H., and Matsuo, M. (2010). Mutation spectrum of the dystrophin gene in 442 Duchenne/Becker muscular dystrophy cases from one Japanese referral center. Journal Of Human Genetics *55*, 379.

Toma, C., Pittenger, M.F., Cahill, K.S., Byrne, B.J., and Kessler, P.D. (2002). Human mesenchymal stem cells differentiate to a cardiomyocyte phenotype in the adult murine heart. Circulation *105*, 93-98.

Turan, S., Farruggio, A.P., Srifa, W., Day, J.W., and Calos, M.P. (2016). Precise correction of disease mutations in induced pluripotent stem cells derived from patients with Limb Girdle Muscular Dystrophy. Molecular Therapy *24*, 685-696.

Uchida, S., De Gaspari, P., Kostin, S., Jenniches, K., Kilic, A., Izumiya, Y., Shiojima, I., grosse Kreymborg, K., Renz, H., Walsh, K.*, et al.* (2013). Sca1-derived cells are a source of myocardial renewal in the murine adult heart. Stem Cell Reports *1*, 397-410.

Ueki, J., Nakamori, M., Nakamura, M., Nishikawa, M., Yoshida, Y., Tanaka, A., Morizane, A., Kamon, M., Araki, T., Takahashi, M.P.*, et al.* (2017). Myotonic dystrophy type 1 patient-derived iPSCs for the investigation of CTG repeat instability. Scientific Reports *7*, 42522.

Valentine, B.A., Cooper, B.J., Cummings, J.F., and deLahunta, A. (1986). Progressive muscular dystrophy in a golden retriever dog: light microscope and ultrastructural features at 4 and 8 months. Acta Neuropathologica *71*, 301-310.

Valentine, B.A., Cooper, B.J., de Lahunta, A., O'Quinn, R., and Blue, J.T. (1988). Canine X-linked muscular dystrophy: An animal model of Duchenne muscular dystrophy: Clinical studies. Journal of the Neurological Sciences *88*, 69-81.

van Agtmaal, E.L., André, L.M., Willemse, M., Cumming, S.A., van Kessel, I.D.G., van den Broek, W.J.A.A., Gourdon, G., Furling, D., Mouly, V., Monckton, D.G.*, et al.* (2017). CRISPR/Cas9-induced (CTG·CAG)n repeat instability in the Myotonic Dystrophy type 1 locus: Implications for therapeutic genome editing. Molecular Therapy *25*, 24-43.

van Berlo, J.H., Kanisicak, O., Maillet, M., Vagnozzi, R.J., Karch, J., Lin, S.C., Middleton, R.C., Marban, E., and Molkentin, J.D. (2014). c-kit+ cells minimally contribute cardiomyocytes to the heart. Nature *509*, 337-341.

van Berlo, J.H., and Molkentin, J.D. (2014). An emerging consensus on cardiac regeneration. Nat Med *20*, 1386-1393.

VanDusen, N.J., and Firulli, A.B. (2012). Twist factor regulation of non-cardiomyocyte cell lineages in the developing heart. Differentiation; research in biological diversity *84*, 79-88.

Veltrop, M., van Vliet, L., Hulsker, M., Claassens, J., Brouwers, C., Breukel, C., van der Kaa, J., Linssen, M.M., den Dunnen, J.T., Verbeek, S.*, et al.* (2018). A dystrophic Duchenne mouse model for testing human antisense oligonucleotides. PloS one *13*, e0193289.

Vieitez, I., Gallano, P., González-Quereda, L., Borrego, S., Marcos, I., Millán, J.M., Jairo, T., Prior, C., Molano, J., Trujillo-Tiebas, M.J.*, et al.* (2017). Mutational spectrum of Duchenne muscular dystrophy in Spain: study of 284 cases. Neurología (English Edition) *32*, 377-385.

Vulin, A., Wein, N., Simmons, T.R., Rutherford, A.M., Findlay, A.R., Yurkoski, J.A., Kaminoh, Y., and Flanigan, K.M. (2015). The first exon duplication mouse model of Duchenne muscular dystrophy: A tool for therapeutic development. Neuromuscular Disorders *25*, 827-834.

Walmsley, G.L., Arechavala-Gomeza, V., Fernandez-Fuente, M., Burke, M.M., Nagel, N., Holder, A., Stanley, R., Chandler, K., Marks, S.L., Muntoni, F.*, et al.* (2010). A Duchenne Muscular Dystrophy gene hot spot mutation in dystrophin-deficient cavalier king charles spaniels is amenable to exon 51 skipping. PloS one *5*, e8647.

Wang, J.-Z., Wu, P., Shi, Z.-M., Xu, Y.-L., and Liu, Z.-J. (2017). The AAV-mediated and RNA-guided CRISPR/Cas9 system for gene therapy of DMD and BMD. Brain and Development *39*, 547-556.

Wojtal, D., Kemaladewi, Dwi U., Malam, Z., Abdullah, S., Wong, Tatianna W.Y., Hyatt, E., Baghestani, Z., Pereira, S., Stavropoulos, J., Mouly, V.*, et al.* (2016). Spell checking nature: Versatility of CRISPR/Cas9 for developing treatments for inherited disorders. The American Journal of Human Genetics *98*, 90-101.

Wu, J., Hunt, S.D., Matthias, N., Servián-Morilla, E., Lo, J., Jafar-Nejad, H., Paradas, C., and Darabi, R. (2017). Generation of an induced pluripotent stem cell line (CSCRMi001-A) from a patient with a new type of limb-girdle muscular dystrophy (LGMD) due to a missense mutation in POGLUT1 (Rumi). Stem Cell Research *24*, 102-105.

Xu, L., Park, K.H., Zhao, L., Xu, J., El Refaey, M., Gao, Y., Zhu, H., Ma, J., and Han, R. (2016). CRISPR-mediated genome editing restores dystrophin expression and function in mdx mice. Molecular Therapy *24*, 564-569.

Yang, J., Mani, S.A., Donaher, J.L., Ramaswamy, S., Itzykson, R.A., Come, C., Savagner, P., Gitelman, I., Richardson, A., and Weinberg, R.A. (2004). Twist, a master regulator of morphogenesis, plays an essential role in tumor metastasis. Cell *117*, 927-939.

Yang, W.-J., Li, S.-H., Weisel, R.D., Liu, S.-M., and Li, R.-K. (2012). Cell fusion contributes to the rescue of apoptotic cardiomyocytes by bone marrow cells. Journal of Cellular and Molecular Medicine *16*, 3085-3095.

Yang, Y., Wang, L., Bell, P., McMenamin, D., He, Z., White, J., Yu, H., Xu, C., Morizono, H., Musunuru, K.*, et al.* (2016). A dual AAV system enables the Cas9-mediated correction of a metabolic liver disease in newborn mice. Nature Biotechnology *34*, 334.

Young, C.S., Hicks, M.R., Ermolova, N.V., Nakano, H., Jan, M., Younesi, S., Karumbayaram, S., Kumagai-Cresse, C., Wang, D., Zack, J.A.*, et al.* (2016). A single CRISPR-Cas9 deletion strategy that targets the majority of DMD patients restores dystrophin function in hiPSC-derived muscle cells. Cell stem cell *18*, 533-540.

Young, C.S., Mokhonova, E., Quinonez, M., Pyle, A.D., and Spencer, M.J. (2017). Creation of a novel humanized dystrophic mouse model of Duchenne Muscular Dystrophy and application of a CRISPR/Cas9 gene editing therapy. Journal of neuromuscular diseases *4*, 139-145.

Zetsche, B., Gootenberg, J.S., Abudayyeh, O.O., Slaymaker, I.M., Makarova, K.S., Essletzbichler, P., Volz, S., Joung, J., van der Oost, J., Regev, A.*, et al.* (2015). Cpf1 is a single RNA-guided endonuclease of a Class 2 CRISPR-Cas system. Cell *163*, 759-771.

Zhang, Y., Long, C., Bassel-Duby, R., and Olson, E.N. (2018). Myoediting: toward prevention of muscular dystrophy by therapeutic genome editing. Physiological Reviews *98*, 1205-1240.

Zhang, Y., Long, C., Li, H., McAnally, J.R., Baskin, K.K., Shelton, J.M., Bassel-Duby, R., and Olson, E.N. (2017). CRISPR-Cpf1 correction of muscular dystrophy mutations in human cardiomyocytes and mice. Science Advances *3*, e1602814.

Zhang, Y., Sivakumaran, P., Newcomb, A.E., Hernandez, D., Harris, N., Khanabdali, R., Liu, G.-S., Kelly, D.J., Pébay, A., Hewitt, A.W.*, et al.* (2015). Cardiac repair with a novel population of mesenchymal stem cells resident in the human heart. STEM CELLS *33*, 3100-3113.

Zincarelli, C., Soltys, S., Rengo, G., Koch, W.J., and Rabinowitz, J.E. (2010). Comparative cardiac gene delivery of adeno-associated virus serotypes 1–9 reveals that AAV6 mediates the most efficient transduction in mouse heart. Clinical and Translational Science *3*, 81-89.

Zincarelli, C., Soltys, S., Rengo, G., and Rabinowitz, J.E. (2008). Analysis of AAV serotypes 1-9 mediated gene expression and tropism in mice after systemic injection. Molecular Therapy *16*, 1073-1080.

Zuris, J.A., Thompson, D.B., Shu, Y., Guilinger, J.P., Bessen, J.L., Hu, J.H., Maeder, M.L., Joung, J.K., Chen, Z.-Y., and Liu, D.R. (2014). Cationic lipid-mediated delivery of proteins enables efficient protein-based genome editing in vitro and in vivo. Nature Biotechnology *33*, 73.